MASSACHUSETTS INSTITUTE OF TECHNOLOGY
DEPARTMENT OF NUCLEAR ENGINEERING

Cambridge, Massachusetts 02139

MIT-3944-1   MITNE-96

REACTOR PHYSICS PROJECT PROGRESS REPORT

September 30, 1968

MASSACHUSETTS INSTITUTE OF TECHNOLOGY

DEPARTMENT OF NUCLEAR ENGINEERING

Cambridge, Massachusetts 02139

MIT-3944-1   MITNE-96

AEC Research and Development Report

UC-34 Physics

(TID-4500, 47th Edition)

REACTOR PHYSICS PROJECT PROGRESS REPORT

September 30, 1968

Editors:

M. J. Driscoll
T. J. Thompson

Contributors:

F. M. Clikeman
J. N. Donohew
M. J. Driscoll
J. D. Eckard
T. L. Harper
Y. Hukai
I. Kaplan
C. H. Kim
Y.-M. Lefevre

T. C. Leung
N. R. Ortiz
N. C. Rasmussen
C. S. Rim
S. S. Seth
A. T. Supple
C. Takahata
T. J. Thompson

DISTRIBUTION

MIT-3944-1   MITNE-96
AEC Research and Development Report
UC-34 Physics

1. USAEC, New York Operations Office, Library

2-4. USAEC, Reactor Physics Branch, Division of
Reactor Development and Technology

5. USAEC, New York Patents Office, Brookhaven National Lab.

6. USAEC, Cambridge Branch, New York Operations Office,
Research Contracts Division

7. USAEC, Division of Reactor Development and Technology

8. USAEC, HWOCR Branch

9. USAEC, Water Projects Branch

10. USAEC, Core Design Branch

11. USAEC, Division of Naval Reactors

12. Advisory Committee on Reactor Physics (E. R. Cohen)

13. ACRP (G. Dessauer)

14. ACRP (R. Fluharty)

15. ACRP (E. Gaerttner)

16. ACRP (R. Ehrlich)

17. ACRP (F. C. Maienschein)

18. ACRP (J. Chernick)

19. ACRP (R. Avery)

20. ACRP (M. Nelkin)

21. ACRP (F. Dawson)

22. ACRP (G. Hansen)

23. ACRP (W. B. Loewenstein)

24. ACRP (L. W. Nordheim)

25. ACRP (T. M. Snyder)

26. ACRP (R. Bayard)

27-29. D. T. I. E., Oak Ridge, for Standard Distribution

30-100. Internal Distribution

101. Combustion Engineering (S. Visner)

102. Brookhaven National Laboratories (H. Kouts)

ABSTRACT

This is the initial annual report in an experimental and theoretical program to develop and apply single and few element methods for the determination of reactor lattice parameters.

During the period covered by the report, January 1, 1968 through September 30, 1968, work was devoted to development and evaluation of methods for the experimental determination of the heterogeneous fuel rod parameters Γ, η and A. The first of these parameters, the thermal constant Γ, is related to the thermal utilization; η is the total fast neutron yield per thermal neutron absorbed; and the epi-thermal absorption parameter, A, is related to the resonance escape probability. Exponential tank experiments were completed which show that Γ and η can be measured using foil activation traverses external to a single fuel element. Numerical experiments were performed using multigroup codes to demonstrate the feasibility of a proposed method for determination of A. Analytic work focused on development of methods for calculation of the material buckling, B_m^2, for full lattices from measured values of Γ, η and A, and on correction of these parameters for interaction effects.

Work was also initiated with the objective of applying advanced gamma spectrometric methods using Ge(Li) detectors to the determination of fuel rod parameters. Capture gamma spectra were measured for a number of low and high enrichment, and depleted, fuel specimens. A report was issued on a computer program developed to extract photopeak energies and intensities from multi-channel analyzer spectra.

TABLE OF CONTENTS

LIST OF FIGURES

LIST OF TABLES

1. INTRODUCTION

1.1 Foreword

This is the first annual progress report of the Reactor Physics Project of the Massachusetts Institute of Technology. This project was initiated January 1, 1968 with the objective of developing and applying single and few rod methods for the determination of reactor physics parameters. Development of these methods should increase the ability to evaluate the reactor physics characteristics of new and promising types of reactor fuel at very low cost. Work is divided into two tasks, with two phases in each task.

Task I is concerned with irradiated fuel containing both fission products and plutonium. Phase I of this work is concerned with development of techniques, including the use of simulated burned or recycled fuel (containing plutonium but no fission products). Phase II will involve use of actual spent fuel.

Task II of the project is devoted to application of single rod methods to clustered fuel. Phase I is concerned primarily with a theoretical demonstration of the applicability of such methods, and Phase II primarily with experimental investigation of selected clean-configuration experiments.

This report summarizes the work completed through September 30, 1968, which has mainly been concerned with Phase I of Tasks I and II.

1.2 Research Objectives and Methods

The following abbreviated discussion will serve to show the motivation for the specific investigations reported upon in subsequent chapters of this report and to unify the presentation. All of this work is based upon heterogeneous reactor theory, which is well known to be applicable to lattices of low enrichment fuel moderated by heavy water: reference 1, for example is a recent confirmation of this assertion.

In heterogeneous reactor theory, a fuel element may be characterized by as few as three parameters:

Γ = asymptotic thermal flux at rod surface per thermal neutron absorbed by rod,

η = fast neutrons emitted per thermal neutron absorbed in the fuel,

A = epithermal absorptions per unit slowing-down density.

Knowledge of these three parameters permits calculation of k_∞:

$$k_\infty \cong \frac{\eta(1-A/V_c)}{1 + \Gamma \Sigma_{am} V_m} , \qquad (1.1)$$

where

V_m = cross-section area occupied by moderator in a unit cell,

V_c = cross-section area occupied by total unit cell,

Σ_{am} = mean cross section for neutron absorption by moderator.

These same three parameters are required as input to heterogeneous theory computer programs such as HERESY (2).

Most previous work in the area of heterogeneous reactor physics has been concerned with methods for calculation of Γ, η and A. In the present work, the emphasis is, instead, on experimental determination of these parameters using one (or a few) rod(s), and the concurrent theoretical and numerical work is primarily designed to help plan or interpret the experiments.

Previous work at M.I.T., summarized in reference 3, has shown that η and A can be inferred from in-rod foil activation experiments. The present work has as its objective the determination of parameters by means of measurements made on the rod surface or in the surrounding moderator. This should obviate the need for cutting into rods containing plutonium and fission products, with the attendant contamination problem.

Two major parallel experimental approaches are being pursued in the development of parameter measurement methods. The first involves classical foil activation, or activity traverse experiments; the second, high resolution gamma-ray spectroscopy using Ge(Li) detectors. Both approaches are discussed in subsequent chapters of this report.

To date, most single rod experiments, and all of those at M.I.T., have been concerned with small-diameter (e.g., 0.5 inch) cylindrical rods and with lattices made up of uniform arrays of such rods, as might be used in large pressurized or boiling water reactors. Since most heavy water moderated reactors are of the pressure-tube type, with more widely separated fuel rod clusters, there is considerable incentive to extend the work to such systems. In theory, this extension is simple, since one need only treat each fuel cluster (plus its surrounding pressure and calandria tubes) as a single "rod" in a larger, widely-spaced array. In practice, one must show that the much larger diameter of such "rods" (e.g., 4 inches) and the inhomogeneous interior structure does not invalidate the experimental methods employed. Some preliminary evidence, both theoretical and experimental, on this question will be discussed in this report.

1.3 Staff

The project staff, including thesis students, during the report period was as follows:

M. J. Driscoll, Assistant Professor of Nuclear Engineering

T. J. Thompson, Professor of Nuclear Engineering

I. Kaplan, Professor of Nuclear Engineering (on sabbatical since July 1, 1968)

N. C. Rasmussen, Professor of Nuclear Engineering

F. M. Clikeman, Associate Professor of Nuclear Engineering

A. T. Supple, Jr., Project Technician

J. N. Donohew, Research Assistant (Fall 1968)

J. D. Eckard, Jr., AEC Fellowship, Part-time Programmer

T. L. Harper, AEC Fellowship, Part-time Data Analyst

Y. Hukai, Pan American Fellowship, Sc.D. Student

C. H. Kim, Research Assistant (Summer 1968)

Y.-M. Lefevre, Research Assistant (Fall 1968)

T. C. Leung, Research Assistant, S.M. Student (Since June 1968)

N. R. Ortiz, Research Assistant (Fall 1968)

C. S. Rim, Research Assistant (Summer 1968)

S. S. Seth, Research Assistant, Sc.D. Student

C. Takahata, Part-time Electronics Assistant (Spring 1968)

1.4 References

(1) Groves, W. E., F. D. Benton, and R. M. Satterfield, "A Comparison of Heterogeneous Nuclear-Reactor Lattice Theory with Experiment," Nucl. Sci. Eng., Vol. 31, No. 1, January 1968.

(2) Klahr, C. N. et al., "Heterogeneous Reactor Calculation Methods," NYO-2680, 1961.

(3) Heavy Water Lattice Project Final Report, MIT-2344-12, MITNE-86, September 30, 1967.

2. CALCULATION OF LATTICE PARAMETERS

S. S. Seth

2.1 Introduction

The ultimate objective of the experimental heterogeneous method is to measure characteristic fuel parameters using single (or a few) fuel elements and, from them, to calculate key properties of complete fuel lattices. The two most important collective properties of the fuel lattice are the infinite multiplication constant, k_∞, and the material buckling, B_m^2.

As noted in Chapter 1, the familiar four-factor formula,

$$k_\infty = \eta' \epsilon p f, \tag{2.1}$$

can be rewritten in terms of the heterogeneous theory parameters η, A and Γ:

$$\eta = \eta' \epsilon,$$

$$A = (1-p)V,$$

$$\Gamma \approx \frac{1/f - 1}{V(1-v)\,\Sigma_{am}} = \frac{\Lambda}{V(1-v)\,\Sigma_{am}}, \tag{2.2}$$

where

V = cross-section area of unit cell (i.e., volume per unit length),

v = volume fraction fuel in unit cell,

Σ_{am} = mean absorption cross section of moderator.

Substitution of the values obtained for η, ϵ, p and f from Eqs. 2.2 into Eq. 2.1 gives:

$$k_\infty = \frac{\eta(1 - A/V)}{1 + \Gamma V(1-v)\,\Sigma_{am}} = \frac{\eta(1 - A/V)}{1 + \Lambda}. \tag{2.3}$$

Equation 2.3 can be modified in a number of respects to improve its capabilities. First of all, instead of assuming that η, A and Γ are

constants independent of lattice spacing, as is implied by Eq. 2.3, the small interaction effects can be taken into account. Secondly, a more accurate relation between Γ and f can be derived. Finally, since the material buckling is the quantity which is directly measured in most lattice experiments, it is convenient to relate k_∞ and B_m^2. According to age-diffusion theory,

$$k_\infty = e^{B_m^2 \tau}(1+L^2 B_m^2),\tag{2.4}$$

where the diffusion area, L^2, and age, τ, can be expressed in terms of the corresponding moderator properties, L_o^2 and τ_o:

$$L^2 = L_o^2 \frac{\Lambda}{1+\Lambda},$$

$$\tau = \tau_o\left(1 - \frac{v}{2}\right)^{-2}.$$

The following sections of this chapter discuss the results of applying the preceding equations to experimental data and present some of the improved theoretical relations derived for the key variables.

2.2 Correction of Γ, η and A for Interaction Effects

Of the three heterogeneous parameters, η will vary most with lattice spacing primarily because it has been defined here to include the fast fission factor. The measured single rod value, η_o, can be corrected to include both epithermal fissions in U-235 and fast fissions in U-238 due to neutrons originating in other fuel elements by summing up the individual contributions over the entire lattice, using methods described in reference 1. Following that work, one obtains the expression:

$$\eta = \eta_o\left[1 + v\left\{\frac{v^{25}\Sigma_{fe}^{25}}{\xi\Sigma_s} + 4\lambda v^{28}\Sigma_{ff}^{28}\exp\left(-\sqrt{\frac{3\pi a}{v\lambda}}\right)\right\}\right]\tag{2.5}$$

where

$$v^{25}, v^{28} = \text{fission yields for U-235 and U-238, respectively,}$$

Σ_{fe}^{25} = epithermal fission cross section for U-235 = $N^{25} \sigma_{fe}^{25}$,

Σ_{ff}^{28} = cross section for U-238 fast fission = $N^{28} \sigma_{ff}^{28}$,

λ = mean free path for first-flight neutrons in D_2O,

$\xi\Sigma_s$ = moderating power of D_2O,

a = fuel rod radius.

Table 2.1 lists both the input parameters to Eq. 2.5 and the result obtained from applying Eq. 2.5 to a representative set of natural uranium lattices. Also shown are experimental full lattice data, interpreted using methods described by Donovan (2). As is evident, the corrections to η_o can amount to several percent and are, therefore, worth making. Further, the relatively simple theoretical expression given in Eq. 2.5 is evidently capable of making this correction with sufficient accuracy.

TABLE 2.1

Comparison of Predicted and Measured Values of η for
One-Inch-Diameter, Natural Uranium Lattices

Lattice Spacing (Inches)	Full Lattice Experiment	η Prediction Using Equation 2.5
4.5	1.44	1.457
5.0	1.42	1.439
5.75	1.41	1.421
∞ (Single Rod)	1.37	1.37

Input parameters to Equation 2.5:

ν^{25} = 2.43 $\qquad$ λ = 11.36 cm

ν^{28} = 2.83 $\qquad$ $\xi\Sigma_s$ = 0.18 cm^{-1}

σ_{fe}^{25} = 280 b $\qquad$ η_o = 1.370

σ_{ff}^{28} = 0.306 b

The other two fuel element characterization parameters, Γ and A, vary much less with lattice spacing than does η. Corrections have therefore not been included in calculations made to date. There are, however, several small corrections which are still under consideration. These will be mentioned briefly. Although the Dancoff shadowing effect is small in widely spaced, D_2O-moderated lattices, the effect on A must eventually be considered. There is also a second correction due to the increasing non-$1/E$ effect as lattice spacing is decreased. An expression for this effect on the effective resonance integral (ERI) has previously been derived for U-238 (3). Since previous work (2) has also shown that A is directly proportional to the ERI, we may write:

$$\frac{\Delta A^{28}}{A^{28}} = 0.03 \cdot A^{28} \cdot v \tag{2.6}$$

Equation 2.6 predicts that lattice effects could modify A by several percent. As noted in Chapter 6, neither the theoretical nor the experimental work has yet progressed to the point where such small corrections are warranted.

Finally, the thermal constant Γ will also vary slightly with pitch, due to spectral hardening effects. Frech (4) has experimentally shown that the change in effective neutron temperature is directly proportional to the volume fraction of fuel; hence, it is conceivable that a simple correction scheme could be developed to account for spectral hardening. Again, because there is an irreducible inherent experimental error of a few percent in the determination of Γ, it is questionable whether such sophistication is warranted.

2.3 Improved Expression for Thermal Utilization

The second major weakness of the simple relation, Eq. 2.3, is that the thermal flux has been assumed constant in the moderator in relating Γ and f. This defect is easily remedied by application of diffusion theory in cylindrical unit cell geometry, assuming a weakly absorbing moderator. One obtains:

$$\Lambda = \frac{1}{f} - 1 = \Gamma \Sigma_{am} V(1-v) + \frac{V}{4\pi L_o^2} \left\{ \frac{v}{2} - \frac{3}{2} - \frac{\ln v}{1 - v} \right\} , \qquad (2.7)$$

where

L_o, Σ_{am} = diffusion length and absorption cross section for D_2O moderator,

Λ = moderator absorptions per fuel absorption.

Comparison of Eqs. 2.2 and 2.7 shows that the latter merely contains a small additive correction (second term on the right-hand side of the equation). As will be discussed in Chapter 3, Eq. 2.7 permits one to calculate f from Γ with quite acceptable accuracy, namely, within about ± 0.1 percent.

2.4 Calculation of Material Buckling

A computer program, HECKLE, has been written to calculate k_∞ and B_m^2 from single rod parameters, using Eqs. 2.3, 2.4, 2.5 and 2.7.

Figure 2.1 shows experimental values of B_m^2 measured using complete lattices of one-inch-diameter, natural uranium fuel rods, as compiled by Palmedo (5). Also shown is the result of inserting the following single rod parameters into the HECKLE code:

η_o = 1.37	Reference 2
Γ = 0.94 cm^{-1}	Chapter 3 of this report
A = 19.0 cm^2	
L_0^2 = 0.9437 × 10^4 cm^2	99.75 mol % D_2O
τ_o = 119 cm^2	99.75 mol % D_2O
Σ_{am} = 0.879 × 10^{-4} cm^{-1}	99.75 mol % D_2O

Because of the lack of reliable single rod measurements, the value of A was estimated using Hellstrand's correlations for U-238, and corrected to include U-235 absorptions by the method described in Chapter 6.

As can be seen from Fig. 2.1, the values of B_m^2 calculated from
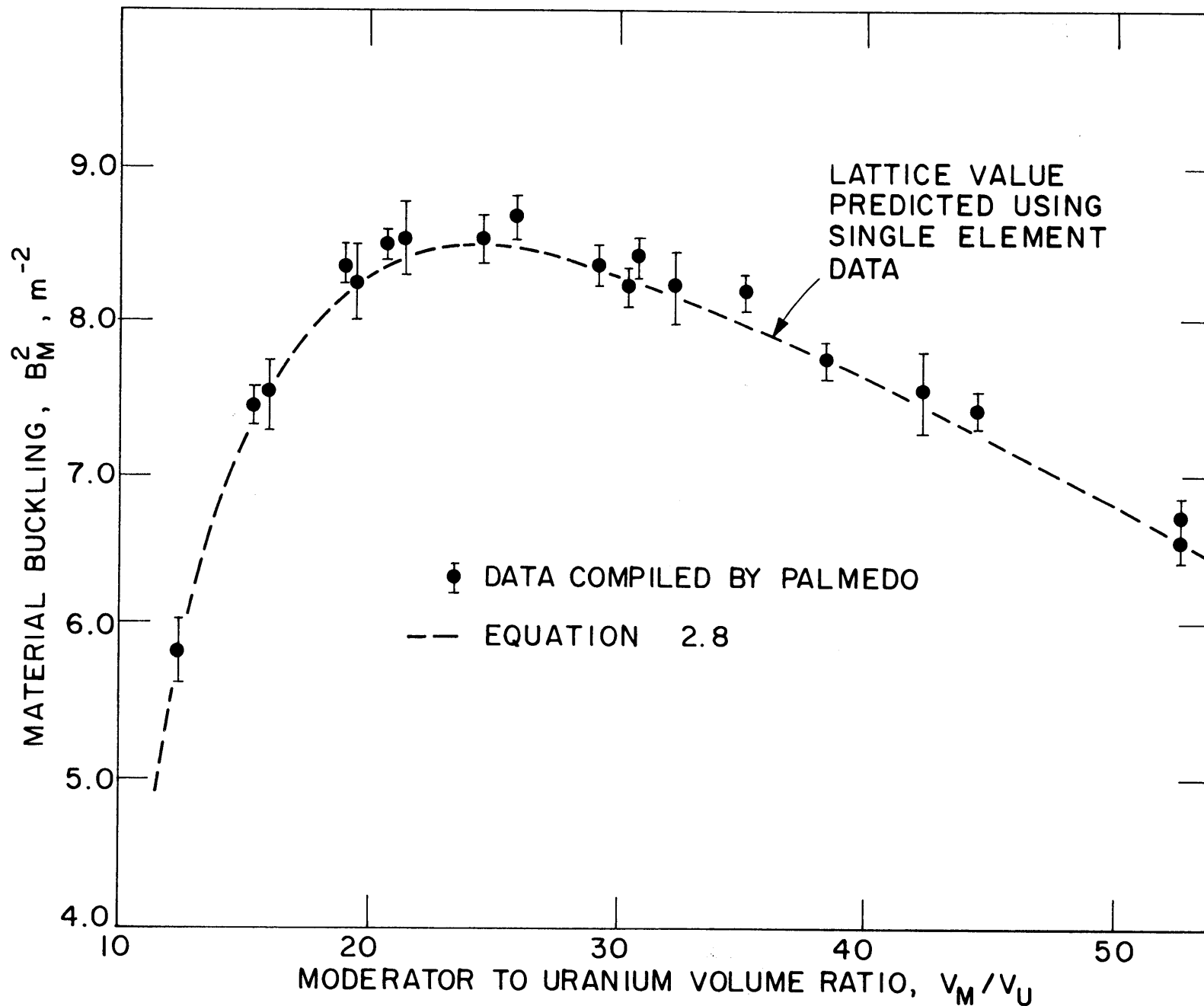
FIG. 2.1 BUCKLINGS OF 1.0 IN. DIAMETER, NATURAL URANIUM RODS
          IN D$_2$O

single rod data and those measured on full lattices are in good agreement.

The HECKLE code has also been used to study the effect on B_m^2 of variations in each of the single rod parameters Γ, η and A. It was found that, in order to determine B_m^2 within $\pm$ 5%, it is necessary to know η within approximately $\pm$ 1% and Γ and A within about $\pm$ 7%. Chapters 3 through 6 of this report discuss the progress achieved to date in developing experimental methods having this capability.

2.5 Future Experimental Work

The problem of applying single rod methods to tightly clustered fuel has also been looked into, and all indications are (see Chapter 3) that the methods developed for individual fuel rods can be applied to clustered fuel. In fact, since there is normally a much wider spacing between clusters than between individual rods in a uniform lattice, the values of η, Γ and A should vary only slightly with the inter-element spacing. Clusters comprising 19 and 31 rods (Fig. 2.2) and of a composition that simulates partially burned natural UO_2 (Table 2.2) are being fabricated, and experiments to determine the heterogeneous parameters for these clusters will be undertaken during the coming year. Full lattices comprising the same fuel have been extensively investigated (6) both analytically and experimentally by the Savannah River Laboratory, and their results should provide an excellent basis for testing the proposed new methods.

TABLE 2.2
Properties of Type B, USAEC-AECL Cooperative Program,
Simulated Burned Fuel

1. Isotopic Composition, wt % of total U + Pu

U-235	U-238	Pu-239	Pu-240	Pu-241	Pu-242
0.30	99.431	0.25	0.016	0.002	0.001

2. Individual Fuel Rods
   Pellets: sintered coprecipitated oxide, 95% theoretical density, 0.500 ± 0.002 inch diameter.
   Clad: 6063 T6 aluminum, ID 0.507 ± 0.004 inch, wall thickness 0.020 ± 0.002 inch, length 54 inches.

FUEL
RODS

0.597"

3.080" OD
3.020" I D

6061 AI HOUSING TUBE
(19 - ROD CLUSTER)

4.000" OD
3.900" I D

6061 AI HOUSING TUBE
(31 - ROD CLUSTER
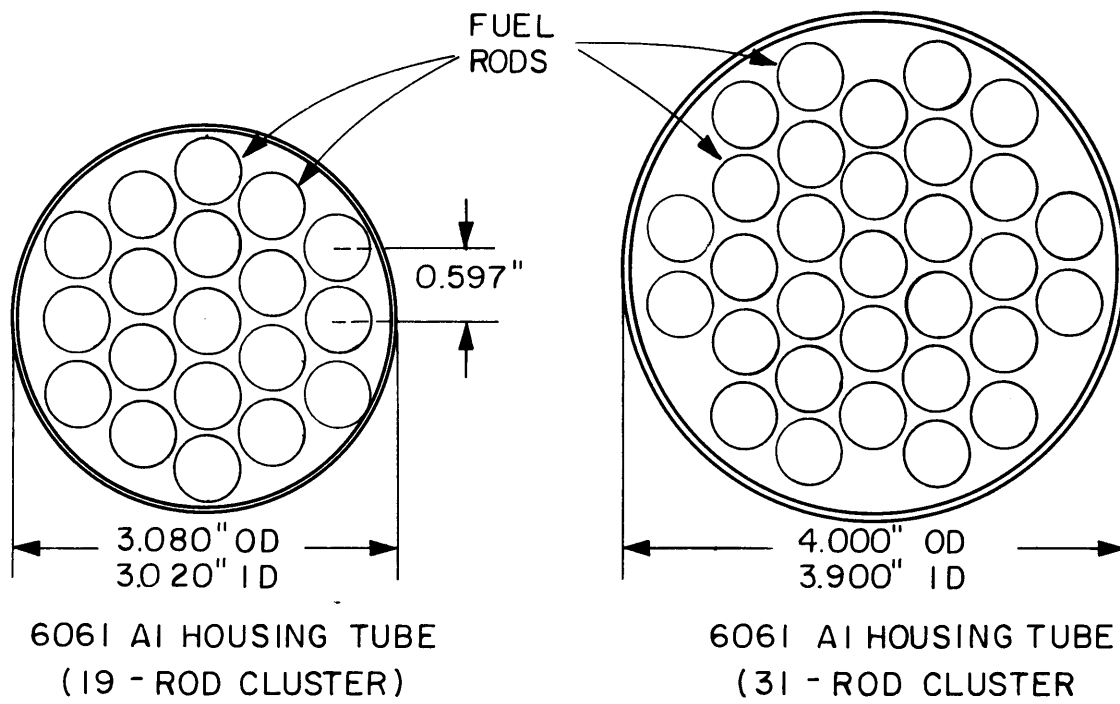
FIG. 2.2 FUEL CLUSTER ARRANGEMENT

2.6 <u>References</u>

(1) Higgins, M. J., Fuel Rod Interaction Kernels, Chapter 9, "Heavy Water Lattice Project Final Report," MIT-2344-12, MITNE-86, September 30, 1967.

(2) Donovan, R., Measurement of Heterogeneous Parameters, Chapter 8, ibid.

(3) Seth, S. S., Measurement of Integral Parameters, Chapter 3, ibid.

(4) Frech, D., Neutron Temperature Measurements Inside Fuel Rods, Chapter 5, ibid.

(5) Palmedo, P. F. et al., "Measurements of the Material Bucklings of Lattices of Natural Uranium Rods in D_2O," MITNE-13, 1962.

(6) Bauman, N. P. et al., "Lattice Experiments with Simulated Burned Fuel for D_2O Power Reactors," DP-1122, February 1968.

3. EXPERIMENTAL DETERMINATION OF
THE THERMAL CONSTANT

S. S. Seth and A. T. Supple

3.1 Introduction

Previous work at M.I.T. by Pilat (1) and by Donovan (2) has demonstrated the feasibility of measuring the thermal constant, Γ, using radial foil traverses about a single fuel element. The objective of the work reported herein was to effect desirable improvements in both the theoretical and experimental methodology.

3.2 Theory

Careful analysis of the single rod experiment using age-diffusion theory has led to improved theoretical expressions relating Γ, η and the thermal flux shape. An abbreviated derivation follows.

First, define Γ as the ratio of the asymptotic thermal flux on the surface of the fuel rod to the net thermal neutron current into the rod. By asymptotic flux, we mean the value of the thermal neutron flux in the moderator extrapolated back to the fuel rod surface using diffusion theory. Thus,

$$\Gamma = \frac{\phi(a)}{2\pi a \, |J|} . \tag{3.1}$$

The thermal neutron balance in the moderator region of a cylindrical exponential tank containing a single central fuel rod then becomes, according to age-diffusion theory:

$$D\nabla^2\phi(r) - \Sigma_a\phi(r) + D\gamma^2\phi(r) + \frac{\phi(a)}{\Gamma} \, \eta \, \frac{e^{\gamma^2\tau_{th} - \frac{r^2}{4\tau_{th}}}}{4\pi\tau_{th}} = 0, \tag{3.2}$$

where

$$\gamma^2 = \text{axial buckling.}$$

The following boundary conditions apply:

(a) at the fuel rod surface, r=a,

$$\phi(a) - 2\pi a \, D\Gamma [\nabla\phi]_{r=a} = 0 \, ;$$

(b) at the extrapolated outer boundary, $r = R$,

$$\phi(R) = 0 \, ;$$

(c) at the thermal flux peak in the moderator, $r = x$,

$$\left[\frac{\partial\phi}{\partial r}\right]_{r=x} = 0 \, .$$

The Green's function for this problem is given by:

$$G(r, \xi) = \begin{cases} -\kappa \left[Y_o(\alpha r) - J_o(\alpha R)\beta \right] \left[J_o(\alpha\xi) - Y_o(\alpha\xi) \dfrac{J_o(\alpha R)}{Y_o(\alpha R)} \right] & r < \xi \\[3em] -\kappa \left[Y_o(\alpha\xi) - J_o(\alpha\xi)\beta \right] \left[J_o(\alpha r) - Y_o(\alpha r) \dfrac{J_o(\alpha R)}{Y_o(\alpha R)} \right] & r > \xi \end{cases}$$

$$(3.3)$$

where

$$\alpha^2 = \gamma^2 - \frac{\Sigma_a}{D} \, ,$$

$$\kappa^{-1} = \frac{2}{\pi} \left[\frac{J_o(\alpha R)}{Y_o(\alpha R)} \cdot \beta - 1 \right] ,$$

and

$$\beta = \frac{Y_o(\alpha a) + 2\pi D\Gamma(\alpha a) \, Y_1(\alpha a)}{J_o(\alpha a) + 2\pi D\Gamma(\alpha a) \, J_1(\alpha a)} \, .$$

The radial flux shape in the moderator can then be solved for:

$$\phi(r) = N \phi(a) \left\{ \left[J_o(\alpha r) - Y_o(\alpha r) \frac{J_o(\alpha R)}{Y_o(\alpha R)} \right] \left[I_2(a, r) - \beta I_1(a, r) \right] \right.$$

$$\left. + \left[Y_o(\alpha r) - \beta J_o(\alpha r) \right] \left[I_1(r, R) - \frac{J_o(\alpha R)}{Y_o(\alpha R)} I_2(r, R) \right] \right\} \qquad (3.4)$$

where

$$N = \frac{J_o(\alpha a) + 2\pi D\Gamma(\alpha a) J_1(\alpha a)}{4D\Gamma \left[I_1(a, R) - \frac{J_o(\alpha R)}{Y_o(\alpha R)} I_2(a, R) \right]}$$

$$I_1(u, v) = \int_u^v J_o(\alpha \xi) \, e^{-\frac{\xi^2}{4\tau_{th}}} \left(-\frac{\xi}{2\tau_{th}} \right) d\xi$$

$$I_2(u, v) = \int_u^v Y_o(\alpha \xi) \, e^{-\frac{\xi^2}{4\tau_{th}}} \left(-\frac{\xi}{2\tau_{th}} \right) d\xi \ .$$

By setting the first derivative of Eq. 3.4 (with respect to r) equal to zero, the thermal constant, Γ, can be expressed in terms of the position of the peak in the thermal flux profile at $r = x$:

$$\Gamma = \frac{\eta \, e^{\frac{\gamma^2 \tau_{th}}{}} \left[\frac{J_1(\alpha x)}{Y_1(\alpha x)} I_2(a, x) - I_1(a, x) \right] - \left[J_o(\alpha a) - \frac{J_1(\alpha x)}{Y_1(\alpha x)} Y_o(\alpha a) \right]}{2\pi D(\alpha a) \left[J_1(\alpha a) - \frac{J_1(\alpha x)}{Y_1(\alpha x)} Y_1(\alpha a) \right]} \ .$$

(3.5)

Equation 3.5 is the desired relation among the thermal constant and other known or measurable system parameters. In particular, it quantifies the relation between Γ and the measured radial distance to the thermal flux peak, x, which is the entire basis for the subject experiment. Before proceeding to a discussion of some experimental applications, a brief discussion of a few other aspects relevant to the practical application of Eq. 3.5 are in order.

As shown by Eq. 3.5, Γ and η are not independently determined in the present experiment. However, detailed numerical studies have shown that η has a weak influence on the relation of Γ to the peak flux value, x. Therefore, it is possible to use a rough approximation for η in determining Γ.

A second point to note is that Eq. 3.5 requires knowledge of the radial buckling, α^2. This can be determined experimentally by measuring the axial buckling and applying the relation $\alpha^2 = \gamma^2 - \dfrac{\Sigma_a}{D}$. However, it is also possible to estimate α^2 from the unperturbed radial buckling $\alpha_o^2 = \left(\dfrac{2.405}{R}\right)^2$:

$$\alpha = \alpha_o + \frac{J_1(\alpha x)}{Y_1(\alpha x)} \frac{Y_o(\alpha_o R)}{J_1(\alpha_o R)} \frac{(\eta - 1)}{R\left[1 - \eta \, e^{\gamma^2 \tau_{th}} I_3(a, x)\right]} , \qquad (3.6)$$

where

$$I_3(a, x) = \frac{J_1(\alpha x)}{Y_1(\alpha x)} I_2(a, x) - I_1(a, x) .$$

Note that α appears on both sides of Eq. 3.6; it may, however, be readily determined iteratively. A simpler but more approximate expression can also be derived:

$$\alpha \approx \alpha_o - \frac{Y_o(\alpha_o R)}{J_1(\alpha_o R)} \frac{(\eta - 1)}{R(4D\Gamma - Y_o(\alpha a))} . \qquad (3.7)$$

While use of the above expressions is somewhat cumbersome, since the integrals I_1 and I_2 must be evaluated by numerical integration, it appears necessary to use these more sophisticated relations instead of the simpler $\eta = 0$ approximations used by Donovan (2) in order to obtain sufficient accuracy. Work is continuing to simplify and systematize the present formalism.

Finally, some work has been done to evaluate the adequacy of age-diffusion theory in the interpretation of the subject experiment. In general, the difference between the actual flux peak position and that implied by age-diffusion theory is much smaller (< 1%) than can be experimentally measured. This has been checked by numerical experiments using the computer program ANISN and analyzing the flux profiles obtained with the diffusion versus S_4 and S_8 approximations. Donovan (2) likewise derived an approximate expression showing that transport corrections would usually be negligible.

3.3 Experiments

In order to test the revised analytical procedure, a series of experiments was performed on the one-inch-diameter, natural uranium rods used by Pilat and Donovan. The mean result of five determinations was $\Gamma = 0.94 \pm .05 \text{ cm}^{-1}$. The result which would have been obtained if the effect of fast neutrons from the rod was neglected in analyzing the data (i.e., $\eta = 0$) is $\Gamma = 1.3$, which is more than 30% larger than the correct value. Thus, it is clearly necessary to use the more complicated expressions of the preceding section to analyze the experimental data.

To test the applicability of a similar approach to fuel rods arranged in a tight cluster, but treated as a single large fuel "rod," a second series of radial gold foil traverses was performed in the moderator surrounding a seven-rod cluster of 1.99% enriched UO_2 fuel rods. The experiment confirmed that the location of the flux peak was not affected by the heterogeneous structure of the cluster. Measurements along radii differing in polar angle by 30° showed no discernible shift in flux peak location, indicating that the fuel cluster can be treated as a homogenized cylinder. The value of Γ was found as a mean of six measurements to be 0.805 ± 0.12.

The comparatively large uncertainty in the last set of experiments showed the need for further refinements in experimental technique beyond those described in reference 2. These now include installation of a submersible light in the exponential tank and provision of a viewing telescope to check foil holder position. Results obtained using these refined experimental techniques will be reported subsequently.

3.4 Relation of the Thermal Constant to the Thermal Utilization

Other theoretical work was carried out to investigate the relation between the thermal constant, Γ, and the thermal utilization, f. While adequate for many purposes, the relation implied in Chapter 1, namely, $f = \dfrac{1}{1 + \Gamma \Sigma_a V_m}$, can be improved upon. For example, the

following more accurate relation can be derived by application of diffusion theory to a cylindrical unit cell:

$$f = \frac{1}{1 + \Gamma \Sigma_{am} V_m + (E-1)} \quad .$$

(3.8)

In Eq. 3.8, (E-1) refers to the "excess" moderator absorptions per fuel absorption, i.e.:

$$(E-1) = \frac{(\text{absorption in moderator}) - \Sigma_{am} V_m \phi(a)}{(\text{absorption in fuel})} \quad .$$

Diffusion theory gives the following result (3) for (E-1):

$$(E-1) = \frac{\kappa_m^2 (b^2 - a^2)}{2\kappa_m a} \left[\frac{I_1(\kappa_m b) K_o(\kappa_m a) + I_o(\kappa_m a) K_1(\kappa_m b)}{I_1(\kappa_m b) K_1(\kappa_m a) - I_1(\kappa_m a) K_1(\kappa_m b)} \right],$$

where κ_m is the inverse thermal diffusion length in the moderator and 'a', 'b' refer to the fuel and cell radii, respectively. The above relation may be usefully approximated (3) and expressed in terms of the volume fraction fuel, v, in the unit cell:

$$(E-1) = \frac{V}{4\pi L_o^2} \left\{ \frac{v}{2} - \frac{3}{2} - \frac{\ln v}{(1-v)} \right\} \quad .$$

Since f is a weak function of Γ in D_2O-moderated lattices, (E-2) can often be ignored when calculating f from Γ. (However, when calculating Γ from f, the converse is true and neglecting (E-1) can cause a large error in Γ.) Table 3.1 lists values of f calculated using Eq. 3.8 together with comparable THERMØS results.

The agreement between the numerical and experimental results is quite good. In fact, since f is so close to unity in such lattices, it would be very difficult to go more than ±1% astray in f. However, because Γ also appears in expressions for η (see Chapter 4), it is still important to measure Γ with the best possible precision, and this will be the primary objective of future work in this area.

TABLE 3.1

Comparison of Heterogeneous and THERMØS Results

1.01-Inch-Diameter, Natural Uranium Metal Fuel Rods ($\Gamma = 0.94$ cm^{-1})

Lattice Spacing (Inches)	$\overline{\Sigma}_{am}$* cm^{-1}	$(E-1)$**	f**	f*	$(E-1)$*	f***
4.5	0.638×10^{-4}	0.0012	0.9924	0.9918	0.0020	0.9916
5	0.664×10^{-4}	0.0016	0.9902	0.9896	0.0027	0.9890
5.75	0.674×10^{-4}	0.0024	0.9865	0.9859	0.0041	0.9848

*THERMØS calculation

**Calculation using Eq. 3.8, diffusion theory (E-1) value, and $\Gamma = 0.94$ cm^{-1}

***Calculation using THERMØS (E-1) value, Eq. 3.8, and $\Gamma = 0.94$ cm^{-1}

3.5 <u>References</u>

(1) Pilat, E. E., "The Use of Experiments on a Single Fuel Element to Determine the Nuclear Parameters of Reactor Lattices," MIT-2344-10, MITNE-81, 1967.

(2) Donovan, R. E., Measurement of Heterogeneous Parameters, "Heavy Water Lattice Project Final Report," MIT-2344-12, MITNE-86, 1967.

(3) Weinberg, A. M. and E. P. Wigner, <u>The Physical Theory of Neutron Chain Reactors</u>, The University of Chicago Press, Chicago, 1958.

4. A FOIL ACTIVATION METHOD FOR MEASUREMENT OF η

T. C. Leung

4.1 Introduction

Although Donovan has reported an in-rod foil activation method for determination of η (1), it is an objective of the present work that all measurements be made outside the fuel rod. In this chapter, a method involving measurement of the cadmium ratio of gold foils in the moderator surrounding the test rod is described.

4.2 Definition of η

There are many definitions of η, and most of them vary only slightly from one another. In the present work, η is defined as the number of fission neutrons produced (by thermal, epithermal and fast fission reactions) per thermal neutron absorbed in the fuel. It is important to note that η as defined here includes a fast fission contribution (e.g., δ_{28}) and an epithermal fission contribution (δ_{25}), where δ_{28} and δ_{25} are defined as follows:

$$\delta_{28} = \frac{\text{total U}^{238} \text{ fission rate in fuel}}{\text{total U}^{235} \text{ fission rate in fuel}} , \qquad (4.1)$$

$$\delta_{25} = \frac{\text{epicadmium U}^{235} \text{ fission rate}}{\text{subcadmium U}^{235} \text{ fission rate}} . \qquad (4.2)$$

The governing equation derived by Donovan (1) is:

$$\eta = \eta_{th}(1 + \delta_{25}) \left[1 + \frac{(\nu_{28,f} - 1 - \alpha_{28,f})\delta_{28}}{\nu_{25,th}} \right] , \qquad (4.3)$$

where

η_{th} = neutrons due to thermal U^{235} fission per thermal absorption in the fuel,

$\nu_{28,f}$ = average number of neutrons produced per U^{238} fast fission,

$$\alpha_{28,f} = U^{238} \text{ fast capture to fission ratio,}$$

$$\nu_{25,th} = \text{average number of neutrons produced per } U^{235} \text{ thermal fission.}$$

The parameter η_{th}, the neutron yield per thermal absorption in the fuel, is, apart from quite small spectral hardening effects, a constant, independent of lattice spacing. However, the fast fission and epithermal fission parameters, $(\delta_{28}, \delta_{25})$ and thus η, as defined in Eq. 4.3 will vary with pitch. If the fuel elements are far apart, the part of the fast effect due to interaction between adjacent elements may be negligible; otherwise, the value of η must be corrected for the lattice effect. The present work will be limited to experimental determination of the infinite-pitch lattice or single rod value of η. Analytic methods for performing the small corrections due to finite lattice spacing have already been discussed in Chapter 2.

4.3 Derivation of Expression for η

Consider Fig. 4.1 which shows a single fuel rod of radius a, immersed in a cylindrical tank of moderator which is fed from below by a thermal neutron source. It is assumed that the thermal flux sufficiently far away from the fuel rod obeys diffusion theory. As noted in Chapter 3, the heterogeneous thermal constant is defined as the asymptotic thermal moderator flux at the surface of the rod per neutron absorbed (per unit length) by the rod.

$$\Gamma \equiv \frac{\phi_{th}(a)}{2\pi a J} . \tag{4.4}$$

Thus, the thermal neutron absorption in the fuel rod is $\dfrac{\phi_{th}(a)}{\Gamma}$, and

the resultant fast neutron source thereby produced is $\eta \dfrac{\phi_{th}(a)}{\Gamma}$.
These fast neutrons emitted by the fuel rod will be slowed down to produce an epithermal flux field. The slowing-down density, q(r), at a distance r from the center of the fuel element is, according to age theory:

¢ FUEL ROD   EDGE OF TANK

MODERATOR

ASYMPTOTIC (DIFFUSION
THEORY) THERMAL FLUX

PEAK FLUX
$\phi(X)$

$\phi(a)$ ACTUAL FLUX, $\phi(r)$
                 INCLUDING
                 TRANSPORT EFFECT

$\Leftarrow$ == J, CURRENT
                 INTO ROD

                                                   $\phi(R)=0$
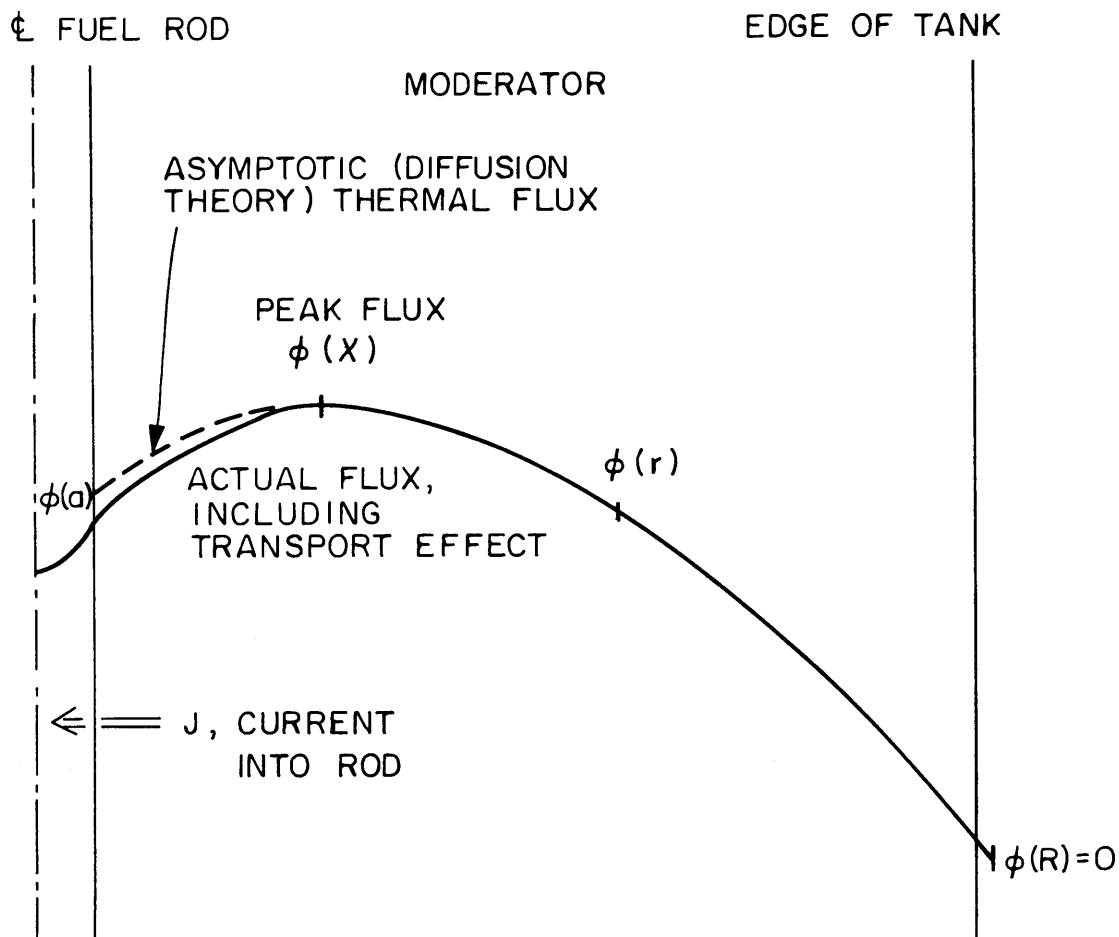
$\phi(a)$ = ASYMPTOTIC MODERATOR THERMAL FLUX
           EVALUATED AT ROD SURFACE

J   = NET NEUTRON CURRENT INTO THE FUEL ROD,
      n/cm^2 - sec.

a   = RADIUS OF FUEL ELEMENT OR "EFFECTIVE"
      RADIUS IN CASE OF CLUSTER FUEL ELEMENT

X   = RADIAL DISTANCE AT WHICH PEAK FLUX OCCURS

R   = EXTRAPOLATED RADIUS OF TANK

FIG. 4.1 SCHEMATIC OF SINGLE FUEL ROD EXPERIMENT IN
        EXPONENTIAL TANK

$$q(r) = \frac{\eta}{\Gamma} \phi_{th}(a) \ e^{\gamma^2 \tau} \ \frac{e^{-(r^2/4\tau)}}{4\pi\tau} \ , \tag{4.5}$$

where

τ = age to foil detector resonance energy (in our case, gold, 4.9 ev),

γ^2 = axial buckling of the exponential tank.

The factor $e^{\gamma^2 \tau}$ in Eq. 4.5 accounts for the effect of the axial gradient $e^{-\gamma z}$ in the exponential tank.

The slowing-down density can also be expressed relative to the epithermal flux in the following form:

$$q(r) = \xi \Sigma_T \phi_{epi}(r) \ , \tag{4.6}$$

where

ξ = average logarithmic energy decrement of moderator D_2O,

Σ_T = total cross section of moderator D_2O.

Combining Eqs. 4.5 and 4.6,

$$\frac{\phi_{epi}(r)}{\phi_{th}(a)} = \frac{\eta}{\xi \Sigma_T \Gamma} \ e^{\gamma^2 \tau} \ \frac{e^{-(r^2/4\tau)}}{4\pi\tau} \tag{4.7}$$

or

$$\eta = \left[(4\pi\tau)(\xi \Sigma_T)(\Gamma) \ e^{(r^2/4\tau) - \gamma^2 \tau} \right] \frac{\phi_{epi}(r)}{\phi_{th}(a)} \ . \tag{4.8}$$

The factor $\dfrac{\phi_{epi}(r)}{\phi_{th}(a)}$ can be expanded:

$$\frac{\phi_{epi}(r)}{\phi_{th}(a)} = \frac{\phi_{epi}(r)}{\phi_{th}(r)} \cdot \frac{\phi_{th}(r)}{\phi_{th}(a)} \ , \tag{4.9}$$

and $\dfrac{\phi_{th}(r)}{\phi_{th}(a)}$ can be determined if the flux distribution in the exponential tank is known. This calculation is discussed in Section 4.5.

The quantity $\dfrac{\phi_{epi}(r)}{\phi_{th}(r)}$ can be expressed in terms of the cadmium ratio (R_{cd}) of gold foils measured at r:

$$\frac{\phi_{th}(r)}{\phi_{epi}(r)} \cdot \frac{\sigma_{th}}{\sigma_{epi}} = (R_{cd}-1)_o \, , \tag{4.10}$$

where the subscript o denotes the infinitely thin foil, and

σ_{th} = effective absorption cross section integrated over thermal energies,

σ_{epi} = effective absorption cross section integrated over epithermal energies.

Since practical experiments require finite thickness foils, a self-shielding correction is necessary to account for foil thickness. The "thickness correction" designated by K is the experimental ratio of $(R_{cd}-1)$ for an infinitely thin foil to that for the finite foils of thickness t:

$$K = \frac{(R_{cd}-1)_o}{(R_{cd}-1)_t} \, . \tag{4.11}$$

Simms (2) gives a plot of K_{exp} vs t, comparing different experimental and calculated values of K_{exp}.

Combining Eqs. 4.8, 4.9, 4.10 and 4.11, one obtains the final expression for η:

$$\eta = \left[(4\pi\tau)(\xi\Sigma_T)(\Gamma) \, e^{(r^2/4\tau)-\gamma^2\tau} \right] \frac{\phi_{th}(r)}{\phi_{th}(a)} \cdot \frac{\sigma_{th}}{\sigma_{epi}} \cdot \frac{1}{K} \cdot \frac{1}{(R_{cd}-1)_t} \, . \tag{4.12}$$

4.4 Comparison Method for Determination of η

An absolute determination of η based on Eq. 4.12 would face many obvious difficulties, the most serious of which would be the experimental uncertainties in the large number of parameters entering into the expression, in particular τ, ξ, Σ_T, σ_{th}, σ_{epi} and K. One way to get around this is by using a comparison method. Using Eq. 4.12 to define η_{ref} for some standard rod (e.g., a natural uranium rod) and dividing it into the same equation for η of an unknown fuel element yields:

$$\frac{\eta}{\eta_{ref}} = \left(\frac{\Gamma}{\Gamma_{ref}}\right) \frac{\left[e^{(r^2/4\tau)-\gamma^2\tau}\right]}{\left[e^{(r^2/4\tau)-\gamma^2\tau}\right]_{ref}} \frac{\left[\dfrac{\phi_{th}(r)}{\phi_{th}(a)}\right]}{\left[\dfrac{\phi_{th}(r)}{\phi_{th}(a)}\right]_{ref}} \frac{(R_{cd}^{-1})_{t,ref}}{(R_{cd}^{-1})_t} . \tag{4.13}$$

Equation 4.13 contains two experimental parameters (Γ and R_{cd}) and two small theoretical corrections. Their determination will be discussed in the following sections.

4.5 Determination of $\phi_{th}(r)/\phi_{th}(a)$ and Γ

In Chapter 3, Seth has derived expressions for the flux distribution in a cylindrical exponential tank of moderator with a single fuel element in its center (Eq. 3.4). The expression will not be repeated here, since all that is required for the present discussion is the resulting functional dependence:

$$\frac{\phi(r)}{\phi(a)} = f(\Gamma, D, \alpha, a, R, \tau) , \tag{4.14}$$

where

τ = age from fission to thermal energy in the moderator,

D = diffusion coefficient of the moderator,

a = effective radius of fuel rod,

R = extrapolated radius of exponential tank,

α^2 = radial buckling of the perturbed system,

Γ = thermal constant of the fuel rod.

The first four of these parameters are readily specified and, as noted in Chapter 3, α^2 can also be determined independently. There remains, then, only the determination of Γ.

It has been shown in Eq. 4.13 that η is directly proportional to Γ. In addition, the flux ratio $\phi(r)/\phi(a)$ also depends on Γ implicitly (Eq. 4.14). The accuracy in an η measurement therefore depends on an accurate concurrent determination of Γ.

A theoretical expression relating Γ to experimentally measurable quantities has also been derived by Seth in Chapter 3 (Eq. 3.5).

Functionally,

$$\Gamma = f(\eta, D, \alpha, a, x, \tau) . \qquad (4.15)$$

It is interesting to note that Γ also depends weakly on η. Thus, in principle, Γ and η can be determined only by an iterative process. For example, Γ is first approximated by assuming a value for η. Using this value of Γ from Eq. 4.15, η can in turn be obtained from Eq. 4.13, and this new value of η can be fed back into Eq. 4.15 to get a better approximation to Γ. Fortunately, the coupling between the two parameters is weak, and one "iteration" usually suffices. Thus, one can view the two experiments for determination of η and Γ as independent, since in either case a rough estimate of the one suffices to allow determination of the other.

As seen from the expression for Γ in Eq. 4.15, Γ also depends on two other quantities: x, the radial distance at which the neutron flux is maximum, and α as previously defined. The distance, x, can be measured experimentally by making a radial foil activation traverse, and this experiment is in fact the basis for the experimental determination of Γ discussed in Chapter 3. For present purposes, we need only assert that Γ can be determined by an independent experiment.

The above procedure has been applied to experimental data for a one-inch-diameter, natural uranium rod. Figure 4.2 shows the flux ratio versus radial position calculated using Eq. 4.14.

Returning to Eq. 4.13, the next quantity to be determined is the ratio of exponential terms of the form $\exp(r^2/4\tau - \gamma^2\tau)$.

4.6 Determination of Exponential Correction Factor

In the derivation of the exponential correction factor, age theory was assumed to hold. However, this assumption is known not to be exact for heavy water. In order to check that the age theory assumption was adequate, the epithermal group flux near gold resonance (3.0 ev to 10.0 ev) was calculated using the SRA code (multigroup diffusion theory, see Chapter 7 of this report). The epithermal flux is
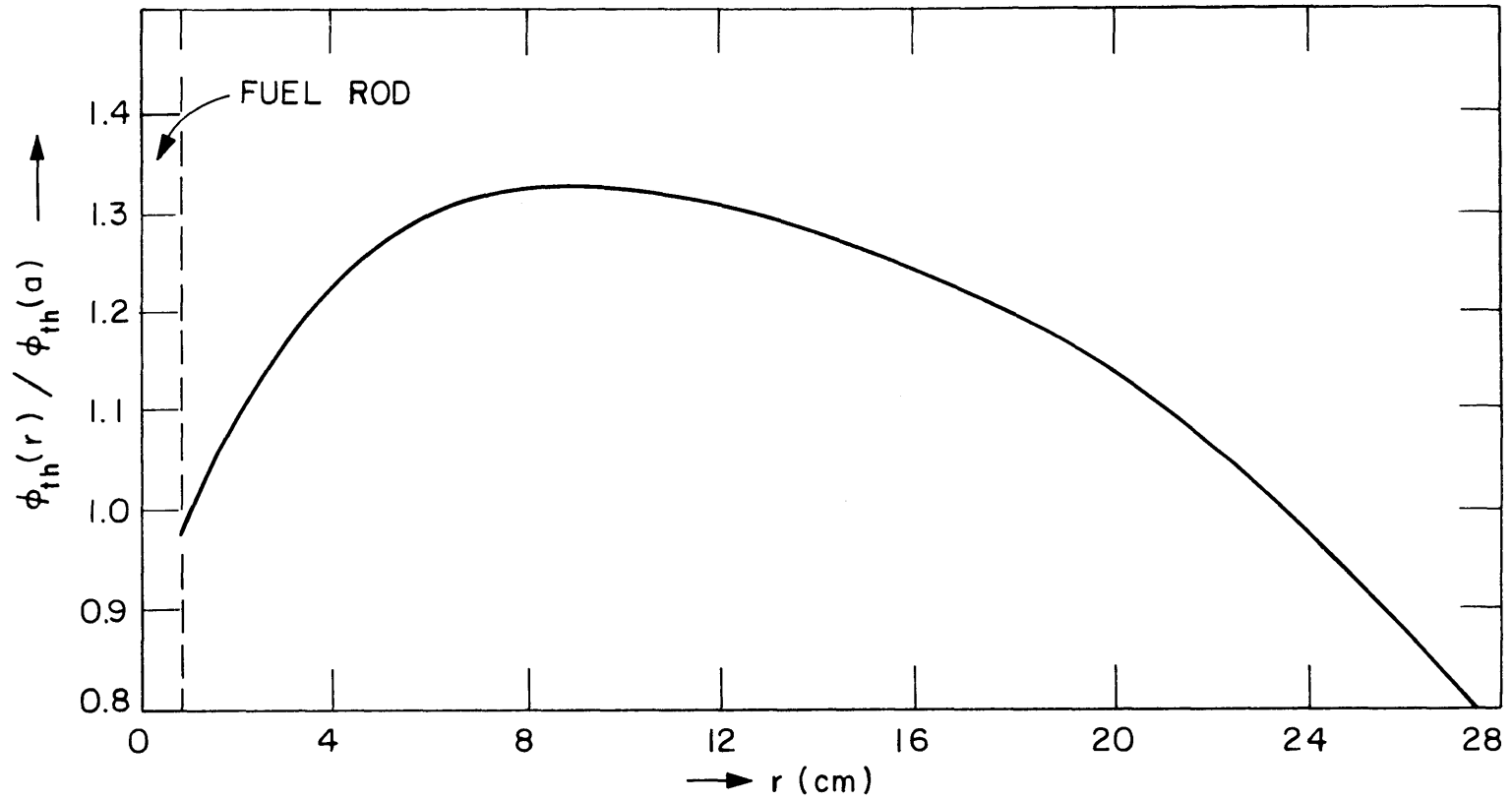
FIG. 4.2 PLOT OF $\phi_{th}(r)/\phi_{th}(a)$ VS r FOR ONE INCH NATURAL URANIUM ROD

$\Gamma = 0.9404$ cm $\tau = 118$ cm^2

$D = 0.81$ cm $a = 1.37$ cm

$\alpha = 0.0484$ $R = 46.72$ cm

fairly well represented by $\exp(-r^2/4\tau)$ in the region of concern as shown in Fig. 4.3. Based upon these results, it was concluded both that age theory was applicable and that the effective age to gold resonance was adequately known.

In the expression for η, errors in the exponential correction term $\exp(r^2/4\tau - \gamma^2\tau)$ should not be too large, so that errors in τ and r do not significantly compromise the accuracy of η. The variance of $\exp(r^2/4\tau - \gamma^2\tau)$ is given by

$$\sigma^2 = \left[\left(\frac{r}{2\tau}\right)^2 \sigma_r^2 + (\tau)^2 \sigma_{\gamma^2}^2 + \left(\frac{r^2}{4\tau^2} + \gamma^2\right)^2 \sigma_\tau^2\right]\left(e^{(r^2/4\tau)-\gamma^2\tau}\right).$$

For a 1-inch-diameter, natural uranium rod, typical parameter values and their uncertainties are:

$$r = 15.70 \text{ cm} \qquad\qquad \sigma_r = \pm\, 0.05 \text{ cm}$$

$$\gamma^2 = 24.47 \times 10^{-4} \text{ cm}^2 \qquad\qquad \sigma_{\gamma^2} = \pm\, 0.2 \times 10^{-4} \text{ cm}^2$$

$$\tau = 95 \text{ cm}^2 \qquad\qquad \sigma_\tau = \pm\, 3 \text{ cm}^2$$

Thus,

$$e^{(r^2/4\tau)-\gamma^2\tau} = 1.516 \qquad\qquad \sigma = \pm\, 0.02$$

The uncertainty is therefore small and acceptable and could be further reduced by improving the accuracy in τ and r. The error due to γ^2 is relatively small.

Since r is experimentally fixed and γ^2 is measured, the exponential correction factor is completely determined upon completion of the experiment described in the next section.

4.7 Experimental Apparatus and Procedure

The experiments to be described in this section were done in the exponential tank of the M.I.T. Heavy Water Lattice Facility. This facility and its use for single rod experiments have been described in detail in a previously published report (3).
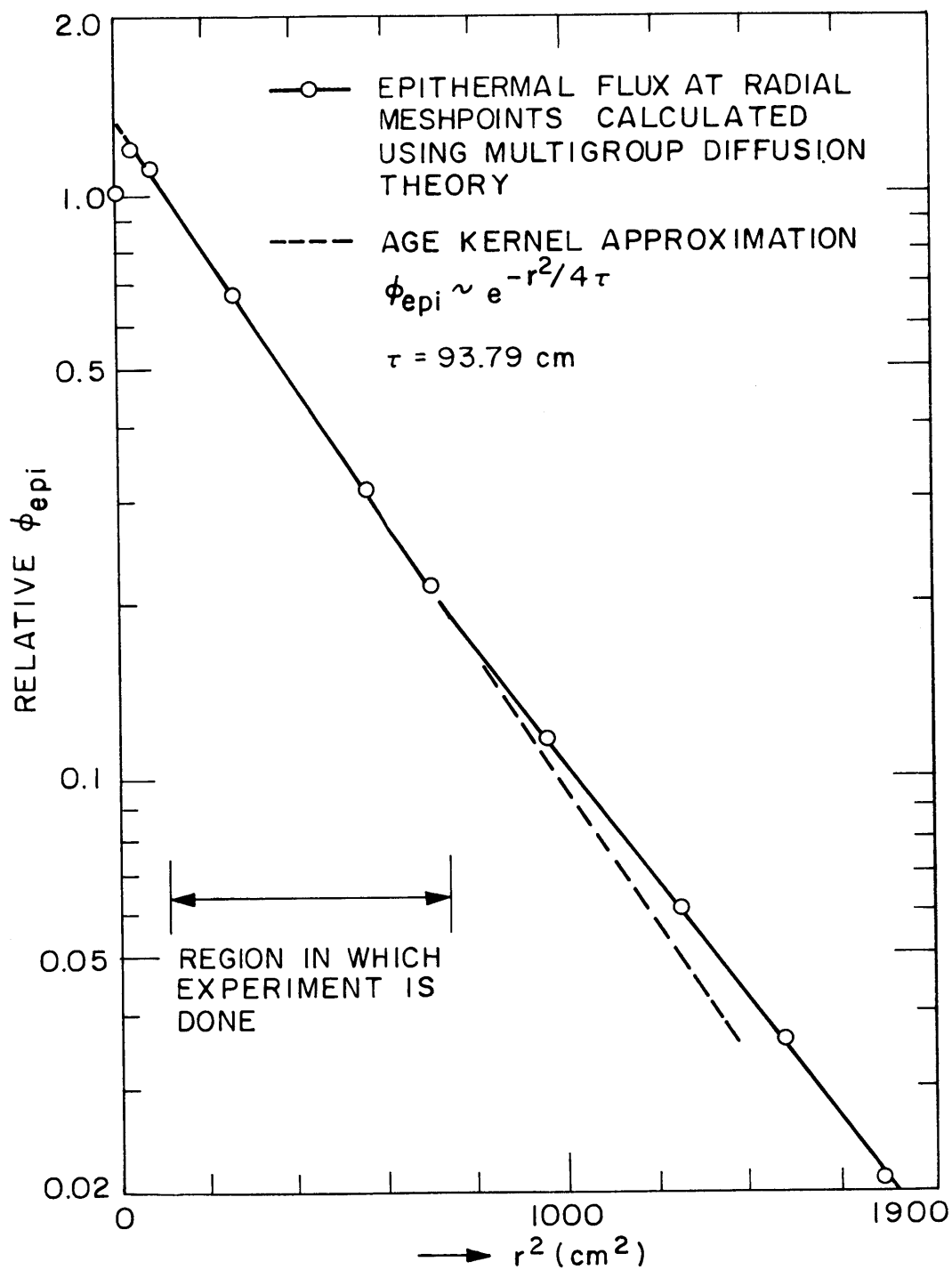
FIG. 4.3 COMPARISON OF AGE VS MULTIGROUP
EPITHERMAL FLUX NEAR GOLD RESONANCE

The method of suspending the fuel rods and foil holders in the present experiments is shown in Fig. 4.4a. The two foil holders were placed on opposite sides of the fuel rod, and thus two separate sets of data could be obtained from each experimental run. Each foil holder consists of two pieces; the shorter piece connects to the support girder, and the longer piece supports the gold foils. The two pieces were pinned together in a flexible joint so that the bottom pieces would hang vertically straight-down under their own weight.

The support girder is slotted every 1-1/8 inches to permit positive reproducible location of the foil holders at various radial positions.

Gold foils were used as activation detectors, since high purity gold can be readily obtained and because gold has high activation cross sections for both epithermal and thermal neutrons. The activation product Au^{198} emits a gamma ray of 0.411 Mev with a convenient 2.7-day half-life. Particularly important for the present purpose is the fact that gold has a large absorption resonance at 4.9 ev, which makes it ideal for cadmium ratio measurements in a weak epithermal flux field, as in the present application.

The gold foils used in these experiments were obtained from the Lattice Facility foil library. Each foil was 1/4 inch in diameter and about 11 mils thick. These foils had been previously punched, cleaned, weighed and ordered according to weight. The variation of weights among the foils was less than 1%. Such uniformity of foils weight is desirable because it makes certain corrections, such as gamma self-shielding, negligible.

Foils were mounted alternately in aluminum cans and cadmium boxes along the foil holders as shown in Fig. 4.4b. The "bare" foils were mounted in aluminum cans for two reasons. In the first place, this method of mounting prevented direct contact between the foils and the mylar mounting tape, thus precluding possible foil contamination or weight loss. Secondly, this technique insured local displacement of the D_2O moderator in a manner equivalent to that experienced with cadmium boxes. The use of the T-shaped aluminum foil holder, with the foils facing the fuel rod, reduced the flux
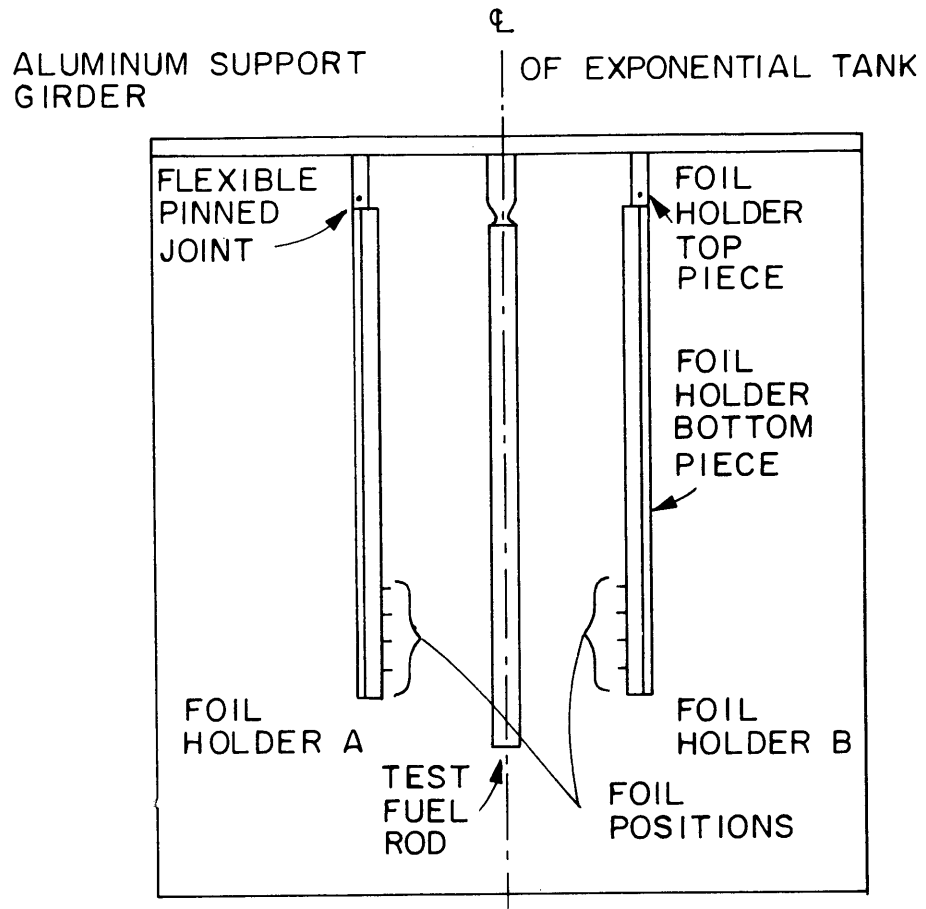
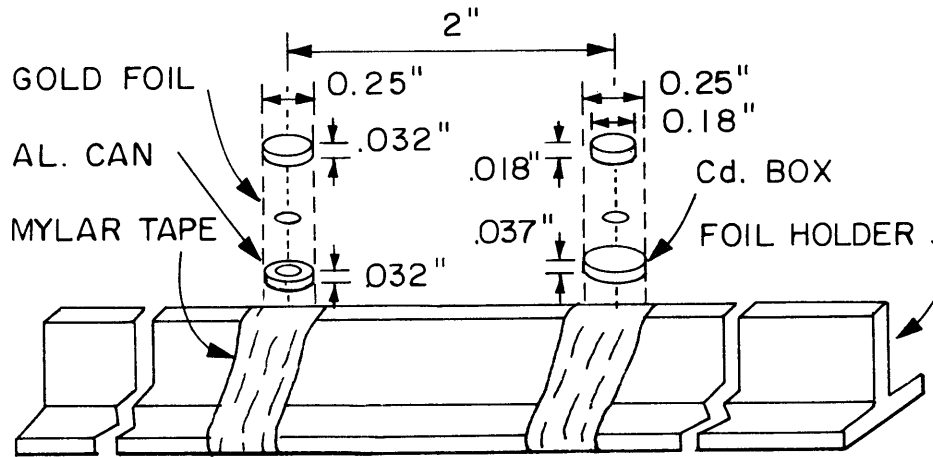FIG. 4.4a POSITION OF FOIL HOLDERS AND FUEL ROD IN EXPONENTIAL TANK

FIG. 4.4b MOUNTING OF FOILS

perturbation due to the holder while still retaining the required rigidity.

Standard NaI counting equipment was used with an automatic sample changer. The gold foils were gamma-counted for the 411-kev photopeak. Base line and window settings in the counting system were established by irradiating a sample foil, and single channel analyzer settings were selected that passed only the desired part of the spectrum.

Experimental runs were made on two fuel "elements": a "reference" rod of 1.01-inch-diameter, natural uranium metal and an "unknown" 7-rod cluster of 2% enriched, 0.431-inch-diameter, UO_2 fuel rods.

Foils were placed at a predetermined radial distance, r, from the fuel rod such that $\phi_{th}(r)$ was approximately equal to $\phi_{th}(a)$, thus minimizing the flux ratio correction factor. For each kind of fuel rod, two separate experimental runs were conducted; since four sets of cadmium ratio are measured per run, this gave a total of eight determinations per fuel type. The exposure time was fixed at about 10 hours in order to accumulate sufficient foil activity. Exact irradiation times were unimportant, since only relative activities were of interest. To insure good statistics, at least 10,000 counts were collected on each foil. The bare foils, whose activities were too high to count immediately after irradiation, were allowed to cool for two or three days to minimize counter dead time corrections. Methods of analyzing and correcting the data are discussed in the next section.

4.8 Data Analysis and Results

Raw data, as printed out by the automatic counting apparatus, was reduced to the form of counts per minute per milligram for each foil irradiated, corrected for background, foil weight, counting time, dead time and decay during counting.

Since the flux has an exponential distribution in the axial direction, the ratio of the activities of the two bare foils on a foil holder is $e^{2\gamma\Delta Z}$, where $2\Delta Z$ is the separation distance between the bare foils. Each bare foil was at a distance ΔZ (2 inches) above its paired

cadmium-covered foil. Therefore, a multiplicative correction factor of $e^{\gamma \Delta Z}$ must be applied to the activity of each bare foil in order to correct for the height difference between the bare and cadmium-covered foils in a pair. It should also be noted that the quantity γ can be determined from the two bare foil activities.

The comparison method for determination of η was discussed in Section 4.4. Equation 4.13 gives the ratio η/η_{ref} in terms of ratios of Γ's, fluxes and cadmium ratios between the unknown and reference rods. In the present work, the reference was chosen to be the 1-inch-diameter, natural uranium rod, and η_{ref} was defined to be 1.37, based upon the experimental and theoretical results obtained by Donovan (<u>1</u>).

The previously described experiments were carried out on both the standard and the unknown. Table 4.1 summarizes the results. In addition, other necessary information required to obtain η from Eq. 4.13 is also given, including the foil position r, the thermal constant Γ, the calculated flux ratio and the measured cadmium ratio.

The experimental result, $\eta = 1.77 \pm 0.02$, is in good agreement with the experimental result obtained by Donovan for a single, 2% enriched rod (1.74 ± 0.09). Correction of the latter value for the small additional fast fission effect due to clustering would further improve agreement, but this does not appear warranted in view of the larger experimental uncertainties.

4.9 Summary and Conclusions

While it is premature to draw definitive conclusions based upon a single test case, the proposed method for experimental determination of η appears to be feasible; it remains to be seen whether the experimental uncertainty can be sufficiently reduced. The foil activation techniques required are well established in the field of experimental reactor physics and are easy to master and apply. The theoretical corrections are small in magnitude.

In particular, the ratio $\dfrac{\phi_{th}(r)}{\phi_{th}(a)}$ is not a strong function of radius in the region where measurements are to be made; thus errors due to foil holder positioning are small. In the case of a one-inch natural

TABLE 4.1

Experimental Results for η of 7-Rod Cluster

Experimental Runs	r cm	Γ cm^{-1}	$\dfrac{\phi(r)}{\phi(a)}$	R_{cd}*	η
Natural Uranium (Standard)	15.7	0.9404	1.245	84.02 ± 0.85	1.37 (Defined)
2% Enriched 7-Rod Cluster (Unknown)	18.5	0.805	0.954	56.23 ± 0.68	1.77 ± 0.02

*Note:- Error shown is SDM of experimental results.

uranium rod, the maximum ratio of $\dfrac{\phi_{th}(r)}{\phi_{th}(a)}$ occuring at x, is only about 1.3. To keep the thermal flux ratio correction small, r can be chosen so that $\phi_{th}(r)$ is approximately equal to $\phi_{th}(a)$. Of course, r could even be chosen such that $\phi_{th}(r) = \phi_{th}(a)$ exactly, and the flux ratio correction factor would be unity. But this is not necessary since $\dfrac{\phi_{th}(r)}{\phi_{th}(a)}$ can always be evaluated.

On the other hand, there exist certain disadvantages in this method, the most important of which is the dependence on a con-current measurement of Γ: one needs a very accurate Γ measurement since η is directly proportional to Γ.

During the coming year, additional applications of the subject method will be performed in order to further evaluate its utility.

4.10 References

(1) R. Donovan, Measurement of Heterogeneous Parameters, Chapter 8 in "Heavy Water Lattice Project Final Report," MIT-2344-12, MITNE-86, September 30, 1967.

(2) R. Simms, I. Kaplan, T. J. Thompson and D. D. Lanning, "Analytical and Experimental Investigations of the Behavior of Thermal Neutrons in Lattices of Uranium Metal Rods in Heavy Water," NYO-10211, MITNE-33, October 1963.

(3) E. E. Pilat, M. J. Driscoll, I. Kaplan, T. J. Thompson, "The Use of Experiments on a Single Fuel Element to Determine the Nuclear Parameters of Reactor Lattices," MIT-2344-10, MITNE-81, February 1967.

5. PULSED NEUTRON AND BUCKLING METHODS

N. R. Ortiz and T. C. Leung

5.1 Introduction

It is well known that established pulsed neutron techniques give useful information about nuclear properties when applied to complete lattices. Much less work has been done on the application of pulsed neutron methods to single fuel elements. Previous experimental work in this area by Kennedy [1] at M.I.T. had proven inconclusive due to the lack of sufficiently sensitive data analysis techniques. Recently, however, Papay [2] has greatly improved pulsed neutron data analysis methods, so that a re-examination of this approach appeared worthwhile.

Thus, in this chapter, η will be expressed in terms of the fractional decrease in time decay constant $\frac{\Delta\lambda}{\lambda}$ due to insertion of a single fuel element into a tank of moderator. The experiments performed by Kennedy [1] will be re-analyzed using the MØMLSQ computer program developed by Papay [2] to obtain $\Delta\lambda$, and thus η. Finally, an equivalence relation between pulsed neutron and axial buckling measurements will be derived and evaluated.

5.2 Relation of $\Delta\lambda$ to η

Simple perturbation theory gives the fractional decrease in λ, due to insertion of a fuel element [1]:

$$\frac{\Delta\lambda}{\lambda} = \frac{\lambda - \lambda'}{\lambda} = \frac{(\nu\Sigma_f - \Sigma_a)_{rod}}{(\Sigma_a + DB^2)_{D_2O}} \left(\frac{\pi a^2}{\pi R^2}\right) \frac{1}{J_1^2(\nu_o)}, \qquad (5.1)$$

where

λ = time decay constant in pure moderator, D_2O,

λ' = time decay constant with a fuel element in the D_2O,

Σ_f = macroscopic fission cross section of the fuel rod,

Σ_a = macroscopic absorption cross section of the fuel rod, or moderator, as noted,

ν = number of neutrons emitted per fission,

a = radius of fuel element,

D = diffusion coefficient of the moderator,

R = extrapolated radius of the exponential tank,

ν_o = 2.405 .

Denoting η_p as the prompt value of η, and β as the delayed neutron fraction:

$$\nu\Sigma_f - \Sigma_a = (\eta_p - 1)\Sigma_a , \tag{5.2}$$

where

$$\eta_p = \eta(1-\beta) . \tag{5.3}$$

Applying heterogeneous theory for a line absorber, we can match neutron losses with the weak central absorber of perturbation theory:

$$\left(\eta_p\, e^{-B_z^2 \tau_{th}} - 1\right) \frac{\phi(a)}{\Gamma} = (\nu\Sigma_f - \Sigma_a)\pi a^2 \phi_o . \tag{5.4}$$

In other words, the net absorptions per unit unperturbed flux, ϕ_o, is:

$$\left(\eta_p\, e^{-B_z^2 \tau_{th}} - 1\right) \frac{\phi(a)}{\Gamma}\frac{1}{\phi_o} = (\nu\Sigma_f - \Sigma_a)\pi a^2 . \tag{5.5}$$

The factor $e^{-B_z^2 \tau_{th}}$ in Eqs. 5.4 and 5.5 accounts for the neutron non-leakage probability during slowing down to thermal energy in the axial direction. (The radial leakage probability is negligible for the centrally located line source.) Introducing Eqs. 5.2 and 5.5 into Eq. 5.1:

$$\frac{\Delta\lambda}{\lambda} = \frac{\left(\eta_p\, e^{-B_z^2 \tau_{th}} - 1\right)}{\Gamma}\left(\frac{\phi(a)}{\phi_o}\right)\frac{1}{(\Sigma_a + DB^2)\pi R^2 J_1^2(\nu_o)} . \tag{5.6}$$

Solving Eqs. 5.3 and 5.6 for η gives:

$$\eta = e^{B_z^2 \tau_{th}}\left[(1+\beta) + \pi R^2 J_1^2(\nu_o)\left(\frac{\phi_o}{\phi(a)}\right)(\Sigma_a + DB^2)\Gamma\,\frac{\Delta\lambda}{\lambda}\right] . \tag{5.7}$$

The flux ratio in Eq. 5.7 is given by the following approximate relation derived by applying diffusion theory in the case of a weakly absorbing moderator:

$$\frac{\phi_o}{\phi(a)} = \left\{ \frac{\ln \frac{1}{\alpha a}}{2\pi D\Gamma} + 1 \right\} ; \tag{5.8}$$

thus,

$$\eta = e^{B_z^2 \tau_{th}} \left\{ 1 + \beta + \pi J_1^2(\nu_o) \left[\Gamma + \frac{\ln \frac{1}{\alpha a}}{2\pi D} \right] [\Sigma_a + DB^2] R^2 \frac{\Delta\lambda}{\lambda} \right\} . \tag{5.9}$$

Equation 5.9 is the desired relation for η in terms of $\Delta\lambda$ and other known characteristics of the exponential tank and fuel rod. The value of λ for D_2O in the exponential tank was measured by D. Kennedy (1) to be 630 sec^{-1}. Thus, the present task is to find $\Delta\lambda$. This is to be discussed in the next section.

5.3 Evaluation of $\Delta\lambda$

The fractional decrease in time decay constant, $\Delta\lambda$, cannot be obtained accurately by simply taking the difference of two independently determined time decay constants. However, the technique of direct comparison between two data sets used by L. Papay (2) in his MØMLSQ computer program permits direct determination of $\Delta\lambda$ in a systematic manner.

The procedure for determining $\Delta\lambda$ is briefly reviewed here. For a more thorough discussion, see reference 2. The subject method assumes the count rate data to be represented by an exponential term plus a background b' as follows:

$$M(t) = A e^{-\lambda t} + b' \tag{5.10}$$

or

$$Y(t) = M(t) - b' = A e^{-\lambda t} . \tag{5.11}$$

For two separate runs, (1) and (2):

$$Y_1(t) = A_1 e^{-\lambda_1 t} , \tag{5.12}$$

$$Y_2(t) = A_2 e^{-\lambda_2 t} . \tag{5.13}$$

If Eq. 5.12 is divided by Eq. 5.13, there results

$$Y(t) = A e^{-\Delta\lambda t},$$ (5.14)

where $A = \dfrac{A_1}{A_2}$ = constant for any two sets of data and $\Delta\lambda = \lambda_1 - \lambda_2$.
It can be shown that $\Delta\lambda$ can be expressed as a function of the 0th,
1st and 2nd moments by

$$\Delta\lambda = \frac{2M_1 - tM_0}{M_2 - tM_1}$$ (5.15)

where

$$M_0 = \sum_i C_i$$

$$M_1 = \sum_i C_i (t_i)_{eff}$$

$$M_2 = \sum_i C_i (t_i)^2_{eff}$$

$$C_i = \frac{C_i^1}{C_i^2} = \frac{\text{count rate in the ith channel for the 1st data set}}{\text{count rate in the ith channel for the 2nd data set}}$$

$(t_i)_{eff}$ = effective time from the beginning of the data
analysis to the centroid of the ith channel

$(t_i)^2_{eff}$ = effective squared time from the beginning of the data
analysis to the centroid of the ith channel.

The procedure for determining the "best" value of $\overline{\Delta\lambda}$ is to per-
form a least square fit of the values of $\Delta\lambda_i$ as the initial channel used
in the analysis is varied for an arbitrarily fixed final channel. Thus,
the least square fit is based on the equation

$$\Delta\lambda_i = a + b(\Delta N_i),$$ (5.16)

where ΔN_i is the number of channels used in the ith evaluation, and
a and b are determined from the least squares fit and have the form

$$b = \frac{\overline{\Delta\lambda\Delta N} - \overline{\Delta\lambda}\,\overline{\Delta N}}{(\overline{\Delta N^2}) - (\overline{\Delta N})^2},$$ (5.17)

$$a = \overline{\Delta\lambda} - b\,\overline{\Delta N}. \tag{5.18}$$

The "best" fit of the data occurs when b = 0. The output of the M∅MLSQ computer code is a set of values for $\overline{\Delta\lambda}$ and b for an arbitrarily fixed final channel. The set of values for $\overline{\Delta\lambda}$ and b will vary slightly as the final channel used in the least square analysis is varied. A typical plot of $\overline{\Delta\lambda}$ and b for different arbitrarily fixed final channels is given in Fig. 5.1. Multiple values of $\overline{\Delta\lambda}$ can be determined graphically by locating those points where b = 0 on the b versus final channel plot (for example, point A in Fig. 5.1) and then reading off $\overline{\Delta\lambda}$ for the same abscissa on the $\overline{\Delta\lambda}$ versus final channel plot (point B in Fig. 5.1). The reported value of $\overline{\Delta\lambda}$ is the average of the values of $\overline{\Delta\lambda}$ determined at each point where b = 0.

5.4 Results of Pulsed Neutron Experiments

Pulsed neutron experiments were performed by D. Kennedy and L. Papay at M.I.T. Table 5.1 lists the experimental runs performed. The change in the prompt neutron decay constant, $\Delta\lambda$, due to insertion of the fuel rod, was evaluated by the present authors using the M∅MLSQ computer program as described in the previous section. The results are given in Table 5.2. One notes immediately that the results are not consistent with the theory presented in Section 5.2: since $\Delta\lambda$ decreases (becomes more negative) as enrichment is increased, Eq. 5.9 would imply that η also decreases. Also note, however, that the probable errors are of the same order as the results.

In any case, a sample calculation will be presented. The following values for the M.I.T. exponential tank and a 1-inch-diameter, natural uranium fuel rod will be substituted in the expression for η, Eq. 5.9:

$$\Gamma = 0.94 \text{ cm}^{-1}$$
$$\beta = 0.0078$$
$$D = 0.804 \text{ cm}$$
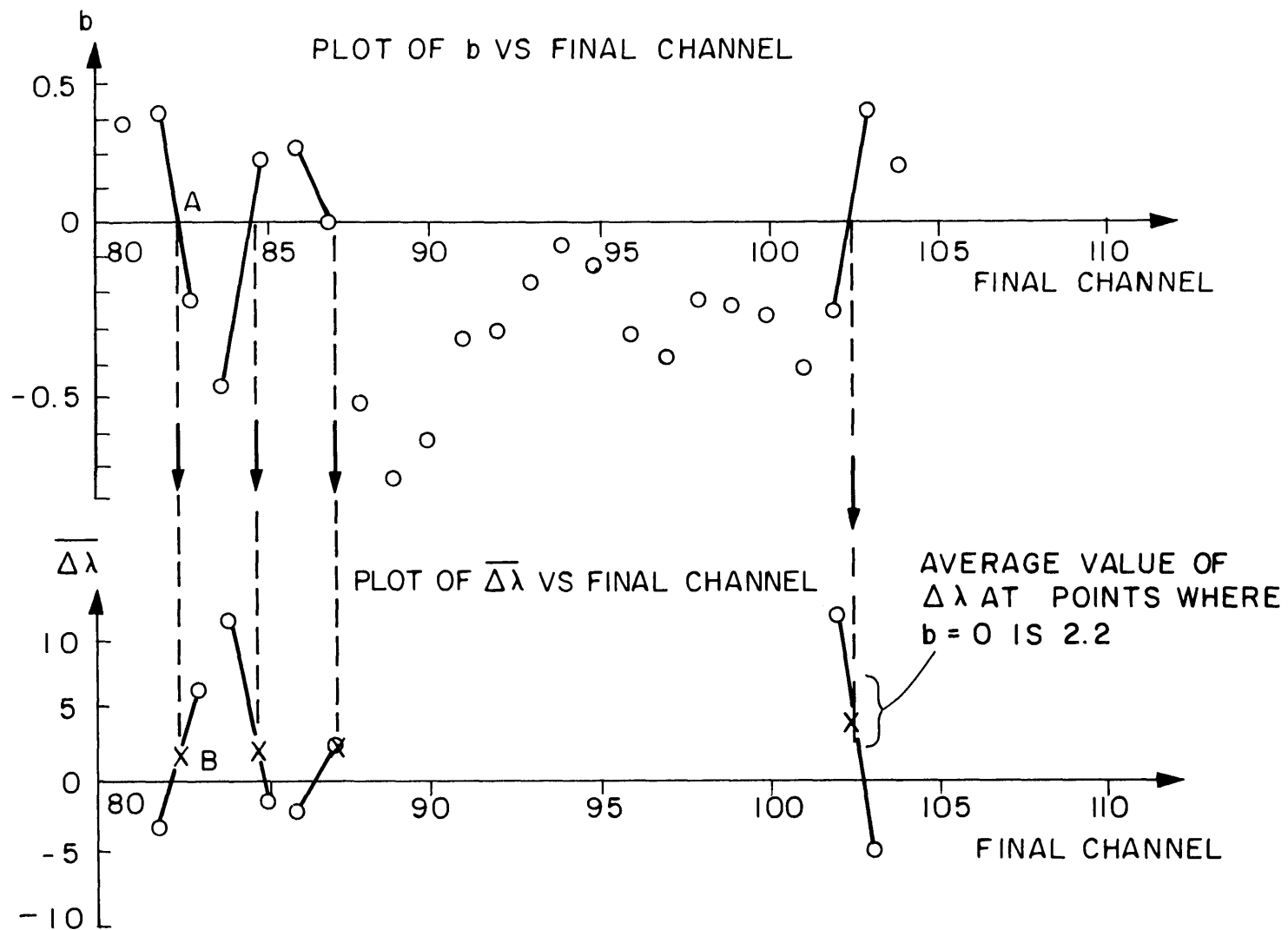$$\tau = 122 \text{ cm}$$
$$a = 1.27 \text{ cm}$$

FIG. 5.1 GRAPHICAL DETERMINATION OF $\overline{\Delta\lambda}$ AT b = O (THE DATA IS TAKEN FROM RUNS 2 AND 4)

TABLE 5.1

Single Element Pulsed Neutron Experiments

Run Number	Type of Run	Remarks	Experimenter
1, 2	Moderator	D_2O	D. Kennedy
3, 4	Single rod in moderator	1-inch natural uranium	D. Kennedy
5, 6	7-rod cluster in moderator	1% enriched, UO_2	D. Kennedy
7	Moderator	D_2O	L. Papay
8, 9	19-rod cluster in moderator	2% enriched, UO_2	L. Papay

TABLE 5.2

Average Values of $\overline{\Delta\lambda}$

$$\lambda_1 - \lambda_2 = 0$$

$$\lambda_5 - \lambda_6 = -8.0$$

$$\lambda_3 - \lambda_4 = -8.2$$

$$\lambda_8 - \lambda_9 = 12.0$$

$$\left.\begin{array}{l} \lambda_1 - \lambda_3 = 14.0 \\[2mm] \lambda_2 - \lambda_4 = 2.2 \end{array}\right\} \text{ Av. } 7.1 \pm 8.0$$

Change in $\overline{\Delta\lambda}$ due to insertion of 1-inch natural uranium rod

$$\left.\begin{array}{l} \lambda_1 - \lambda_5 = -6.4 \\[2mm] \lambda_2 - \lambda_6 = -7.2 \end{array}\right\} \text{ Av. } -6.8 \pm 8.2$$

Change in $\overline{\Delta\lambda}$ due to insertion of 7-rod cluster

$$\left.\begin{array}{l} \lambda_7 - \lambda_8 = -14.0 \\[2mm] \lambda_7 - \lambda_9 = -32.0 \end{array}\right\} \text{ Av. } -23.2 \pm 12$$

Change in $\overline{\Delta\lambda}$ due to insertion of 19-rod cluster

$$R = 47.5 \text{ cm}$$

$$\Sigma_a = 1.24 \times 10^{-4} \text{ cm}^{-2}$$

$$\pi J_1^2(\nu_o) = 0.85$$

$$B_g^2 = \left(\frac{\pi}{H}\right)^2 + \left(\frac{\nu_o}{R}\right)^2 = 31 \times 10^{-4} \text{ cm}^{-2}$$

$$\ln \frac{1}{\alpha a} = \ln \left(\frac{R}{\nu_o a}\right)$$

to give

$$\eta = [1.067] \left[1.0078 + 4.84(0.94 + 1.07)\frac{\Delta\lambda}{\lambda} \right].$$

From Kennedy's data (1), $\lambda = 630$ for the pure moderator case. After the insertion of the 1-inch-diameter, natural uranium rod, $\Delta\lambda = 7.0 \pm 8.0$ (from Table 5.2), and thus

$$\eta \cong 1.2 \pm 0.2 .$$

This η value for the natural uranium rod is about 15% lower than the accepted value, $\eta = 1.37$.

Data for the clustered rods are inconsistent with the theory since the measured $\Delta\lambda$ decreases with enrichment. The reason for the discrepancy is not clear; one possibility is that the position of the detector in the experiments was such that it picked up higher mode decay constants. To resolve this problem, it is clear that either a major experimental evaluation would be necessary or an alternate procedure would have to be adopted. Analytical and numerical studies were therefore initiated with the results reported in the following sections.

5.5 Equivalence of Pulsed Neutron and Buckling Experiments

The fundamental mode decay constant describing neutron die-away for a pulsed neutron experiment performed on a large sub-critical assembly is given by (3):

$$\lambda = \overline{v\Sigma_a} + \overline{vD}\, B_g^2 - \overline{v\Sigma_a}(1-\beta)\, k_\infty(F(B^2)) , \qquad (5.19)$$

where

$F(B^2)$ = fast nonleakage probability,

β = delayed neutron fraction,

B_g^2 = geometric buckling = $B_r^2 + B_z^2$ for a cylinder.

If the same assembly is used in a classical exponential experiment,

$$D\gamma^2 = \Sigma_a + DB_r^2 - \Sigma_a(1-\beta)\, k_\infty\, F(B^2)\,, \tag{5.20}$$

where

γ = exponential die-away constant characterizing the axial flux dependence.

Now define a reference nonmultiplying state ($k_\infty \equiv 0$) denoted by the subscript "o". Then one can show from Eqs. 5.19 and 5.20 that changes in λ and γ^2 are related by:

$$\frac{\Delta\lambda}{\lambda_o} = \frac{\Delta\gamma^2}{\gamma_o^2 + B_{z,o}^2}\,, \tag{5.21}$$

provided that the average neutron velocity and diffusion coefficient do not change appreciably between the two states in question.

Equation 5.21 is quite interesting because it suggests that insofar as the present application is concerned, axial buckling measurements can be substituted for pulsed neutron experiments. Moreover, axial buckling measurements can be done far more rapidly, hence more economically, and with equal if not better accuracy.

Because of the importance of this conclusion to the future course of single rod experimentation, additional work was carried out to validate the applicability of the results. Some previously available experiments were re-analyzed, and in addition a number of numerical experiments were performed using the ANISN code described in Chapter 7.

5.6 Analysis of Buckling Experiments

Malaviya (4) reports both pulsed neutron and buckling data for two cases of interest: thermally black (cadmium) control rods of various radii were inserted along the axis of an exponential assembly,

first containing only pure D_2O moderator, and then into a multiplying lattice. His data are plotted in Fig. 5.2. As predicted by Eq. 5.21, the relation between λ and γ^2 is linear. The intercept differs for the two sets of data because two different size tanks (3- and 4-foot diameter) were used. In Fig. 5.3 the same data are plotted in another form, namely, as $\frac{\Delta\lambda}{\lambda_o}$ versus $\frac{\Delta\gamma^2}{\gamma_o^2 + B_z^2}$. As is evident, Eq. 5.21 is confirmed by the data.

Finally, the data were used to test Eq. 5.9 in the limiting case $\eta = 0$, when the following rearrangement is valid:

$$\left(\frac{-\Delta\lambda}{\lambda}\right)^{-1} = C \cdot \left[\frac{(\Sigma_a + DB^2)R^2}{(1+\beta)}\right] \cdot \left[\Gamma_b + \frac{\ln 1/\alpha_o a}{2\pi D}\right], \qquad (5.22)$$

where

C = constant, predicted to have the value $\pi J_1^2(\nu_o) = 0.85$ according to perturbation theory;

Γ_b = thermal constant for a black rod, which can be calculated from the extrapolation distance, d, for the black rod of radius a:

$$\Gamma_b = \frac{d}{2\pi a D} .$$

The following parameter values are appropriate for the subject experiment:

$\beta = 0.0078$

$R = 47.5$ cm

$\alpha_o = 0.0506$ cm^{-1}

$\Sigma_a + DB^2 = 0.0026$ cm^{-2}

Substitution of these data into Eq. 5.22 permits determination of C from the slope of a plot of $\left(\frac{-\Delta\lambda}{\lambda}\right)^{-1}$ versus $\left[\Gamma_b + \frac{\ln 1/\alpha_o a}{2\pi D}\right]$. The result was found to be $C = 0.86$, in good agreement with the predicted value, $C = 0.85$.

In Section 5.5, the relation between $\Delta\lambda$ and $\Delta\gamma^2$ was derived using cross sections homogenized over the exponential facility. Therefore, the preceding experimental verification of the subject relations for a
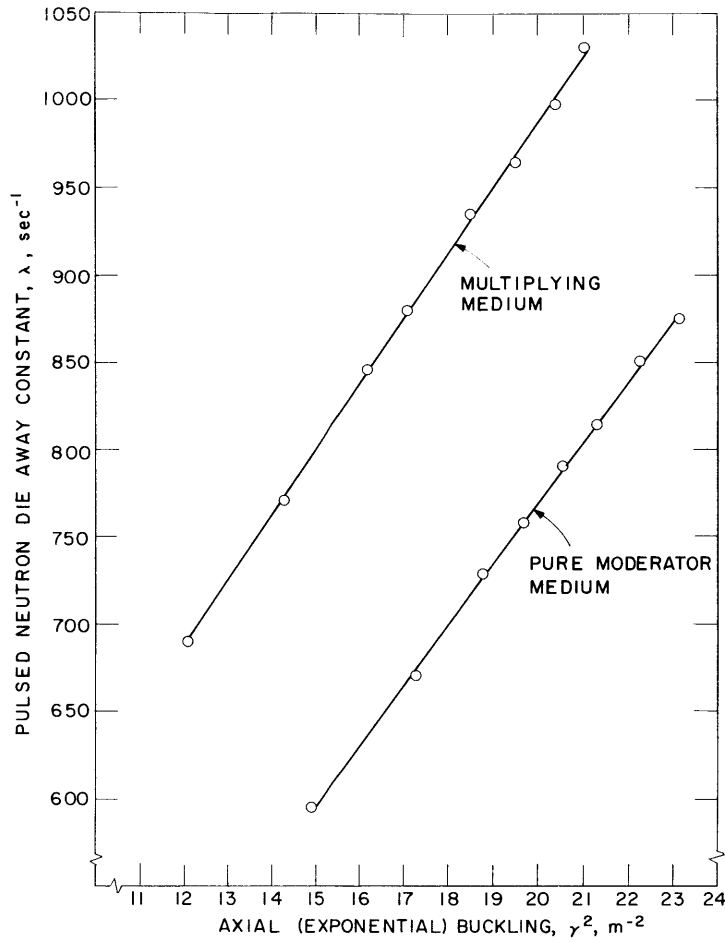
FIG. 5.2 DIRECT COMPARISON OF PULSED NEUTRON AND AXIAL
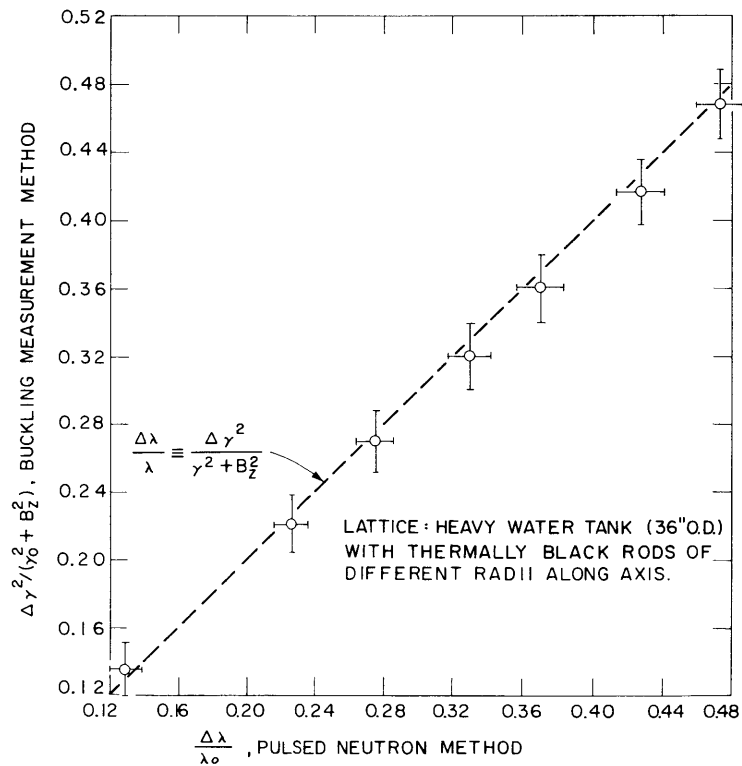BUCKLING EXPERIMENTS

FIG. 5.3 DIFFERENTIAL COMPARISON OF PULSED NEUTRON EXPERIMENTS
AND BUCKLING MEASUREMENTS

highly heterogeneous case is of particular importance. In order to obtain additional evidence, a series of numerical calculations were also performed.

5.7 Numerical Studies

Because no experimental data exist giving both pulsed neutron and buckling data on identical single fuel rod assemblies, a series of multigroup calculations was performed to verify the predicted linear relation between λ and γ^2 for the case in which $\eta > 0$. The ANISN computer code was used for this work, as is described in detail in Chapter 7 of this report. The approach employed was to calculate the die-away constant λ for a simulated pulsed neutron experiment and then to calculate the axial buckling, γ^2, for the same configuration used as an exponential experiment. Figure 5.4 is a plot of the results obtained from these calculations. The linear results show that the extension to multiplying test rods poses no essential difficulty.

5.8 Summary and Conclusions

The analyses reported in this chapter clearly show that present pulsed neutron methods are not capable of extracting meaningful data from single rod experiments. However, for the present purpose, namely, the determination of η, the theoretical equivalence of the pulsed neutron and axial buckling experiment allows one to substitute the latter method. During the coming year, single rod experiments will be carried out in the M.I.T. exponential facility in order to test the practical utility of the axial buckling method. Data will be analyzed by differential methods similar to those discussed in Section 5.3, and η will be determined relative to a known standard.
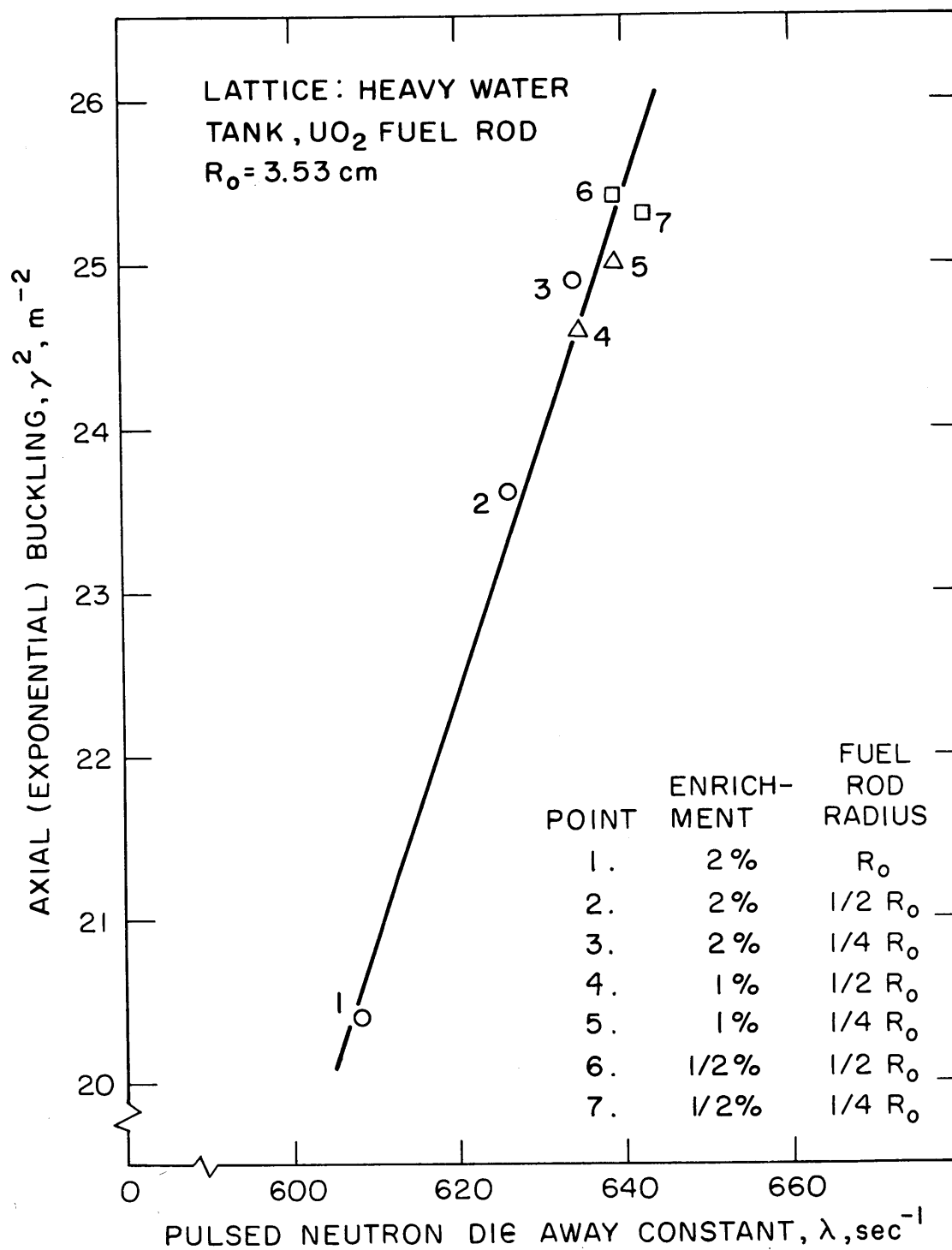
FIG. 5.4 COMPARISON OF PULSED NEUTRON AND AXIAL
BUCKLING NUMERICAL CALCULATIONS

5.9 <u>References</u>

(1) Kennedy, D., Pulsed Neutron Measurements on Single Fuel Elements, Chapter 13 in "Heavy Water Lattice Project Final Report," MIT-2344-12, MITNE-86, September 30, 1967.

(2) Papay, L. T., "Coolant Void Reactivity Effects in Heavy Water Moderated, Low Enriched Uranium Rod Clusters," ScD Thesis, M.I.T., October 1968.

(3) Bliss, H. E., I. Kaplan, and T. J. Thompson, "Use of a Pulsed Neutron Source to Determine Nuclear Parameters of Lattices of Partially Enriched Uranium Rods in Heavy Water," MIT-2344-7, MITNE-73, September 1966.

(4) Malaviya, B. J., I. Kaplan, T. J. Thompson, and D. D. Lanning, "Studies of Reactivity and Related Parameters in Slightly Enriched Uranium Heavy Water Lattices," MIT-2344-1, MITNE-49, May 1964.

6. DETERMINATION OF THE EPITHERMAL PARAMETER, A

Y.-M. Lefevre

6.1 Introduction

The parameter A is defined to be the epithermal absorptions per unit slowing-down density. It is closely related to the more familiar resonance escape probability, p:

$$p = 1 - A/V, \tag{6.1}$$

where V is the cross-section area of the unit cell.

Donovan (1) has shown how A can be determined from fuel rod integral parameters such as ρ_{28}. His method requires in-rod foil irradiations, however, which is not compatible with a major objective of the present work — namely, the use of external measurements to avoid the necessity for exposing fuel containing plutonium or fission products. Therefore, it has been necessary to evaluate alternate approaches for determination of A.

6.2 Numerical Calculations

The close relation between A and the resonance capture probability, (1-p), as expressed in Eq. 6.1, suggested that A could be related to the ratio of epithermal fluxes below and above the major U-238 and U-235 capture resonances. In order to test this hypothesis, a series of numerical calculations was performed using the ANISN code described in Chapter 7.

The ANISN code was used to compute 16 group flux traverses external to a centrally located, single fuel element immersed in D_2O moderator in a 3-foot-diameter exponential tank. The element's diameter was varied to cover the range of current interest ($10 \leqslant A \leqslant 100$ cm^2).

Two of the epithermal flux groups were then chosen to evaluate

the proposed experiment for measurement of A. The following considerations governed the choice of groups:

(a) Resonance absorbers must be available to permit experimental realization of the method. For all practical purposes, this limits consideration to a dozen resonance absorbers and their corresponding energies (2).

(b) The lower group must be below the large U-238 resonance at 6.7 ev but above the cadmium cutoff at about 0.4 ev.

(c) The upper energy group must be above the lower four U-238 resonances, which typically account for over 90% of the resonance absorption. On the other hand, because the measurement is being made on a single element, the energy should be low enough to avoid including the effect of first-flight captures in the rod. Price (3) has shown that as much as 20% of the epithermal captures can be first-flight for isolated fuel elements, but that the percentage is far smaller in full lattices. Another reason for choosing an energy corresponding to multiply-collided neutrons is the potential applicability of age theory.

The above requirements led to choice of molybdenum and gold as the two resonance absorbers (resonances at 480 ev and 4.9 ev, respectively) and to selection of the corresponding groups 9 and 12 in the ANISN code ($100 \leq E \leq 550$ ev and $3 \leq E \leq 10$ ev, respectively). The epithermal flux ratio, R, was then defined as the ratio of group-12 to group-9 fluxes. Figure 6.1 shows plots of R versus radial distance from the center of fuel rods of various diameters. It can be seen that beyond about 10 cm from the rod the flux ratio profiles are parallel. This suggested that experimental determinations of R can be performed at approximately 20 cm from the exponential tank center line in order to avoid perturbations in flux shape due only to differences in rod size.

The next step was to examine the variation of the epithermal flux ratio at r = 20 cm from the rod, R(20), with the epithermal absorption parameter, A. The value of A was calculated for each case in the
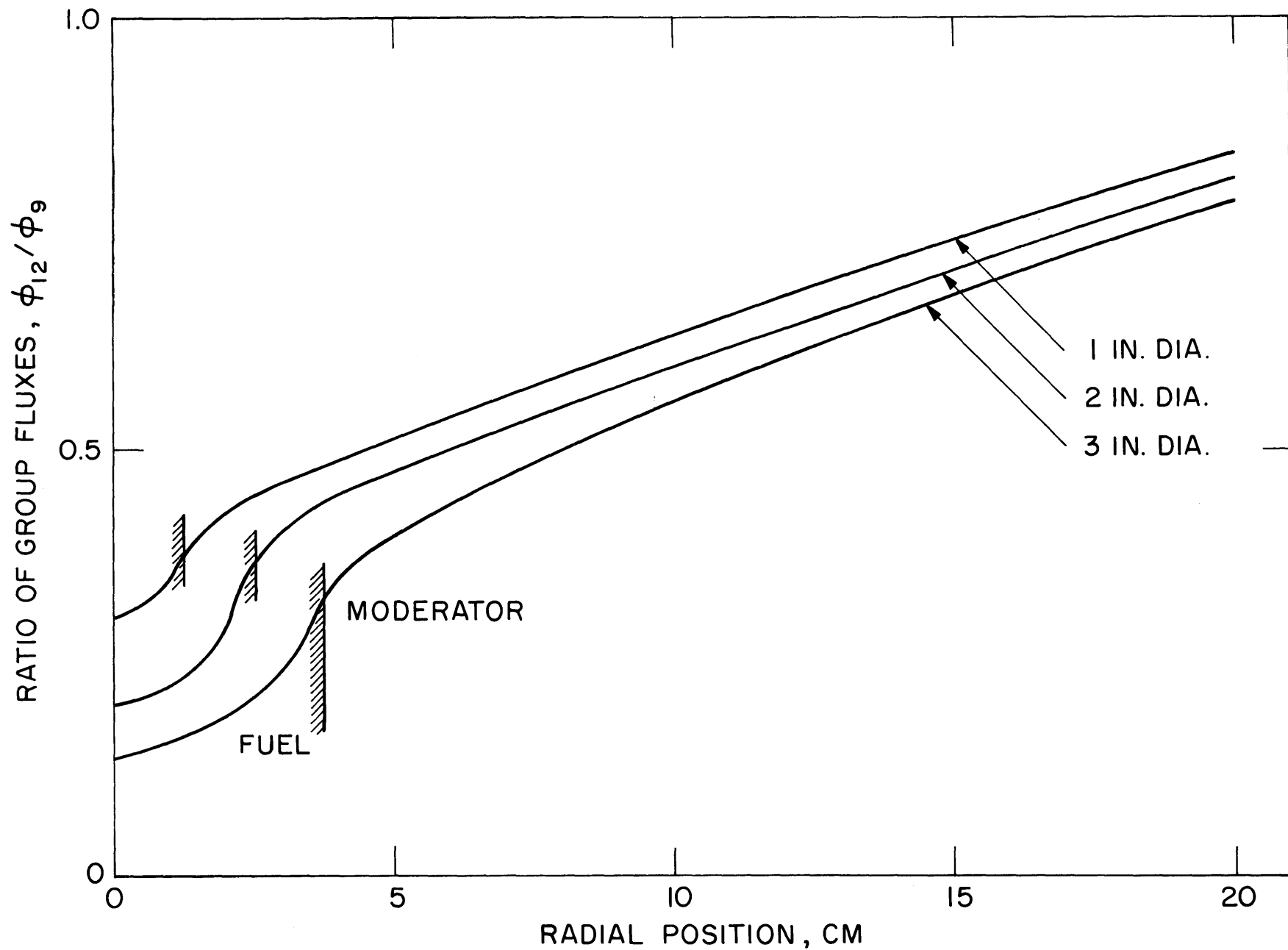
FIG. 6.1   EPITHERMAL FLUX RATIO AS A FUNCTION OF DISTANCE FROM NATURAL URANIUM METAL RODS

following manner.

Donovan ([1]) has derived the following relation between A and the effective resonance integral for a full lattice:

$$A = \frac{N \cdot ERI \cdot V_f}{\xi \Sigma_s} , \qquad (6.2)$$

where

$\xi \Sigma_s$ = slowing-down power of moderator ≈ 0.18 cm^{-1},

N, V_f = atomic concentration and cross-section area of fuel.

Since U-238 and U-235 are the predominant resonance absorbers, the total A value is given by:

$$A = [N^{28} \cdot ERI^{28} + N^{25} RI_\infty^{25}] \frac{V_f}{\xi \Sigma_s} , \qquad (6.3)$$

where resonance self-shielding in the dilute U-235 has been neglected. Seth ([5]) and others have examined this approximation and found it valid; therefore, one can take RI_∞^{25} = 420 barns ([6]). Equation 6.3 then simplifies to:

$$A = \frac{N^{28} V_f ERI^{28}}{\xi \Sigma_s} \cdot \left[1 + \frac{\epsilon}{1 - \epsilon} \cdot \frac{420}{ERI^{28}} \right] , \qquad (6.4)$$

where ϵ is the fuel rod enrichment.

Equation 6.4 was used to calculate values of A for each fuel type studied. Hellstrand's correlation was used to evaluate the effective resonance integral ([7]):

$$ERI^{28} = 4.25 + 26.8 \sqrt{\frac{S}{M}} \text{ barns,} \qquad (6.5)$$

where S/M = surface-to-mass ratio for fuel rod.

It is important to note that Eqs. 6.1 through 6.5 apply to resonance absorption in a full lattice, while the subject experiment is to be performed on a single rod. In a full lattice the resonance flux, $\phi(u)$, is essentially constant, while at a single rod, $\phi(u)$ is proportional to $1/\tau(u)$, as predicted by age theory and as confirmed by the SRA code (see Chapter 7) calculations shown in Fig. 6.2.
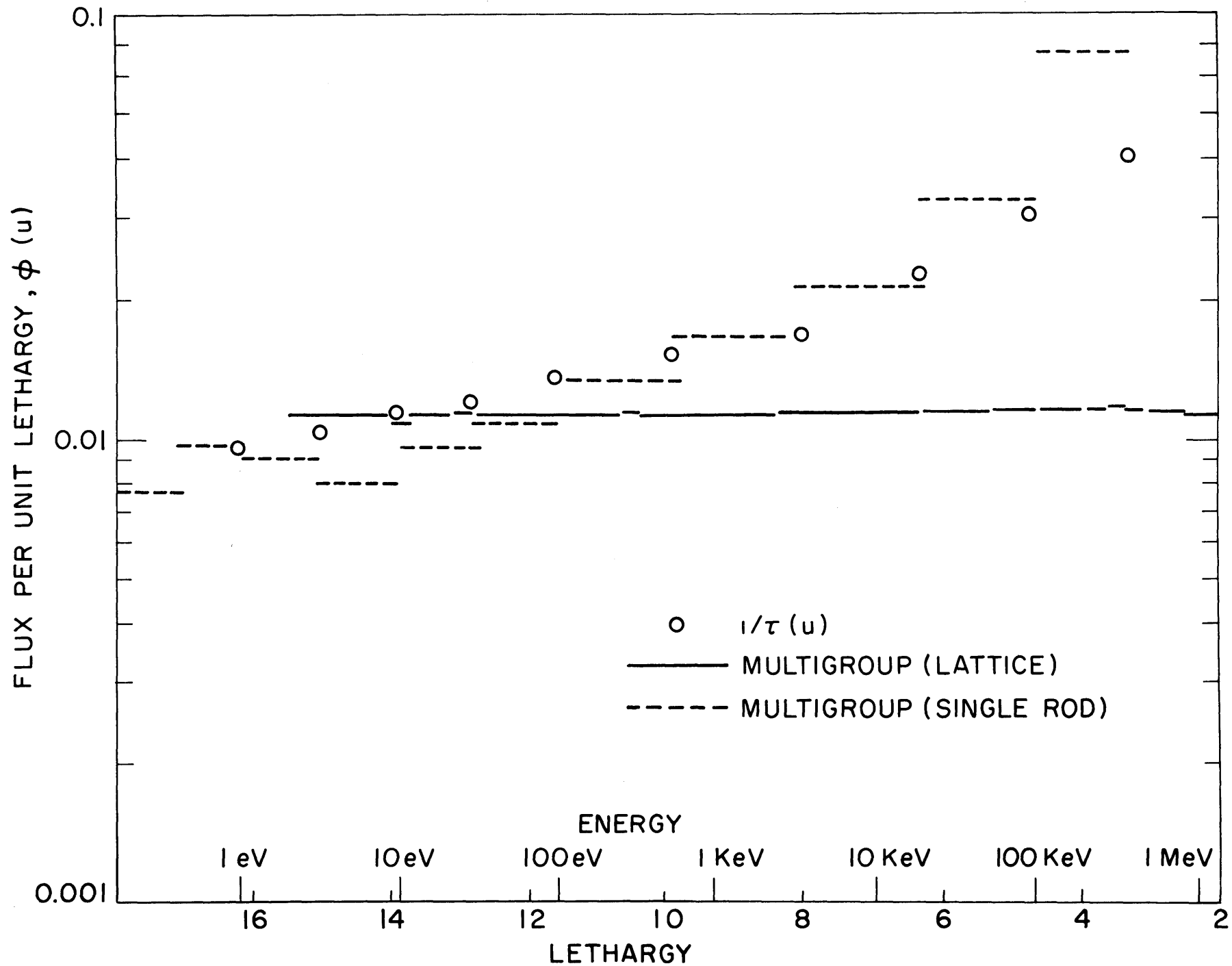
FIG. 6.2   COMPARISON OF EPITHERMAL SPECTRA

Higgins ($\underline{8}$) has shown, however, that if one assumes all absorptions take place at an effective resonance lethargy, u_r, then the preceding lattice equations still apply, but with $V = 4\pi\tau(u_r)$. If it is assumed that $\tau(u_r)$ does not vary with fuel properties, then it is still valid to assume that A is directly proportional to the resonance capture probability and hence a unique function of the flux ratio R.

Figure 6.3 shows a plot of R(20) versus A: as can be seen, it is essentially linear. Also shown is a plot of the flux ratio on the surface of the rod. The variation with A is larger than at a position 20 cm from the rod. However, it is anticipated that surface flux ratios may be more difficult to interpret due to rod size and internal structure effects.

6.3 Evaluation of Results

As is shown in Fig. 6.3, for values of A between 10 and 100 cm^2, R(20) varies only between 0.8 and 0.9. Since it should be possible to measure R(20) with a reproducibility of approximately $\pm$ 1% using conventional foil activation techniques, this would result in a corresponding uncertainty of about $\pm$ 10% in A. Fortunately, as can be seen from Eq. 6.1, the corresponding effect on the resonance escape probability will be reduced to about $\pm$ 1%. Thus, the proposed method appears feasible but only if careful attention is paid to achieving the highest precision.

As was the case with the methods for measurement of η described in Chapter 4, the use of the ratio of cadmium-covered gold to molybdenum activities does not lend itself well to an absolute determination of A. Instead, a relative measurement again appears best, in which unknowns are compared to a standard fuel rod such as 1-inch-diameter natural uranium metal, for which A has been previously determined. There are also other unresolved problems pertinent to the proposed method.

One problem which must be considered is the $1/v$ contribution to epithermal absorptions in molybdenum: at 20 cm from a single rod, $\phi(u)$ is approximately constant, just as in a full lattice, and therefore
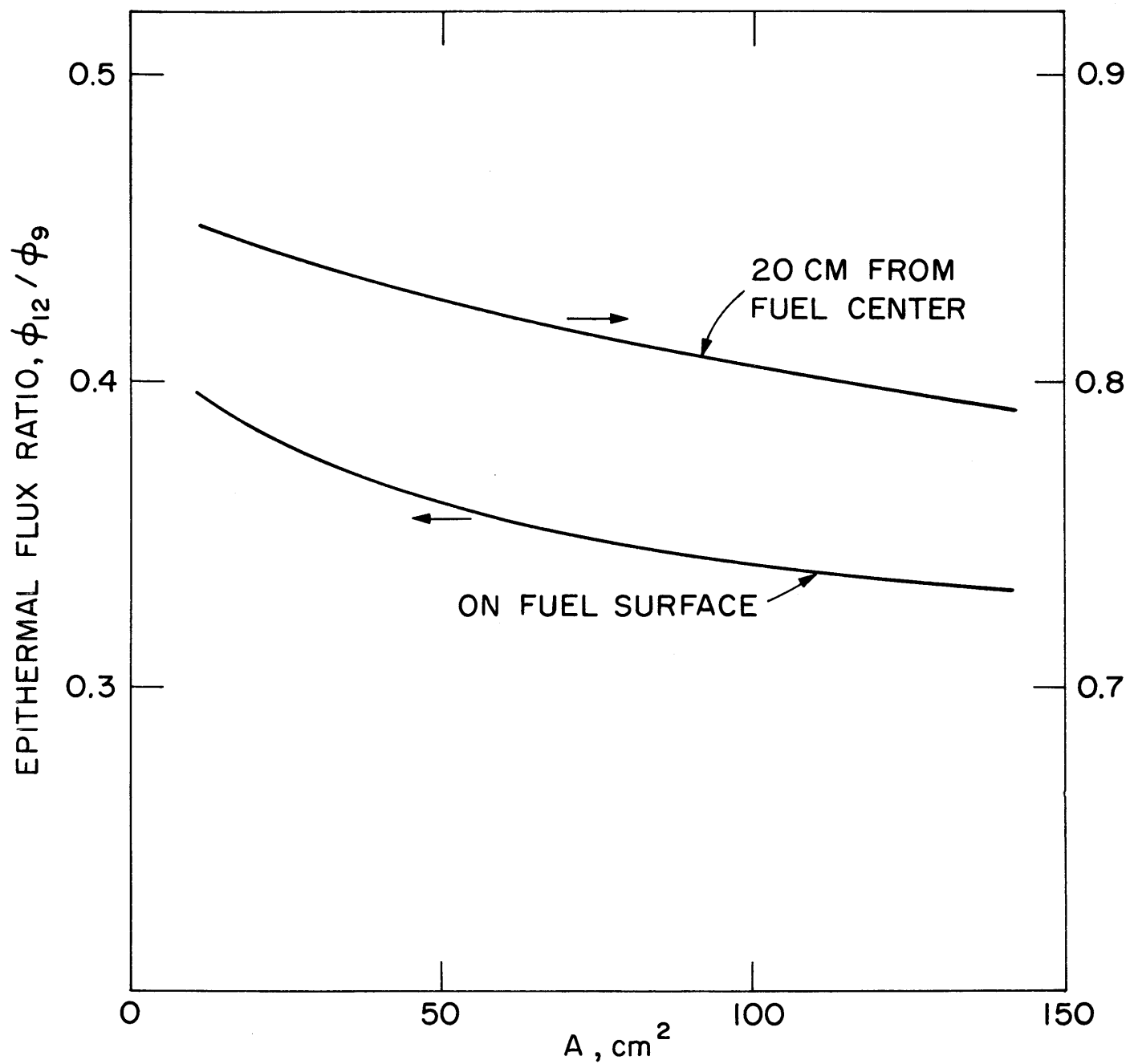
FIG. 6.3   EPITHERMAL FLUX RATIO VS. RESONANCE
ABSORPTION PARAMETER, A

the epithermal cross section due to 1/v absorptions is approximately one-half of the 2200 m/sec cross section. For molybdenum, then, RI(1/v) $\approx$ 0.26 barns, as compared to an infinite dilution resonance integral of 9 barns (6). Thus, the non-resonant capture contribution should be small enough to correct for with sufficient accuracy.

Other problems currently under consideration are the effects of finite source and sink size on the flux ratio. It is not clear, for example, that rods having different size and composition, but the same A, will give rise to the same flux ratio. Further ANISN calculations should help clarify this point. However, even ANISN involves some gross approximations in that the resonance absorption is smeared out over rather broad energy bins instead of being very nearly discrete as in nature.

Exponential irradiation experiments and additional calculations are planned to complete evaluation of the subject Au/Mo method for measurement of the epithermal absorption parameter, A, during the coming year.

6.4 References

(1) Donovan, R., Measurement of Heterogeneous Parameters, Chapter 8 in "Heavy Water Lattice Project Final Report," MITNE-86, MIT-2344-12, September 30, 1967.

(2) Reactor Physics Constants, ANL-5800, 2nd Ed., 1958.

(3) Casver, J. G. and W. R. Morgan, "Selection of a Set of Radioactivants for Investigating Slow Neutron Spectra," Proc. International Conference: Modern Trends in Activation Analysis, Texas, 1961.

(4) Price, L. N., "A Systematic Study of Foil Correction Factors in the Measurement of δ_{28}, δ_{25}, ρ_{28} and C^* in Slightly Enriched D_2O Moderated Lattices," S.M. Thesis, Massachusetts Institute of Technology, Department of Nuclear Engineering, August 1966.

(5) Seth, S. S., "Measurement of Integral Parameters," loc. cit., ref. (1), Chapter 3.

(6) Drake, M. K., "A Compilation of Resonance Integrals," Nucleonics, August 1966.

(7) Helstrand, E., "Measurement of Resonance Integrals," in Reactor Physics in the Resonance and Thermal Regions, Vol. 2, p. 151, Eds. A. J. Goodjohn and G. C. Pomraning, M.I.T. Press, 1966.

(8) Higgins, M. J., "Fuel Rod Interaction Kernels," loc. cit., ref. (1), Chapter 9.

7. NUMERICAL METHODS

J. N. Donohew and J. D. Eckard

7.1 Introduction

In order to facilitate planning and interpretation of single rod experiments, two available computer codes were modified to permit numerical experiments on simulated single rod assemblies in an exponential tank of D_2O moderator. Previous chapters have cited the results of some of these calculations. The purpose of the present chapter is to explain in more detail the general mechanics of the calculational methods.

7.2 The Single Rod Assembly (SRA) Code

The SRA code has been described in considerable detail in reference 1. Basically, it is a multigroup diffusion theory (transport approximation) code designed to calculate the radial flux behavior in cylindrical geometry for a single rod assembly, as shown in Fig. 7.1. The assembly is treated as infinite in the axial dimension, and axial leakage is accommodated through inclusion of variable axial buckling. The program is designed to iterate on the axial buckling to achieve a steady state neutron balance.

Although the internal structure of the code is of no particular concern to the average user, one unique feature of SRA is worth pointing out: namely, that it is based on an integral theory formulation of the multigroup equations rather than on the more common differential-difference formulation.

The cross-section set used with the SRA code to date has been the LASL (Hansen-Roach) 16-Group Set (2). Resonance self-shielding in U-238 is taken into account by the following approximate prescription. For all epithermal groups in which no fissioning occurs in U-238, the absorption cross section is multiplied by the ratio of the
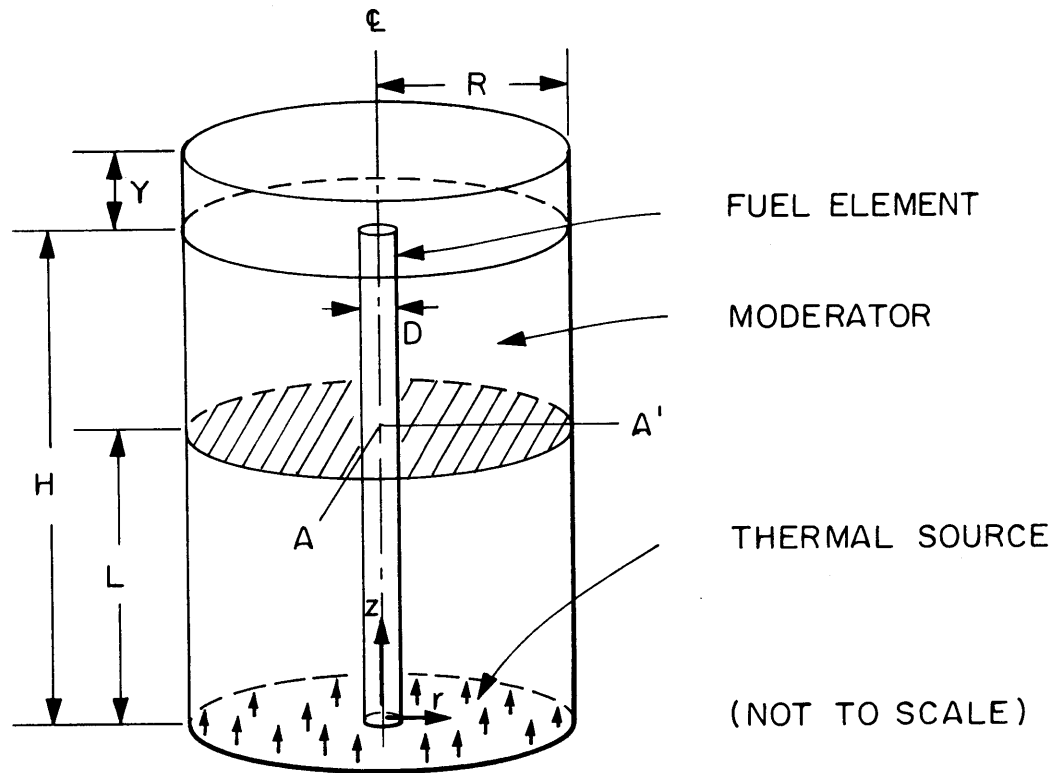
FIG. 7.1 SKETCH OF ASSEMBLY TREATED BY THE
SRA CODE

effective resonance integral to the infinite dilution resonance integral. The transport cross section is likewise modified to take this reduction into account. Since there is very little epithermal flux depression in the fuel for the rather coarse group structure used, this prescription only slightly overestimates resonance capture in the fuel.

The cases investigated are described in Table 7.1. Except for Run 1, which had no rod in the moderator, all runs used a 1.01-inch-diameter, natural uranium metal rod (with the cladding neglected). Run 1 was simply a preliminary check on the fidelity of the mathematics and program. As expected, for this run all energy groups were found to have the same shape, the familiar J_o shape. The value of the axial buckling, γ^2, which gave an effective multiplication ratio of unity was found to be:

$$\gamma^2 = 0.002678 \text{ cm}^{-2} .$$

One can derive the following relationship between the radial and axial buckling:

$$-\alpha^2 \approx \kappa_{th}^2 - \gamma^2 \tag{7.1}$$

(assuming that the thermal flux is much larger than the epithermal fluxes). For the J_o shape,

$$\nabla^2 J_o(\alpha r) = -\alpha^2 J_o(\alpha r) ,$$

and

$$\alpha^2 = \left(\frac{\nu_o}{\tilde{R}}\right)^2 = \left(\frac{2.4048}{47.47}\right)^2 \text{ cm}^{-2} = 0.0025664 . \tag{7.2}$$

For this case,

$$\kappa_{th}^2 = 0.0001115 \text{ cm}^{-2} ,$$

and

$$\gamma^2 - \kappa_{th}^2 = 0.0025665 . \tag{7.3}$$

The near equality of Eqs. 7.2 and 7.3 verifies Eq. 7.1 and also provides a consistency check on the SRA code.

Figure 7.2 presents the spatial variation of three representative groups (each normalized to unity at the center). The data for these plots were taken from Run 2, which involved a moderator purity of

TABLE 7.1

List of Cases Run

Run No.	$\dfrac{(D_2O)}{(D_2O)+(H_2O)}$	η/η_o	Cross Sections	Comments
1	0.995	1	Shielded	No rod
2	0.995	1	Shielded	1.01-inch rod
3	0.995	0.5	Shielded	1.01-inch rod
4	0.995	0.25	Shielded	1.01-inch rod
5	0.995	0	Shielded	1.01-inch rod
6	1.000	1	Shielded	1.01-inch rod
7	0.990	1	Shielded	1.01-inch rod
8	0.000	1	Shielded	1.01-inch rod
9	0.995	1	Unshielded	1.01-inch rod
10	0.995	0.5	Unshielded	1.01-inch rod

99.5 mole % D_2O and a 1.01-inch diameter, natural uranium metal rod. The uppermost curve is for the thermal group (group 16), the middle curve is for an epithermal group (group 13), and the lowest curve is for the high energy group (group 1). The thermal group has its maximum at a position r_o from the fuel centerline. The maxima for progressively higher energy groups occur nearer the center. (This is not always a monotonic occurrence: some epithermal groups have maxima at greater r_o's than other epithermal groups even though the former groups represent higher energy neutrons.) As noted in a previous chapter, calculation of the thermal constant, Γ, is based on experimental determination of r_o using foil activation techniques.
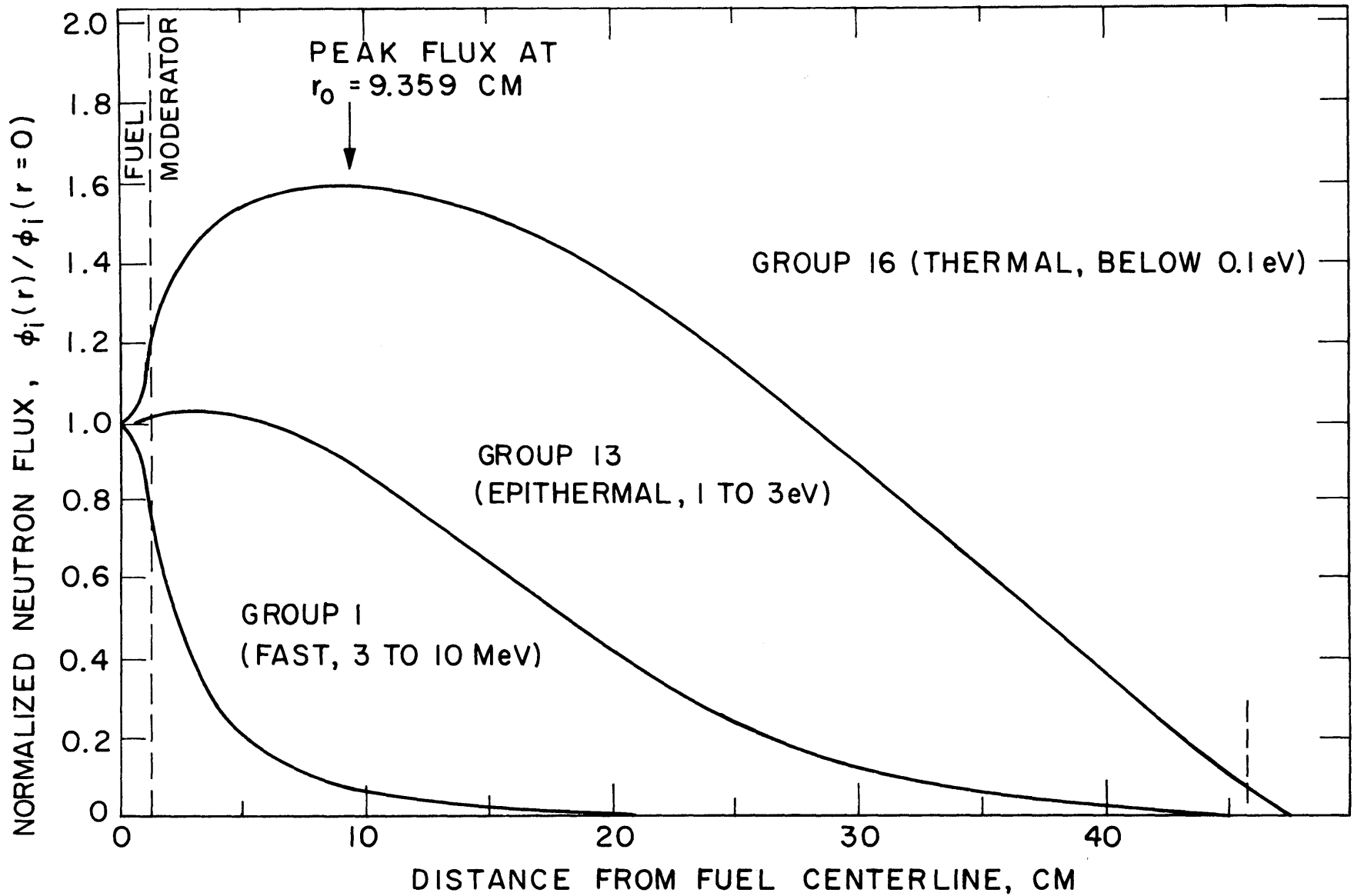
FIG. 7.2 SPATIAL VARIATION OF SELECTED FLUX GROUPS IN A SINGLE ROD ASSEMBLY

Figure 7.3 illustrates the energy-dependent flux at several positions in the SRA. Flux per unit lethargy ($\phi_i/\Delta u_i$) is plotted against lethargy and normalized so that $\sum_i \phi_i = 1$. The fission spectrum $\dfrac{\chi_i}{\Delta u_i}$, likewise normalized, is also given and indicated by the single dots in the figure. The general behavior of the spectra is as one would expect: harder in the fuel rod center, becoming more thermal with distance from the rod. Noting that the ordinate of Fig. 7.3 is logarithmic, one sees that all the spectra are relatively thermal, the normalized (group-integrated) thermal flux ranging from 0.4272 at the rod's center to 0.9899 near the edge of the assembly. An interesting spectrum occurs at $r = 13.13$ cm from the center in the SRA. The epithermal flux $\phi(u)$ is nearly constant up to the six highest energy groups. This means that $\phi(E)$, which is equal to $\phi(U)/E$, is proportional to $\left(\dfrac{1}{E}\right)$, and this is essentially the epithermal spectrum seen by a fuel rod in a full lattice. Few-rod assemblies (with, for example, 3 rods) with rods mutually spaced at this "critical" distance may be able to take advantage of this phenomenon to simulate a complete lattice.

It is important to know how the experimental parameters depend upon one another. Therefore, at this point we will examine the behavior of r_o, which is defined as that thermal flux peak radius for which K (the numerical growth rate) is made equal to unity by varying γ^2 (the axial leakage parameter). The variation of r_o with γ^2 can be seen in Fig. 7.4, and further, as can be seen in Fig. 7.5, K is in turn fairly sensitive to γ^2 so that it is necessary to determine K quite accurately to maintain accuracy in r_o. From these two figures, it is found that

$$\frac{dr_o}{dK} = \frac{dr_o}{d\gamma^2} \frac{d\gamma^2}{dK} = 2715 \text{ cm}^3 \cdot \frac{1}{30 \text{ cm}^2} = 90.5 \text{ cm}.$$

The distance r_o is about 9.5 cm, so to have r_o accurate to 1%, one must calculate K to about ± 0.001. In the calculations, an accuracy of ± 0.00005 was maintained and, additionally, a linear interpolation was made to determine r_o from the values of r_o corresponding to the
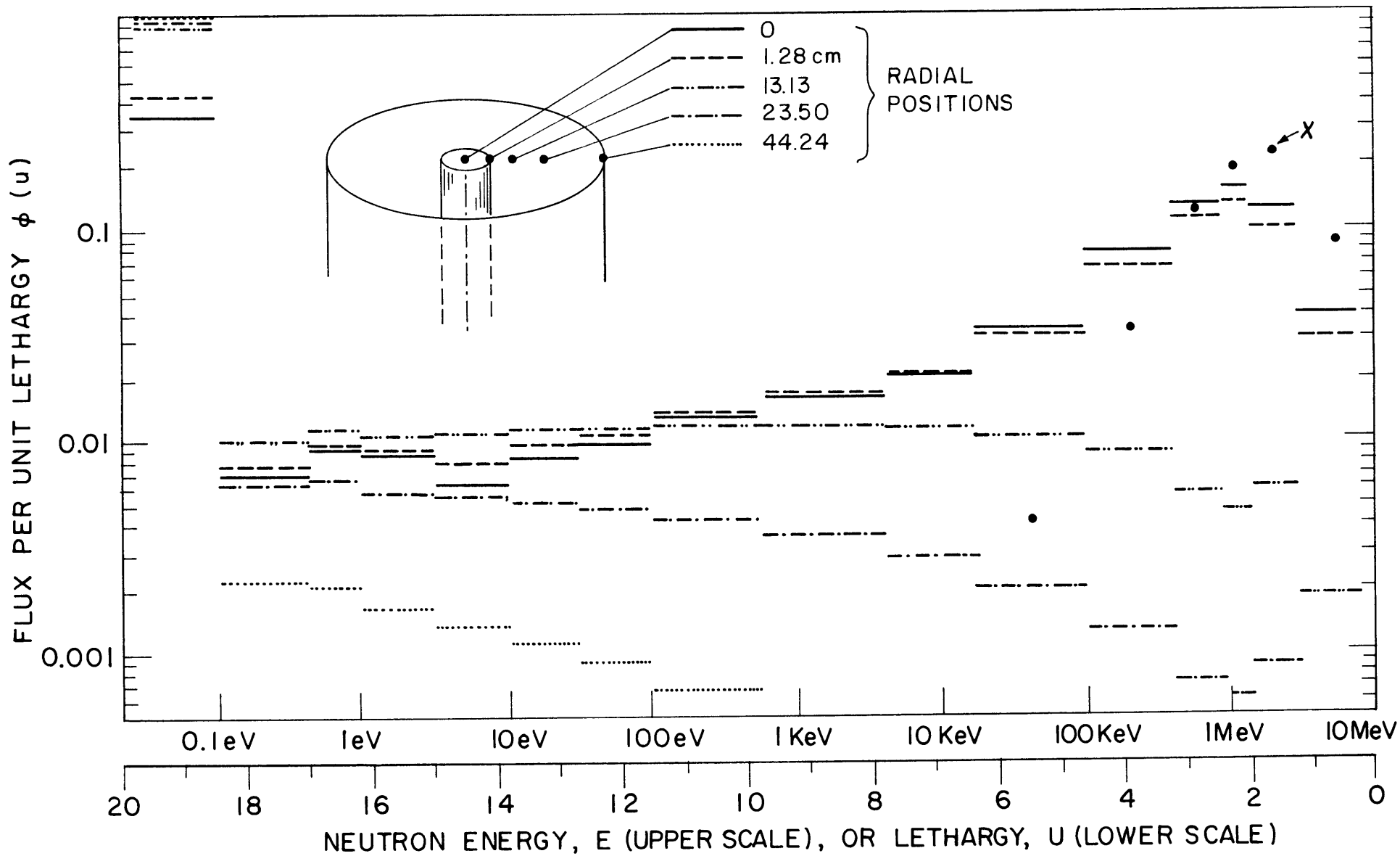
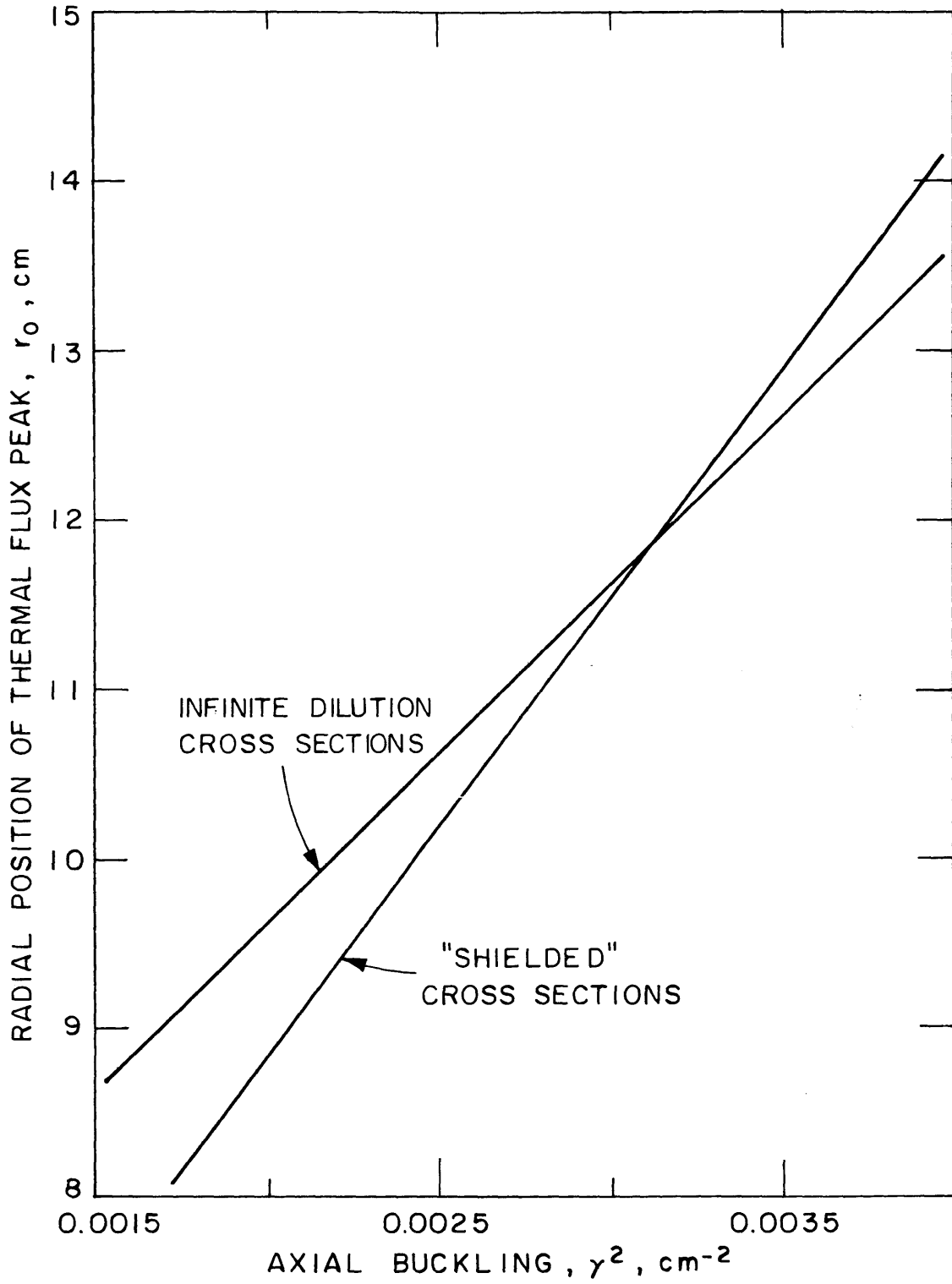FIG. 7.3 SPECTRA AT VARIOUS POSITIONS IN A SINGLE ROD ASSEMBLY

FIG. 7.4 A PLOT OF THERMAL FLUX PEAK POSITION,
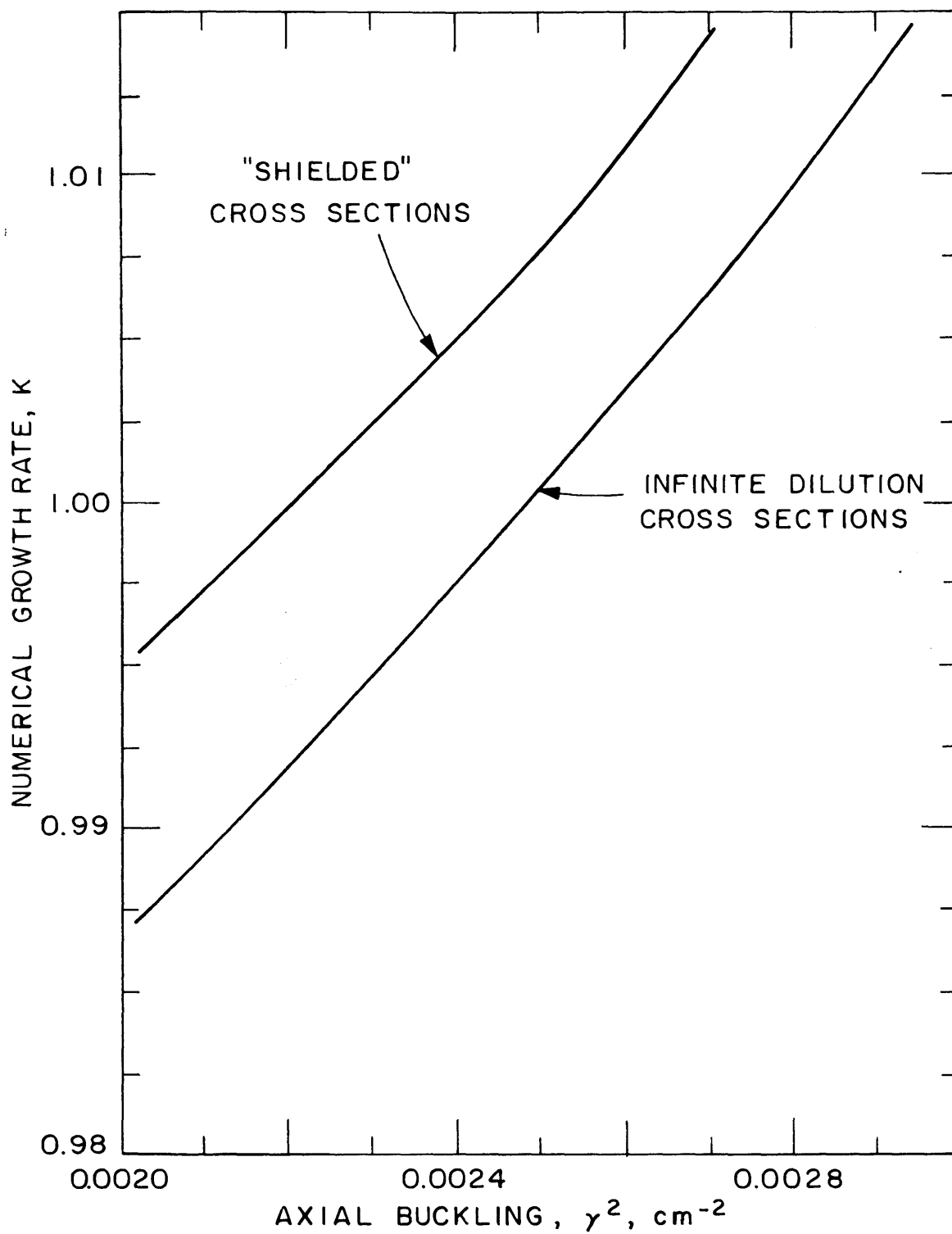r_0 , vs AXIAL BUCKLING, γ^2

FIG. 7.5 A PLOT OF NUMERICAL GROWTH RATE, K, vs
AXIAL BUCKLING, γ^2

K's most closely bracketing 1.00000. This information is given in Table 7.2 together with other pertinent information. It should be noted that the corresponding experimental precision in determining r_o will be about 1% at best.

To obtain the variation of r_o with η, the neutron yield per absorption in fuel, the following procedure has been followed. The full value of η has been designated as η_o, and fractions of this obtained by varying $(\nu\sigma_f)_{th}$ of U-235 have been used to calculate new r_o's. Figure 7.6 depicts the results of this series of calculations. In all cases, the absorption cross sections have remained unchanged. The variation of r_o with (η/η_o) is linear, and a measure of the sensitivity is:

$$\frac{dr_o}{d\left(\dfrac{\eta}{\eta_o}\right)} = -1.034 \text{ cm}.$$

At the value of r_o for $(\eta/\eta_o) = 1$, this is -0.11% in r_o per percent (η/η_o). Thus, r_o is not particularly sensitive to η. However, it is clear that the effect of η upon r_o must be taken into account when determining the thermal constant, Γ.

Figure 7.7 shows how r_o varies with the contamination of D_2O by H_2O. For values of the ratio of concentrations $(H_2O)/((H_2O) + (D_2O))$ between 0.0 and 0.005, r_o decreases slowly as would be expected, since the peaking in an H_2O reflector is nearer the interface than in a D_2O reflector. This is, of course, related to the L^2 of the moderator medium. However, due to the increased absorption in H_2O compared to D_2O, the γ^2 must be increased to maintain $K = 1$. As was seen, r_o is a very sensitive (increasing) function of γ^2. Therefore, the downward trend of r_o is halted and r_o begins to increase. The range of the abscissa from 0.0 to 0.01 covers the range of interest for D_2O assemblies. As can be seen, the variation in r_o is not significant. As a point of interest, the value of r_o for 100% H_2O was calculated to see if SRA's with a light water moderator are feasible. As can be seen from Fig. 7.8, γ^2 increases by an order of magnitude to 0.01846. The corresponding r_o, shown in Fig. 7.7, is

TABLE 7.2

Summary of Results for Runs 1 Through 9

γ^2 (cm^{-2})	K	r_o (cm)	Run No.
No Rod, 99.5% D$_2$O			
0.00268	1.00000	0.0	1
$\eta/\eta_o = 1$			
0.00219	0.99948	9.359	
0.00221	1.00000	9.414	
0.00225	0.00098	9.517	2
0.00234	1.00267	9.759	
0.00249	1.00747	10.170	
0.00324	1.04399	12.210	
$\eta/\eta_o = 1/2$			
0.00200	0.98146	7.823	
0.00260	0.99665	9.691	
0.00266	1.00000	9.928	3
0.00268	1.00080	9.985	
0.00273	1.00249	10.126	
$\eta/\eta_o = 1/4$			
0.00250	0.98274	8.504	
0.00280	0.99516	9.800	
0.002895	0.99998	10.170	4
0.002895	1.00000	10.183	
0.002896	1.00005	10.214	
0.00325	1.02618	11.736	
$\eta/\eta_o = 0$			
0.00318	1.00586	10.823	
0.003133	1.00024	10.516	5
0.003131	1.00000	10.448	

(continued)

TABLE 7.2 (concluded)

| γ^2 (cm^{-2})	K	r_o (cm)	Run No.
100% D_2O			
0.00200	0.99679	9.040	
0.00211	0.99859	9.347	6
0.00217	1.00000	9.476	
0.00219	1.00045	9.517	
99% D_2O			
0.00200	0.99388	8.936	
0.00225	0.99902	9.430	
0.00229	0.99994	9.594	7
0.00229	1.00000	9.599	
0.00260	1.00850	10.287	
100 % H_2O			
0.014000	0.98127	5.600	
0.01820	0.99801	7.149	
0.01846	1.00000	7.398	8
0.018699	1.00170	7.632	
Unshielded			
0.00200	0.98647	9.604	
0.00248	0.99975	10.599	
0.00249	1.00000	10.615	9
0.00260	1.00326	10.833	
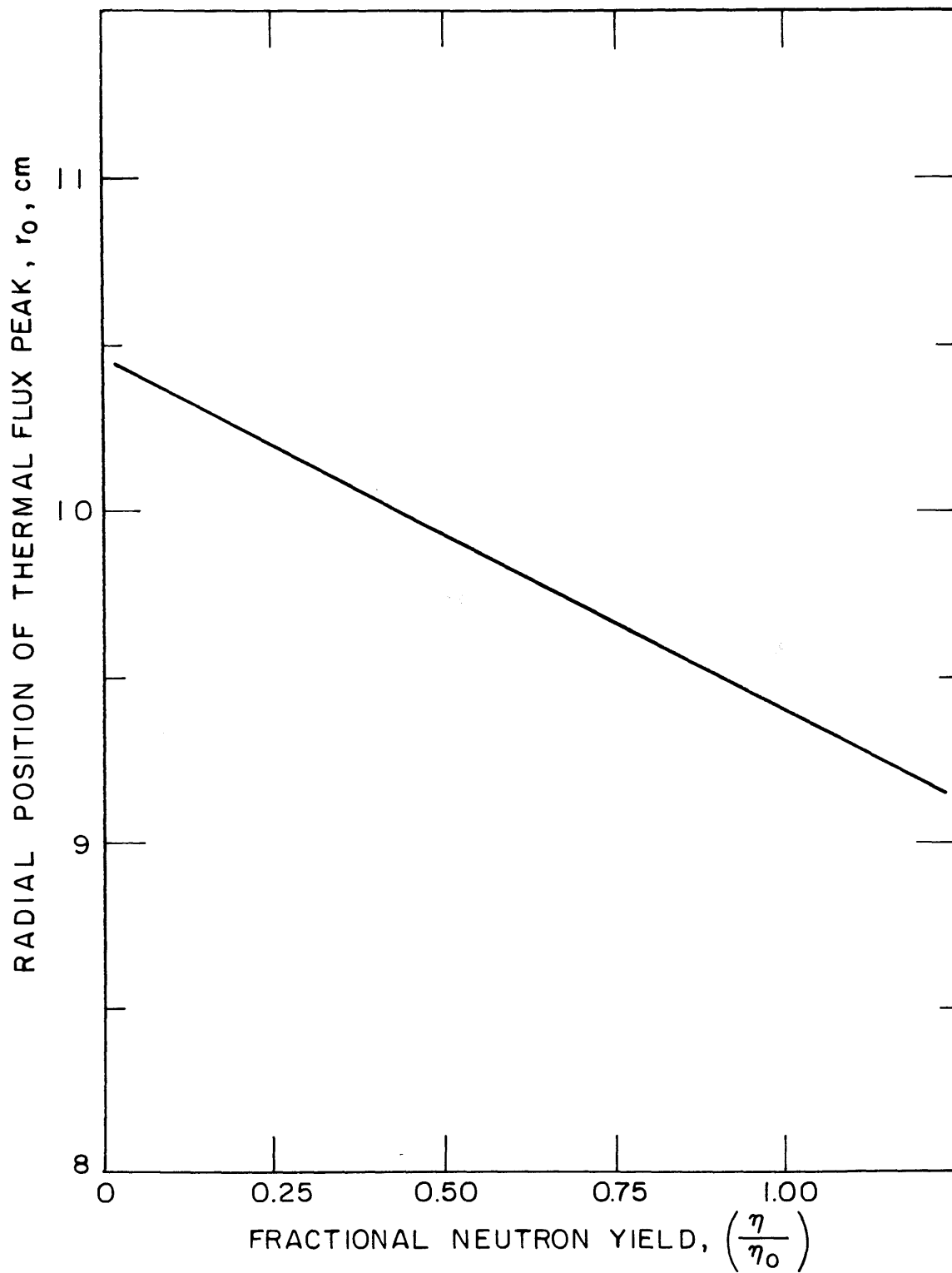
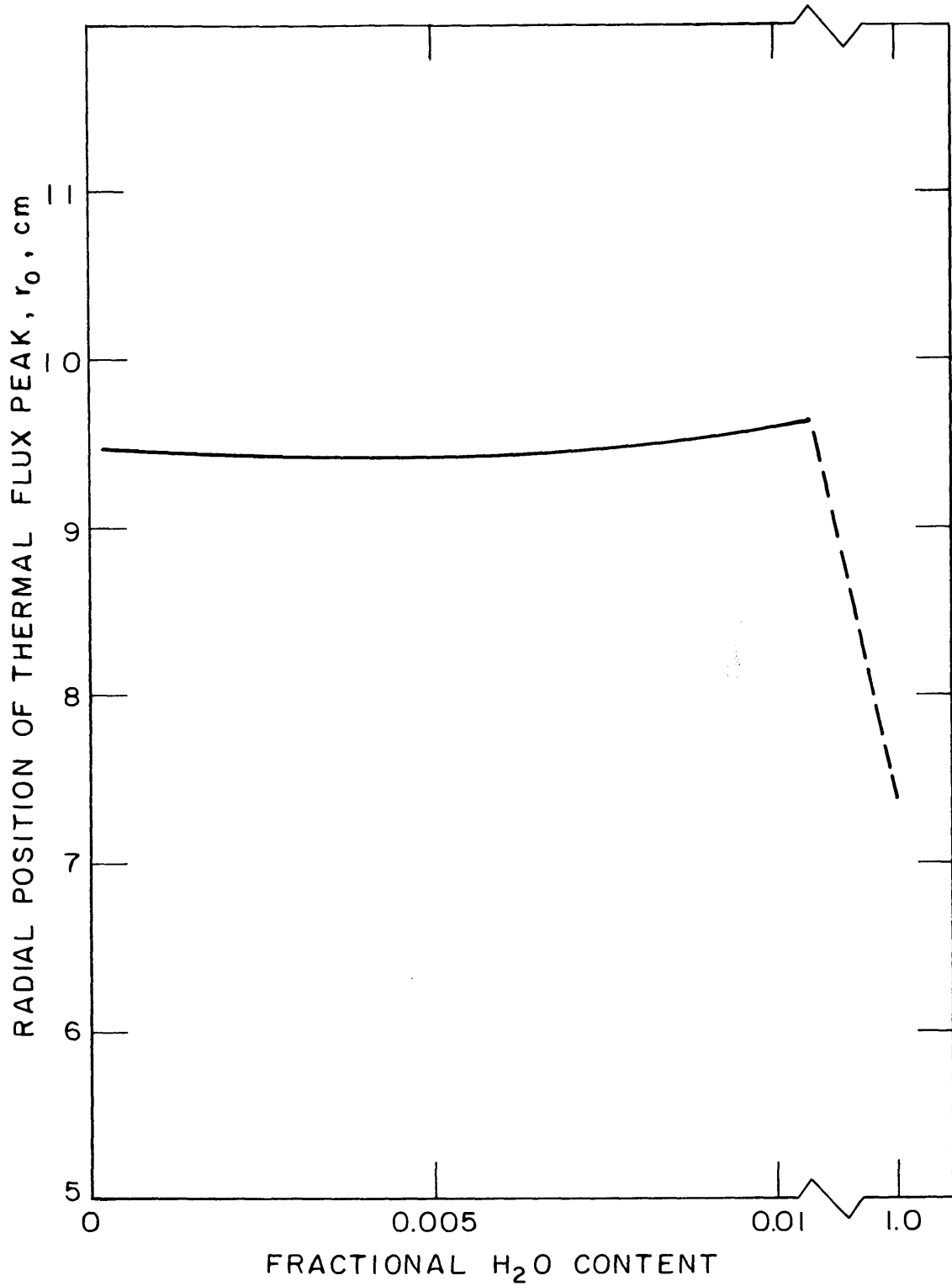FIG. 7.6 VARIATION OF THERMAL FLUX PEAK POSITION
WITH NEUTRON YIELD

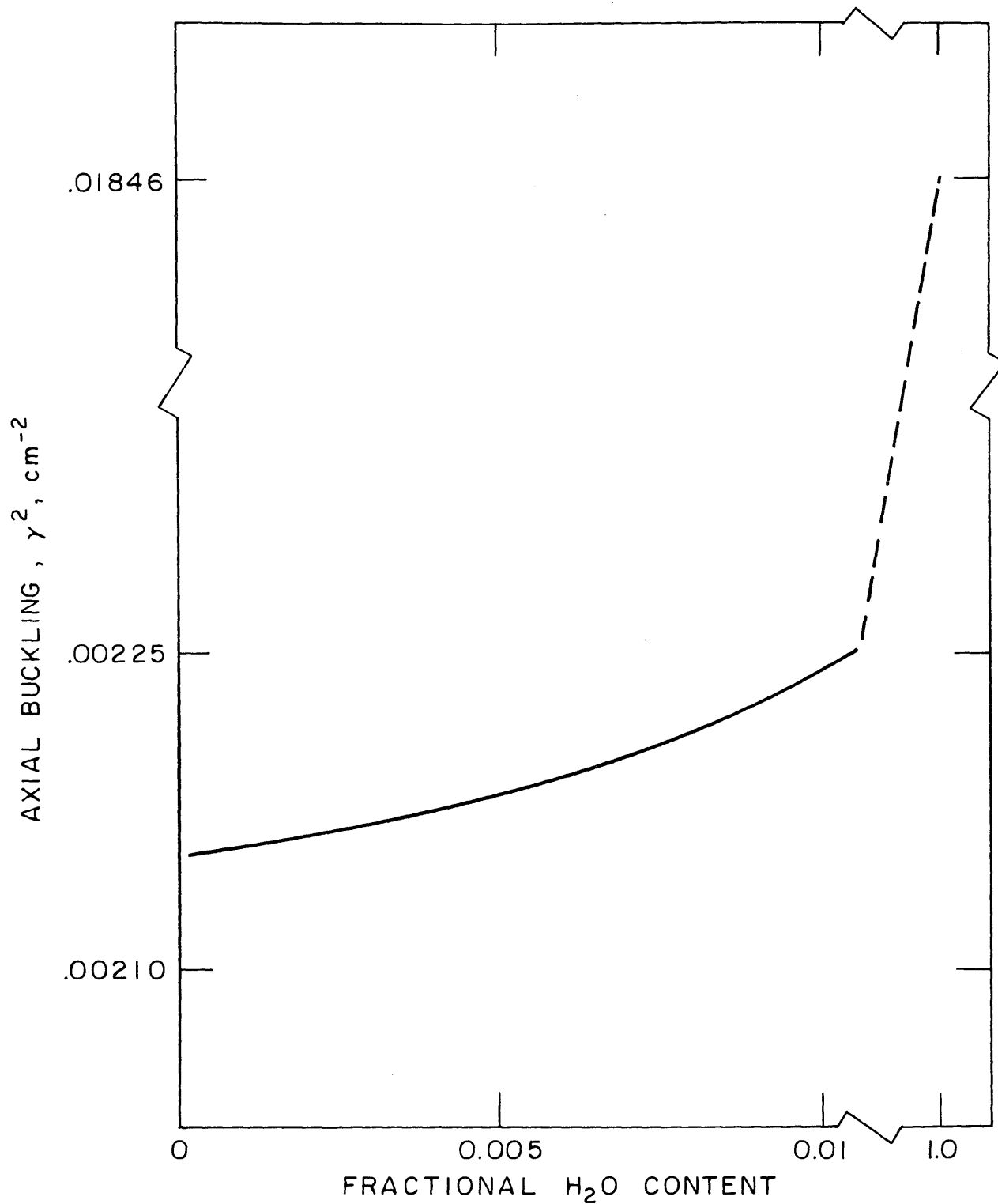FIG. 7.7 VARIATION OF THERMAL FLUX PEAK POSITION, r_0, DUE TO H_2O CONTAMINATION OF D_2O MODERATOR

FIG. 7.8 VARIATION OF AXIAL BUCKLING, γ^2, DUE TO H_2O CONTAMINATION OF D_2O MODERATOR

only 2 cm less than for the 100% D_2O case. This is somewhat surprising and indicates that the peak of the thermal flux occurs sufficiently far outside the fuel rod to be accurately measured. However, the large value of γ^2 means that the axial decay of the flux will be very rapid, and there will therefore undoubtedly be problems in achieving sufficent foil activation and an increased sensitivity to foil-holder tilt.

In conclusion, the SRA code has proven to be a particularly useful tool for studying the single rod experiment. Its only major weaknesses are the oversimplified resonance treatment, a disadvantage shared by all multigroup methods, and the fact that it is based upon diffusion theory. In order to evaluate the effect of this latter restriction, the work reported upon in the following section was undertaken.

7.3 The ANISN Code

The ANISN code is a one-dimensional multigroup transport program which solves the neutron transport equation for slab, cylindrical or spherical geometry using the discrete S_N approximation (3). The version used in the present work was adapted from the original Union Carbide code by workers at Atomics International for operation on an IBM 360, Model 50H. Further trivial modifications were necessary to permit its use on the IBM 360, Model 65 at the M.I.T. Information Processing Center: for example, elimination of the various plotting subroutines. ANISN is an updated version of the DTF-II code (4). Since reference 3 describes how to load and run the ANISN program, the present discussion will be limited to a description of the procedure through which ANISN was induced to calculate single rod experiments.

Two general types of experiments were simulated: exponential and pulsed neutron.

Exponential experiments were simulated by adding a fictitious nuclide to the moderator and fuel regions. The concentration of the fictitious nuclide was taken as the desired axial buckling, γ^2, and the absorption cross section required as input data in each energy group

was set equal to minus the group diffusion coefficient calculated for the other materials in that region. This added a negative leakage cross section $\Sigma_i = -D_i \gamma^2$, to each group in the ensuing calculations. A series of cases was then run for different values of γ^2 to find the one which permitted a steady state neutron balance. Note that different cross sections are required in regions having different D values; hence, one separate fictitious element is required for each region.

For pulsed neutron calculations, a similar procedure was followed. The fictitious nuclide concentration was now taken as the prompt neutron decay constant λ, and the group absorption cross sections as $-1/v$, where v is the average neutron velocity for the group. Here, only one fictitious element is required common to all regions. An axial buckling is also specified, equal to $(\pi/H)^2$, where H is the extrapolated assembly height. In both numerical experiments the other cross sections for the fictitious nuclide are set equal to zero (i.e., transport, fission and intergroup scattering removal), except for the intragroup scattering cross section, which must be specified as minus the absorption cross section.

If the above subterfuge is employed, ANISN will correctly calculate single rod exponential or pulsed neutron experiments. The only caveat worth noting in regard to the output data is the fact that the eigenvalue quoted by the code is not the required value since it is based only on neutrons produced by fissile material. It is a simple matter, however, to calculate the correct multiplication constant as the ratio of fission rate to absorptions plus leakage in the system summary output.

As with the SRA code described in the preceding section of this chapter, Hansen-Roach cross sections were employed as input data, and a self-shielding correction was applied to U-238 in the epithermal energy region. Thermal group properties of D_2O and the thermal neutron velocity were adjusted so as to match known experimental values of D and vD.

Most of the numerical experiments performed using ANISN have been discussed in preceding chapters, and the results displayed in

graphical form. Therefore, only a few selected additional results will be discussed here. The first is the typical pulsed neutron experiment in which moderator height (hence axial buckling) is varied and the prompt neutron decay constant measured at each height. The results are plotted in Fig. 7.9; as can be seen, the expected linear variation of λ with B_z^2 is indeed obtained.

A second use of the ANISN code has been to test approximations made in some of the simple one-group and age-diffusion derivations employed in previous chapters. Its use to test for transport effects upon r_o has already been noted. A second application of this type involved testing approximations made in establishing the equivalence of pulsed neutron and axial buckling experiments. For example, strictly speaking, one must neglect delayed neutrons in the pulsed neutron experiments, thus reducing k_∞ by the factor $(1-\beta)$. Since $\beta \ll 1$, this term was set equal to unity in the simple one-group treatment. ANISN calculations performed with and without this correction for two of the data points plotted in Fig. 7.9 showed that this approximation was indeed valid: λ values of 765 and 608 sec^{-1} changed very slightly, to 762.5 and 609 sec^{-1}, respectively, when the $(1-\beta)$ correction was applied.

Perhaps the most important single conclusion which may be drawn from the ANISN code results is that since transport effects are found to be negligible, the simpler SRA code can be used in the future for most numerical experiments involving single rod assemblies.

7.4 References

(1) Eckard, J. D., Jr., "Characteristics of the Energy-Modal Approximation in Fast Reactor Neutron Spectrum Calculations": Appendix C, Integral Formulation of the Multigroup Equations; and Appendix D, Single Rod Assembly Results, Ph.D. Thesis, Massachusetts Institute of Technology, Department of Nuclear Engineering, December 1968.

(2) Templin, L. J., Editor, "Reactor Physics Constants," 2nd Edition, ANL-5800, pp. 568-576, Argonne National Laboratory, 1963.
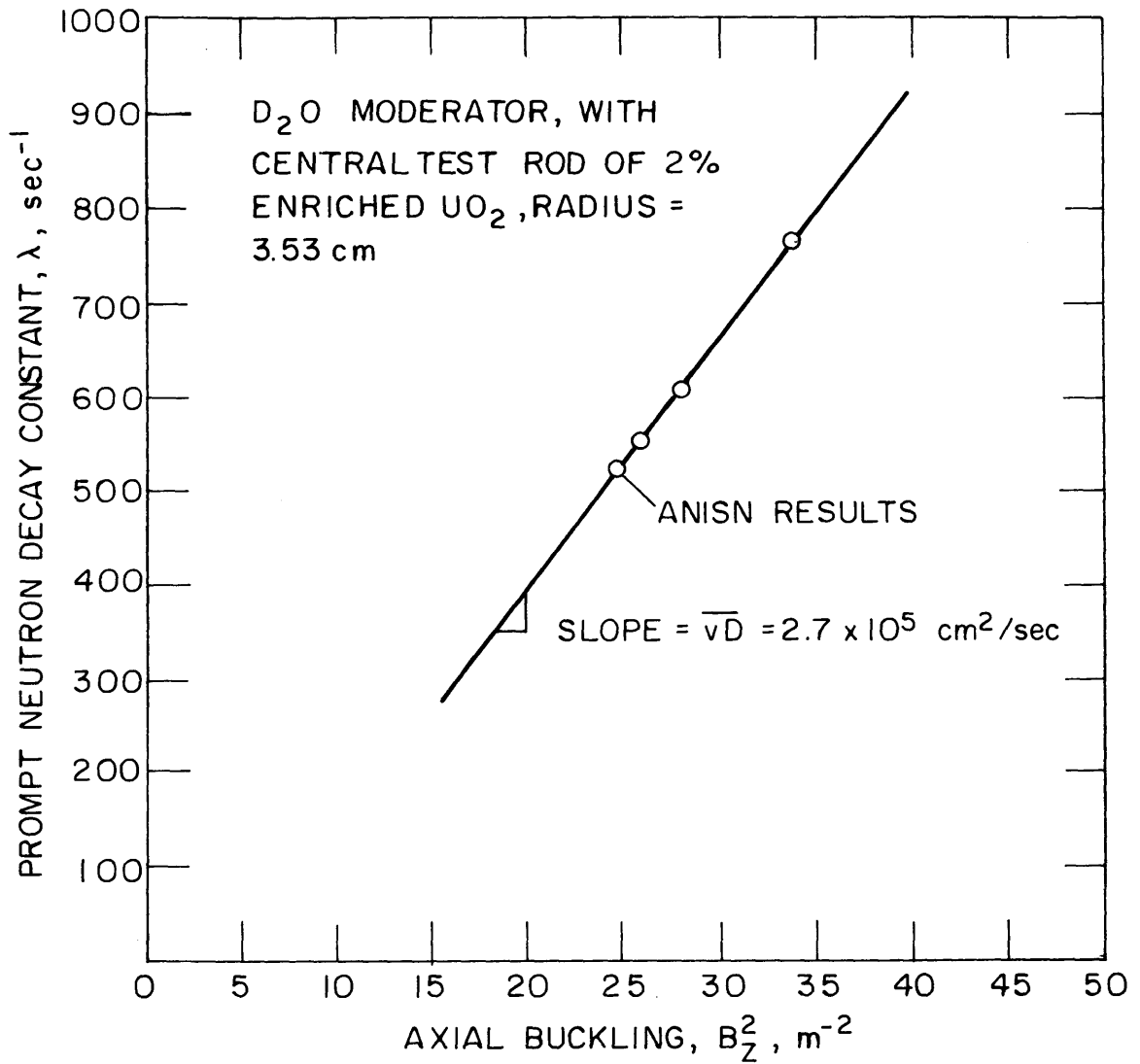
FIG. 7.9 RESULTS OF A SIMULATED PULSED NEUTRON EXPERIMENT

(3) Boling, M. A. and W. A. Rhoades, "ANISN/DTFII Conversion to IBM System 360," AI-66-Memo 171, Volume 1.

(4) Engel, W. W., M. A. Boling and B. W. Colston, "DTF II, A One-Dimensional, Multigroup, Neutron Transport Program," NAA-SR-10951 (1966).

8. GAMMA SPECTROSCOPY

Y. Hukai, T. L. Harper and N. C. Rasmussen

8.1 Introduction

The ultimate objective of the work described in this chapter is to extract useful reactor physics data from fuel rod gamma spectra obtained using high resolution semiconductor spectrometers. In particular, it is to be determined whether relative fertile and fissile capture and fission rates can be measured, from which it may be possible to extract heterogeneous parameters such as η. This particular application of Ge(Li) gamma spectroscopy is still in an early stage of development, but sufficiently encouraging results have been obtained at M.I.T. and elsewhere (1) to indicate that a considerable amount of information can be obtained from this approach.

During the report period, work was carried out in two primary areas: measurement of gamma-ray spectra and analysis of gamma-ray spectra. In the first category, a Ge(Li) gamma spectrometer was set up in front of MITR beam port 4TH1 to permit measurement of the prompt and delayed gamma spectra emitted by fuel rods. Non-coincident, triple coincidence, and Compton suppression modes of operation are possible with this apparatus (2). The other major problem encountered in the use of gamma-ray spectroscopy for the determination of reactor physics parameters occurs in the analysis of the data obtained. Typically, one must deal with many photopeaks and a high Compton background. Sonstelie, for example, found this problem to be the major factor limiting the development of a new method for measurement of δ_{28} (the ratio of U-238 to U-235 fissions) using Ge(Li) gamma-ray spectroscopy (3). Therefore, work has been initiated to extend computer methods previously developed at M.I.T. (4) to such data. Substantial success has already been achieved, in that the results presented in this chapter were analyzed using the subject program. A topical report was issued describing the program:

T. Harper, T. Inouye and N. C. Rasmussen,
"GAMANL, A Computer Program Applying Fourier Transforms
to the Analysis of Gamma Spectral Data." MIT-3944-2,
MITNE-97, August 1968.

8.2 Experimental Measurements

Most of the work during the report period was concerned with
setting up, adjusting and debugging the spectrometer and associated
shield cave in front of a thermal neutron beam port at the MITR. A
number of runs have been made, however, to obtain standard prompt
capture gamma spectra for the individual fertile and fissile nuclides,
and a series of oxide fuel rods have been irradiated to examine com-
bined gamma spectra.

Capture gamma spectra have been measured for highly depleted
uranium metal (18 ppm U-235) and for high purity ThO_2 powder. A
typical spectrum, for Th-232, is shown in Fig. 8.1. Tables 8.1 and
8.2 present the resolved gamma peak energies and intensities
obtained by data analysis with the computer code GAMANL. As can
be seen, some 24 lines were resolved in the U-238 spectrum and 43
in the Th-232 spectrum. These data have been compared with other
results reported in the literature by Sheline et al. (5) and by Groshev
(6). The agreement is, in general, good. These results are
encouraging since they suggest it will be possible to use prompt
gamma spectroscopy for conversion ratio measurements. The strong
4.059 meV line of U-238, which occurs approximately 10 times for
every 100 captures, should prove particularly useful.

Fuel rod irradiations have also yielded interesting results. A
series of half-inch-diameter, UO_2 fuel rods having various U-235
enrichments (1.1, 1.3, 1.6 and 2.0 percent) were irradiated in the
thermal beam port facility and their prompt gamma spectra analyzed.
In addition to the characteristic fertile and fissile nuclide spectra, all
displayed a prominent line at 693.1 keV. This has now been identified
as coming from the inelastic scattering of fission neutrons by Ge-72
in the Ge(Li) detector crystal. Moreover, since Ge-71 does not exist
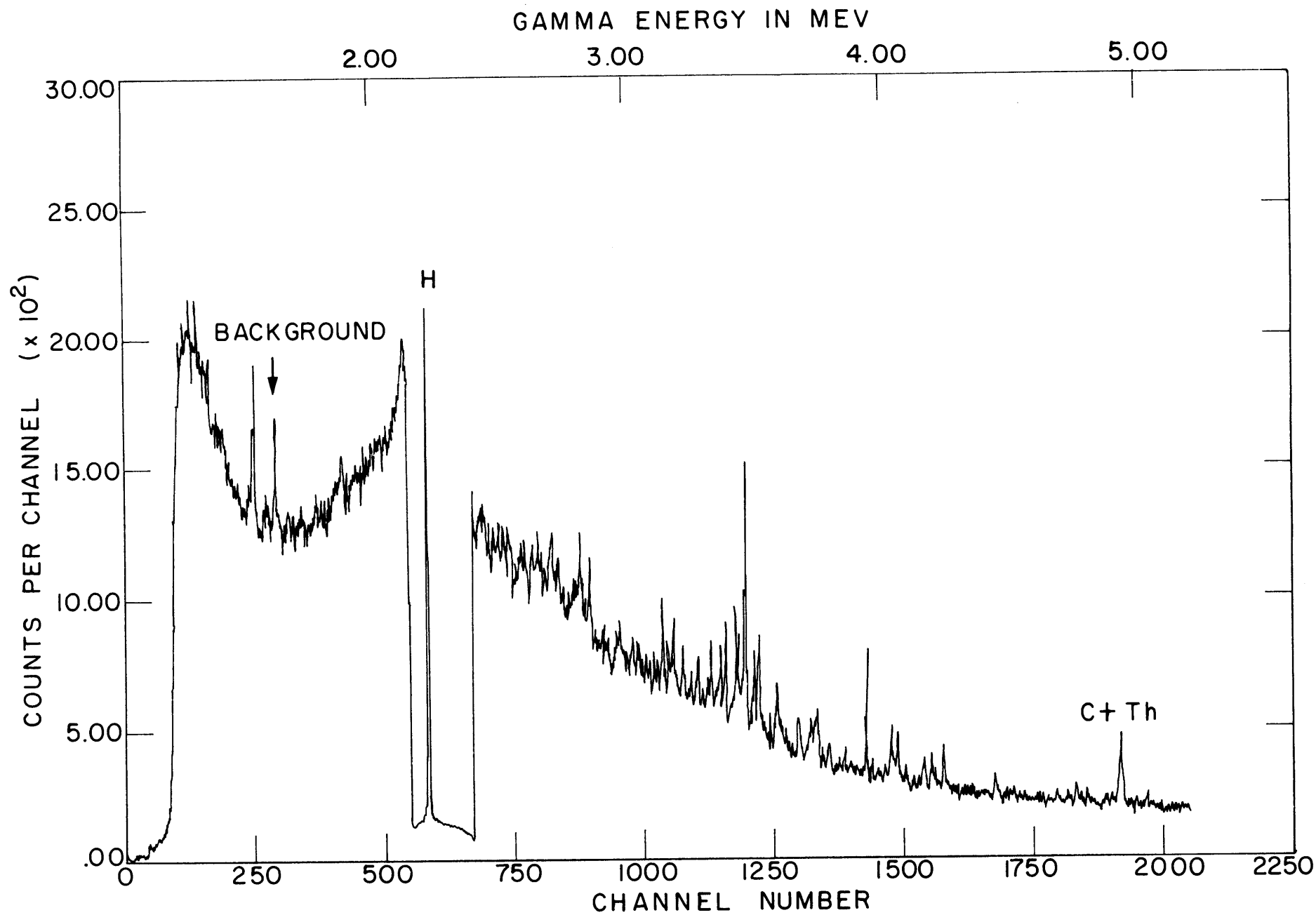
FIG. 8.1 CAPTURE GAMMA RAY SPECTRUM FOR Th-232

TABLE 8.1

Capture Gamma Rays for Uranium-238

Peak Number	Energy (keV)	Intensity (Per 100 captures)
1	523.9	1.67
2	540.3	2.31
3	553.9	6.54
4	562.4	1.10
5	580.7	1.40
6	612.2	3.68
7	661.7	1.03
8	683.7	1.19
9	708.5	1.28
10	1498.1	1.41
11	1889.1	3.09
12	2999.8	0.60
13	3196.1	0.71
14	3312.0	0.56
15	3583.0	2.14
16	3611.5	0.81
17	3637.5	0.77
18	3844.6	0.54
19	3938.0	1.05
20	3988.8	1.03
21	4042.7	0.49
22	4059.7	9.06
23	4170.1	0.46
24	4659.8	0.28

TABLE 8.2

Capture Gamma Rays for Thorium-232

Peak Number	M.I.T.		Groshev (Ref. 6)	
	Energy (keV)	Intensity (Per 100 captures)	Energy (MeV)	Intensity (Per 100 captures)
1	300.3	0.88		
2	335.4	1.16		
3	458.5	0.63		
4	472.8	1.57		
5	522.7	0.56		
6	558.7	0.59		
7	566.8	1.59		
8	578.1	0.72		
9	584.0	0.69		
10	628.7	0.69		
11	666.5	0.74		
12	681.7	0.66		
13	715.8	0.52		
14	1582.8	0.61		
15	2202.5	0.48		
16	2315.8	0.89		
17	2824.7	0.69		
18	2860.4	0.71		
19	3148.9	0.89		
20	3172.2	0.30		
21	3197.2	0.43		

(Continued)

TABLE 8.2 (Concluded)

Peak Number	M.I.T.		Groshev (Ref. 6)	
	Energy (keV)	Intensity (Per 100 captures)	Energy (MeV)	Intensity (Per 100 captures)
22	3229.0	0.42		
23	3292.3	0.27		
24	3325.9	0.27		
25	3341.5	0.49		
26	3377.9	0.34		
27	3397.9	0.66		
28	3435.8	0.68	3.45	0.6
29	3448.1	0.53		
30	3472.8	1.75		
31	3509.5	0.48		
32	3527.7	0.63	3.53	1.1
33	3602.4	0.28		
34	3634.5	0.15		
35	3755.4	0.26	3.75	0.4
36	3802.1	0.14		
37	3863.2	0.16		
38	3946.3	0.71	3.94	0.5
39	4044.5	0.24		
40	4072.6	0.20		
41	4202.1	0.15		
42	4246.6	0.19	4.25	0.3
43	4944.7	0.21	4.92	0.3

in nature, there is no background due to thermal neutron capture in the detector. Thus, it is possible to use the Ge(Li) crystal as a fission neutron yield detector as well as a capture gamma detector. This may make it feasible to measure both ν and η using a single detector system. Figure 8.2 shows a plot of the fast neutron-induced signal versus fuel rod enrichment. The excellent results suggest that this method may also prove useful as an enrichment measurement device.

Work has also been done on the prompt capture plus fission gamma spectra of highly enriched U-235 and Pu-239. The stray neutron background and dense line spectra have so far thwarted acquisition of sufficiently useful data. Feasibility studies are also under way to evaluate whether a spectrometer can be installed in the D_2O exponential tank to permit eventual use of this approach in direct in-pile single rod experiments.

8.3 Data Analysis

Since, as noted in the introduction, a detailed report has been issued describing the subject data analysis procedures, the present discussion will be limited to an abbreviated synopsis.

The computer code developed for this work is a modification of a precursor used to analyze capture gamma-ray spectra obtained with the MIT triple coincidence spectrometer (2). The general objective of the program is to automatically locate all spectral peaks and determine their center and area (energy and intensity). The method employed is an improved version of the Fourier transform method described in reference 4. Four steps are involved: data smoothing by rejecting high frequency components in the Fourier transformed data; background subtraction; resolution improvement by factoring in the response characteristics of the detector (7); and finally, determination of the energy and intensity of the peaks.

A key feature of the latest code modification is the use of the fast Fourier transform algorithm described by Cooley and Tukey (8).

The program, designated GAMANL, is written in FORTRAN IV for the IBM 360, Model 65 computer. Complete analysis of a typical
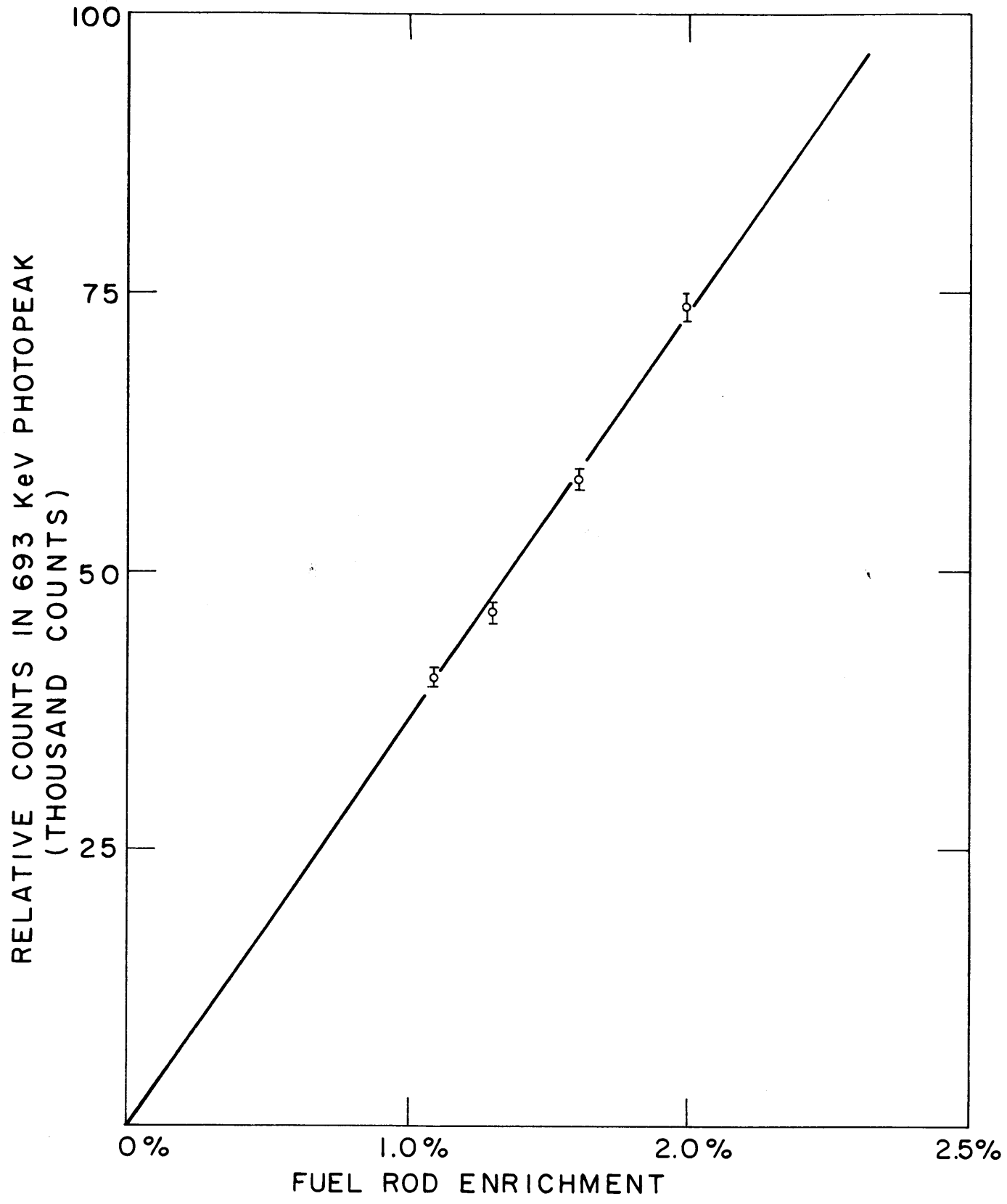
FIG. 8.2 ENRICHMENT MEASUREMENTS USING Ge-72 (n,n')
REACTION

4096 channel spectrum requires about 75 seconds. In addition to the present application, the program has also been used under another government contract in the analysis of a wide variety of gamma-ray spectra (9), with very satisfactory results.

The four major steps in the data analysis are as follows:

1. Data Smoothing

The smoothing of the observed data is accomplished by a Fourier analysis technique similar to that often used to separate the signal from the noise in communication theory. In communication theory, a function of time is transformed into frequency space, multiplied by an appropriate filter function and then transformed back into time space. In the present case, the original data is a function of energy or, more exactly, a function of channel number, so the transformation is into inverse channel number space. By analogy, we shall call this "energy frequence space," and use the symbol ω which has units of radians/channel for the variable.

To describe the method mathematically, let the observed data f(E) be represented as the sum of two components

$$f(E) = s(E) + n(E) \tag{8.1}$$

where s(E) is the true spectral information and n(E) is the noise, which in this case is due principally to random fluctuations in the number of counts in a channel. The Fourier transform of f(E), denoted $F(\omega)$, can be written in the usual notation as

$$F(\omega) = \int_{-\infty}^{\infty} f(E)\, e^{-i\omega E}\, dE \tag{8.2}$$

or

$$F(\omega) = S(\omega) + N(\omega), \tag{8.3}$$

where $S(\omega)$ and $N(\omega)$ stand for the Fourier transforms of the components of f(E).

The success of the method depends upon $S(\omega)$ and $N(\omega)$ being different functions so that a filter function can be chosen which will eliminate at least part of $N(\omega)$ without seriously affecting $S(\omega)$.

Fortunately, this is true in most spectra since the spectral peaks are spread over a number of channels, and so $S(\omega)$ is made up principally of low frequencies. The noise, on the other hand, is channel-to-channel fluctuations and so $N(\omega)$ contains many higher frequencies. Thus, there will be a significant difference in $N(\omega)$ and $S(\omega)$ for cases when the spectral peaks are several or more channels wide and the method will be applicable.

Let us define the inverse transform

$$s(E) = \frac{1}{2\pi} \int_{-\infty}^{\infty} F(\omega) P(\omega) e^{i\omega E} d\omega, \tag{8.4}$$

where $P(\omega)$ is the filter function and $s(E)$ will be a smoothed version of the original spectrum. The method of choosing $P(\omega)$ is discussed later. For simplicity, we have expressed all the transforms in their integral form; however, when the technique is applied to discrete data, the transformations must be used in their discrete form.

2. Background Subtraction

In most cases, the spectral peak sits on a background which must be subtracted in order to accurately determine the peak area. This background is the result of a number of processes in the source and in the detector, and it often cannot be expressed accurately analytically. We have found that to a good approximation the background can be represented as a slowly varying function which connects all the minima in the smoothed data $s(E)$. Care must be exercised in applying this definition, however, since the minima which occur in the case of partially resolved peaks must be excluded. This is accomplished by setting a maximum value for the slope of the background. When the slope connecting two successive minima exceeds this maximum value, the minima are ignored and the background line is connected to the next minima which will give an acceptable slope. The smoothed background subtracted data are designated $g(E)$.

3. Resolution Improvement

In complicated spectra such as those from (n, γ) reactions, there are a number of cases where lines are only partially resolved. In order to determine the peak centers accurately, it would be helpful to have a higher energy resolution. Because of our knowledge of the response of the detector to a monoenergetic gamma ray, the mathematical limit of resolution is somewhat better than the apparent limit usually expressed as the FWHM (full width of half maximum) of a peak. The detailed theory underlying this method has already been described in the literature by Inouye (7) where it was applied to NaI spectra. Here we briefly restate the results and show their applicability to Ge(Li) spectra as well. To understand the method, let us consider Eq. 8.5:

$$g(E) = \int_{-\infty}^{\infty} h(E-E') \, j(E') \, dE' , \qquad (8.5)$$

where g(E) is the smoothed, background subtracted data, which can be expressed analytically as the above integral, where h(E-E') is the response function of the detector and j(E') is the incident spectra which in this case may be considered to be a series of δ functions in energy as expressed in Eq. 8.6:

$$j(E') = \sum_i A_i \, \delta(E'-E_i) . \qquad (8.6)$$

Since Eq. 8.5 is a convolution integral, its transform can be expressed as

$$G(\omega) = H(\omega) \, J(\omega) . \qquad (8.7)$$

Now, since we can experimentally determine g(E) and h(E'-E), we can calculate G(ω) and H(ω) and can therefore determine j(E), the incident spectrum as shown by Eq. 8.8:

$$j(E) = \frac{1}{2\pi} \int_{-\infty}^{\infty} G(\omega)/H(\omega) \, e^{i\omega E} \, d\omega$$

$$= \frac{1}{2\pi} \int_{-\infty}^{\infty} G(\omega) \, W(\omega) \, e^{i\omega E} \, d\omega , \qquad (8.8)$$

where $W(\omega) = \frac{1}{H(\omega)}$ is the resolution improvement filter function. The problem in practice is that g(E) has some noise in it, since the smoothing processes eliminate only part of noise n(E) and the background subtraction also introduces some error. Thus, there is no function $W(\omega)$ which will exactly reproduce the input δ functions. Nevertheless, as will be evident in the next section, it is possible to obtain a significant increase in the apparent resolution using this procedure. The principal thing which limits this procedure is the statistical accuracy of the original data.

4. Peak Selection and Intensity Determination

The peak selection is accomplished by identifying each maximum in the smoothed, background subtracted data g(E). The peak center is obtained by finding the point of zero slope of a second-order fit to the top of the peak. The accuracy of this procedure was checked by comparing the results for a number of peaks to those obtained by finding the centroid of a Gaussian which had been fit to the peak by a least squares method. The results agreed within ± 0.1 channels on peaks with a σ = 1.5 channels. In terms of energy, this was an accuracy of about ± 0.2 keV and was considerably better than the overall reproducibility of about 0.7 keV of typical runs. However, where greater accuracy is required, more sophisticated peak fitting methods could be used. The peak center in channel number is converted to energy using calibration lines of known energy and a correction is made for the small nonlinearities of the system.

The area under a single peak is found by summing all the counts between successive zeros in the background subtracted data. Multiplets, where there are nonzero minima between successive zeros, are treated separately. In this case, two or more Gaussian functions of appropriate width, and centered at the positions determined by using the resolution improvement technique, are fitted to the data. The total counts in the multiplets are then divided in proportion to the amplitudes of the Gaussians which best fitted the data.

8.4 Application of Data Analysis Method

To determine the proper smoothing filter function, it is useful to plot $|F(\omega)|$ vs. ω. Such a plot for two typical 4096 channel spectra is shown in Fig. 8.3. The x's represent a run where the gain was adjusted to produce a channel width of 0.971 keV. The circles represent a lower gain which gave a 2.063-keV channel spacing. The approximate shape of the components of $F(\omega)$ are shown as the solid lines. As expected, in the 0.971-keV run where the peaks contain more channels, the signal component $S(\omega)$ contains less high frequencies. The filter function must be of a form that passes frequencies below the break in the curve but eliminates those frequencies above the break where the noise component $N(\omega)$ dominates. A filter function shape that was found to work well is shown in Fig. 8.4. The three different curves represent functions with different cutoffs. A Gaussian shape used to reduce the curve from unit to zero has a $\sigma = 128$. It is important that the filter function be a smoothly varying function in order that oscillations not be introduced in the inverse transformation. To illustrate the effect of changing the cutoff frequency, those data used to obtain the 0.971 keV/channel curve of Fig. 8.3 were processed using the three different filter functions shown in Fig. 8.4. A portion of the 4096 channel spectrum showing the effect of each of these filter functions on a doublet is shown in Fig. 8.5. The cutoff that begins at $412 \left(\frac{2\pi}{4096} \right)$ rad/channel is the one predicted from Fig. 8.3, and it produces considerable smoothing action without decreasing the peak-to-valley ratio in the doublet. Careful analysis also revealed that the peak centers were not shifted by the smoothing process. As expected, the function with the higher cutoff does not produce as much smoothing and the very low cutoff produces so much smoothing that considerable spectral information is lost.

The proper choice of the resolution-improvement filter function, $W(\omega) = 1/H(\omega)$, where $H(\omega)$ is defined by Eq. 8.8, is somewhat more difficult than the choice of the smoothing filter function. By trial and error, it has been found that a Gaussian plus a constant is a very satisfactory function for accomplishing the desired result. This function
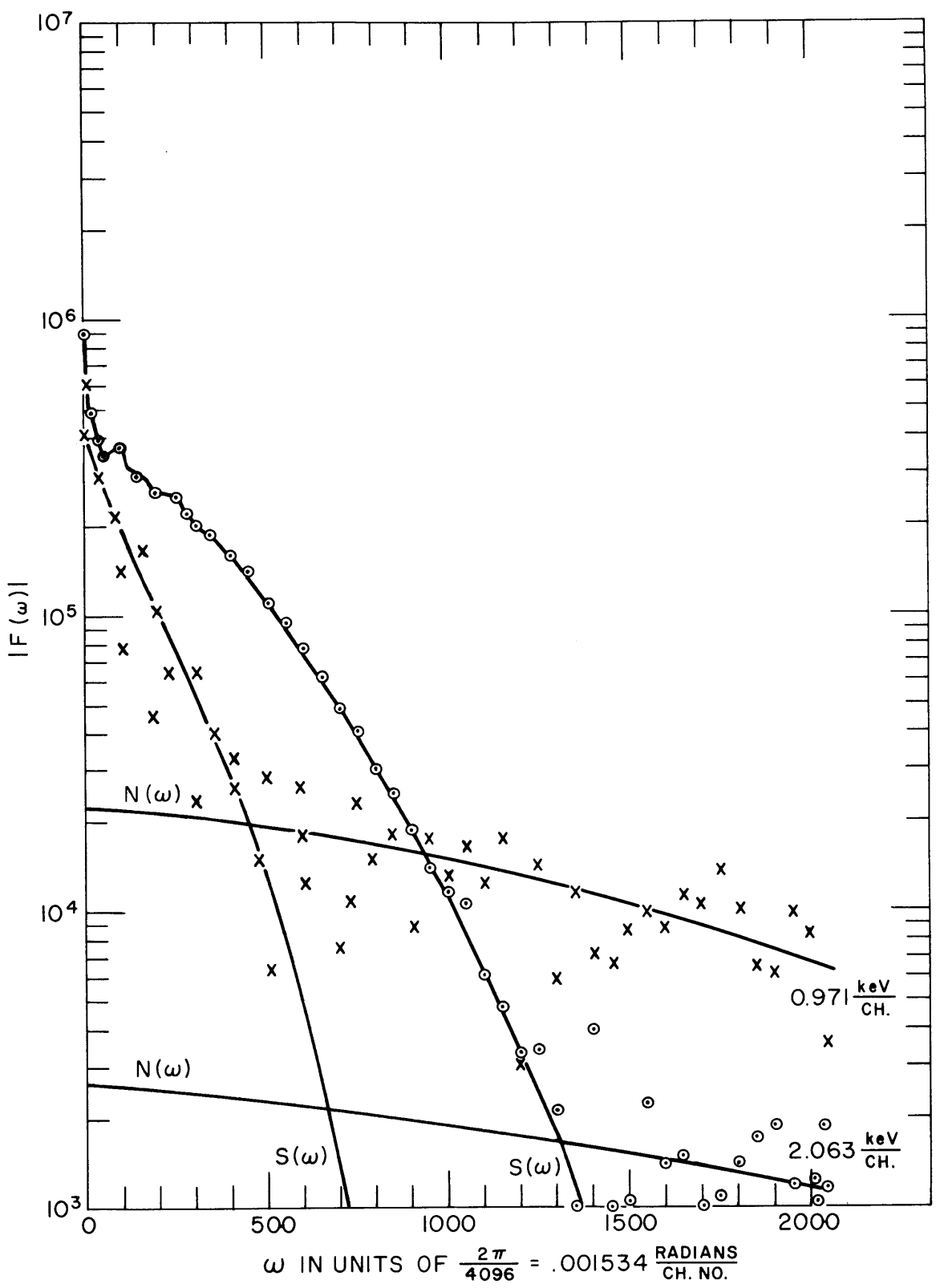
FIG. 8.3 THE ABSOLUTE VALUE OF THE FOURIER TRANSFORMS
FOR TWO DIFFERENT 4096 CHANNEL γ-RAY SPECTRA.
THE ENERGY WIDTH OF A CHANNEL WAS CHANGED AS
INDICATED. THE SOLID LINES INDICATE THE APPROXIMATE
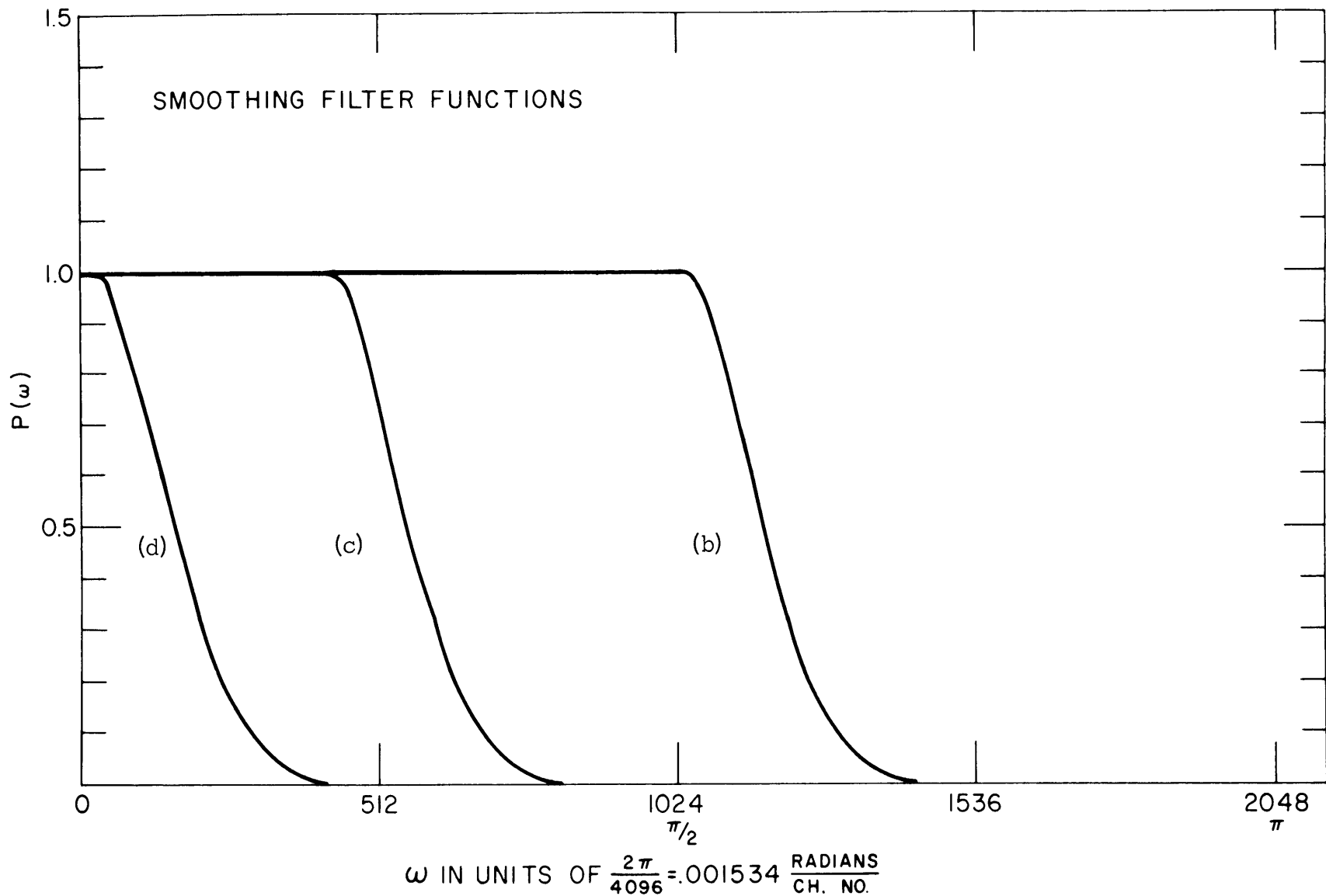SHAPE OF THE TWO COMPONENTS OF $|F(\omega)|$

FIG. 8.4 THE SMOOTHING FILTER FUNCTION P(ω) SHOWING THE SHAPE FOR 3
DIFFERENT CUTOFFS USED FOR THE RUNS PLOTTED IN FIG. 8.5.
A GAUSSIAN SHAPE WITH A σ OF 128 (2π/4096) RADIAN / CHANNEL
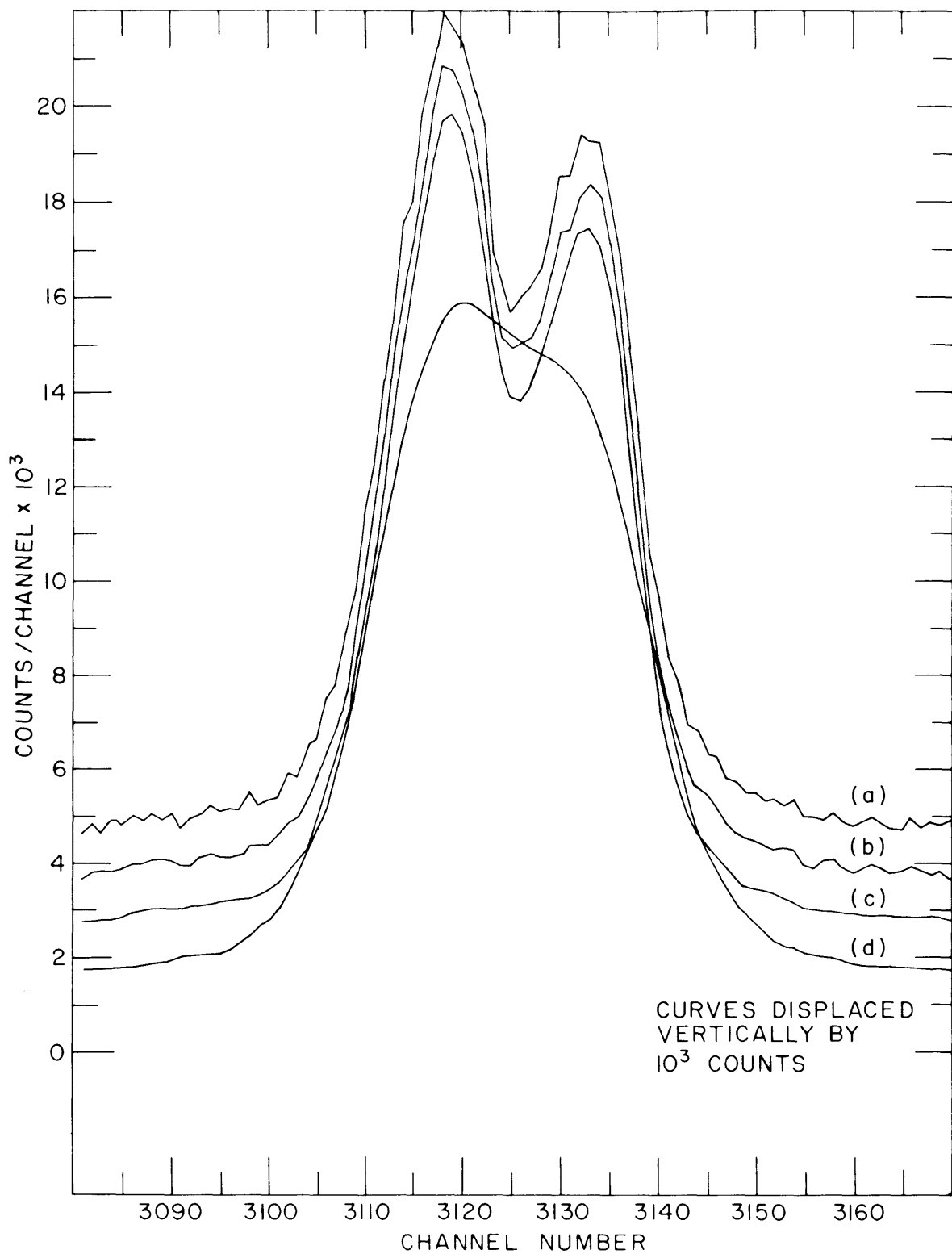IS USED TO REDUCE FUNCTION FROM UNITY TO ZERO

FIG. 8.5 THE EFFECTS OF THE THREE DIFFERENT FILTER
FUNCTIONS OF FIG. 8.4 ON A DOUBLET TAKEN FROM
THE 0.971 keV/CHANNEL DATA. CURVE (a) IS THE
ORIGINAL DATA, CURVES (b, c AND d) RESULT WHEN
FILTER FUNCTIONS (b, c, d) ARE USED. THE FOUR
CURVES ARE ARBITRARILY DISPLACED BY 10^3
COUNTS FOR CLARITY OF PRESENTATION.

has four adjustable parameters: the center, amplitude, standard deviation of the Gaussian and the constant, all of which must be optimized for the data being analyzed. Once this is done for runs of a given gain, it works equally well for subsequent runs at approximately the same gain.

In order to demonstrate the method, the doublet of Fig. 8.5 was recorded under conditions which produced a much worse energy resolution in the system. The original data from this run in the region of the doublet are shown in Fig. 8.6. Figure 8.7 shows the results of smoothing and background subtraction as described above. The curve marked $|G(\omega)|$ in Fig. 8.8 is the transform of the smoothed, background subtracted data. This was multiplied by the function $W(\omega)$ and the inverse transformation produced the doublet shown in Fig. 8.9.

Note that although a dramatic increase in resolution is possible, the process introduces small fictitious peaks on either side of the doublet. The result is that the technique is fine for examining a specific doublet to determine its components, but it cannot be applied in this drastic a manner to the entire spectrum without introducing a number of small spurious peaks which will interfere with the identification of real, small peaks. In addition, the area under a peak is sometimes changed by a spurious peak from a nearby true peak. In practice, therefore, all peaks are identified and their areas, centers and widths determined prior to the second transformation. Then those peaks with widths greater than expected are examined by the above process to locate the position of their components. The amplitude of the components is then determined by adjusting them to best fit the unresolved doublet in the smoothed data.

It has been found that if the function $W(\omega)$ is not properly chosen, it can shift the position of the components by as much as one to two channels in data of the type shown here. It is necessary, therefore, to test the function prior to using it. The check that has been used consists of locating the peak centers of the single isolated peaks of the spectrum as described earlier and then performing the transformation using the proposed $W(\omega)$. If there is no resulting shift in the centers of single isolated peaks, then the function is assumed to be satisfactory.
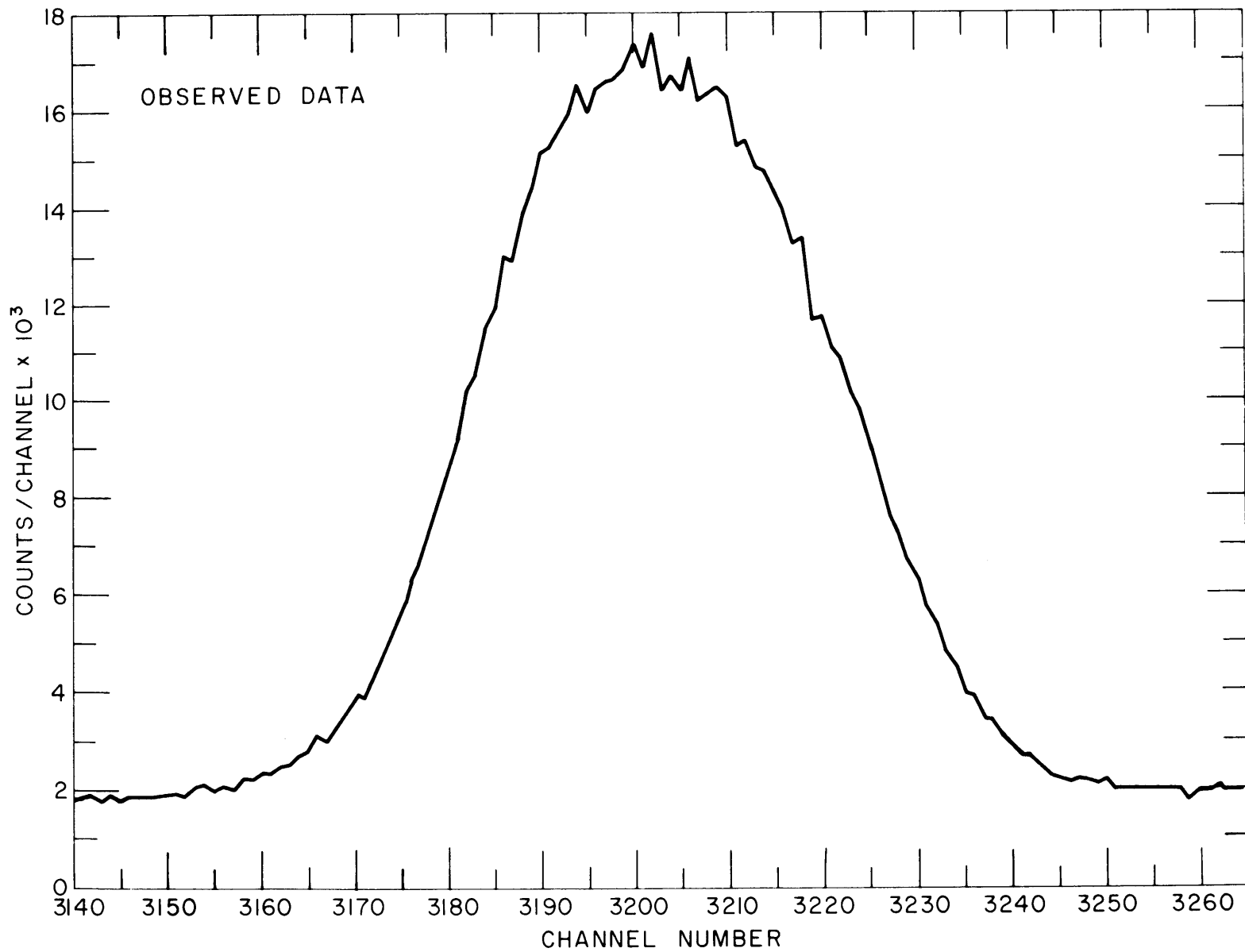
FIG. 8.6 THE OBSERVED DATA OF AN UNRESOLVED DOUBLET FROM A 4096 CHANNEL
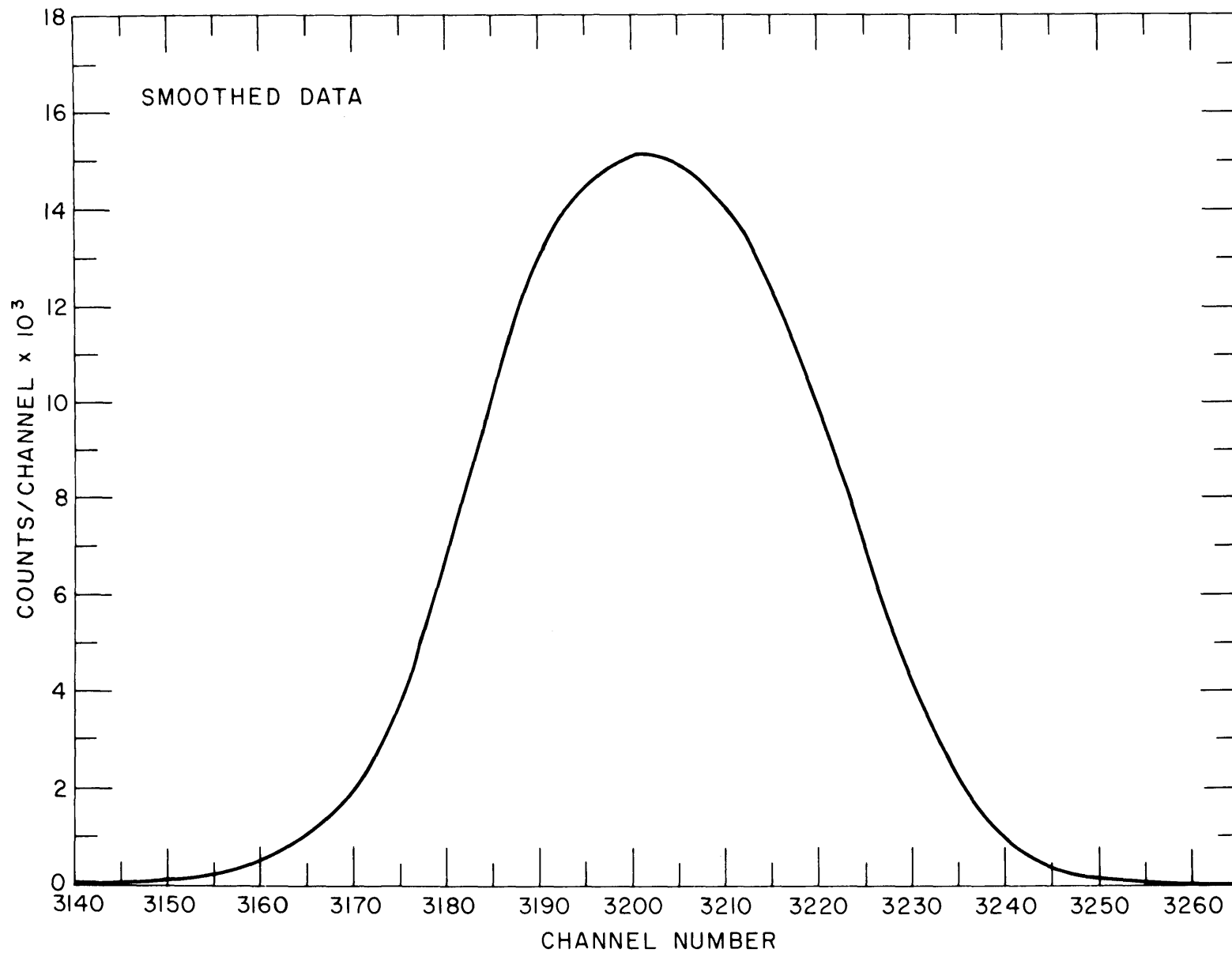SPECTRUM HAVING A 0.724 - keV CHANNEL WIDTH

FIG. 8.7 THE DOUBLET OF FIG. 8.6 FOLLOWING SMOOTHING AND BACKGROUND
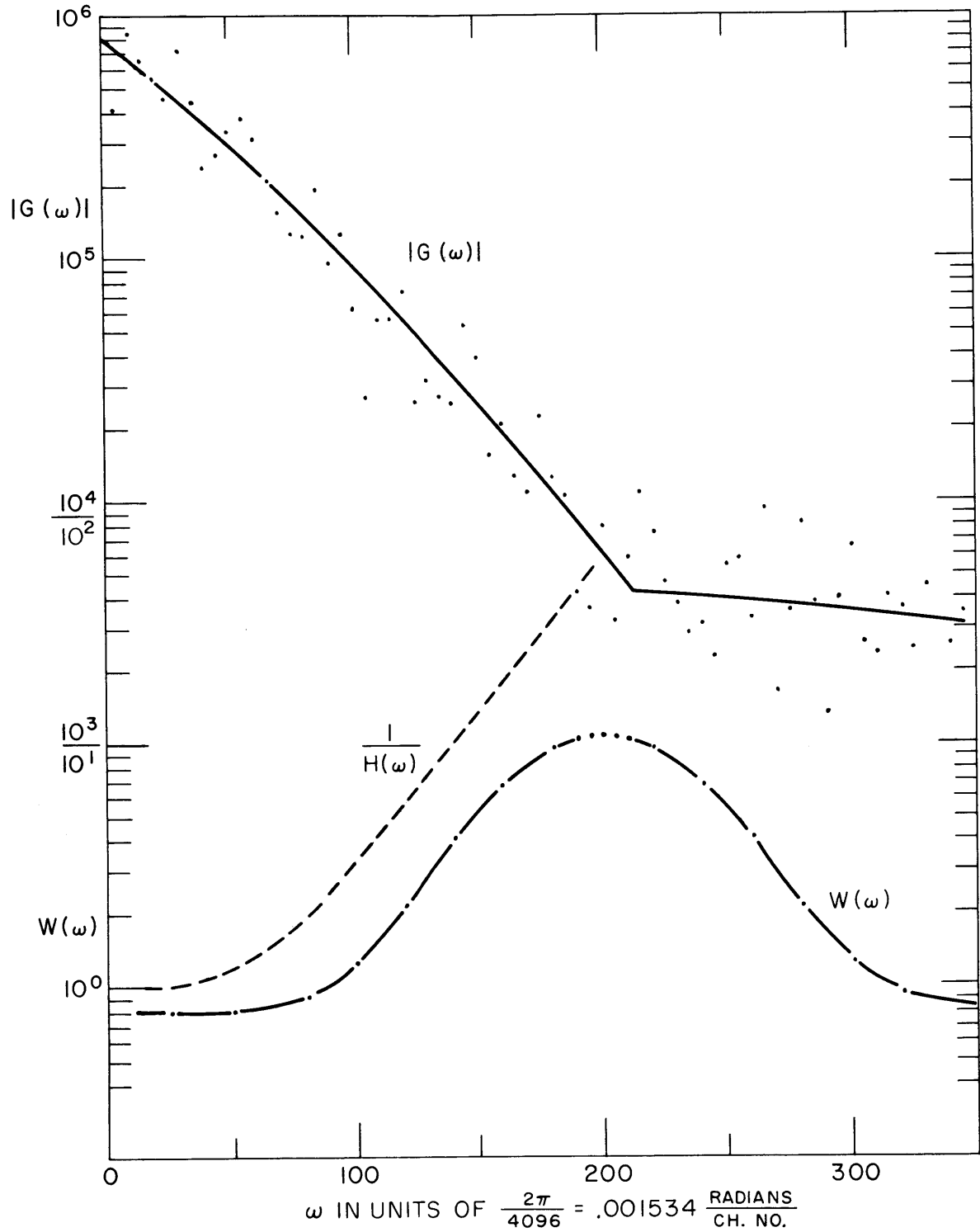SUBTRACTION

FIG. 8.8 THE UPPER CURVE IG(ω)I IS THE ABSOLUTE VALUE OF
FOURIER TRANSFORM OF THE SMOOTHED BACKGROUND
SUBTRACTED DATA OF THE 0.724 – keV / CHANNEL
SPECTRUM. THE LOWER CURVE W(ω) IS THE
RESOLUTION IMPROVEMENT FILTER FUNCTION USED TO
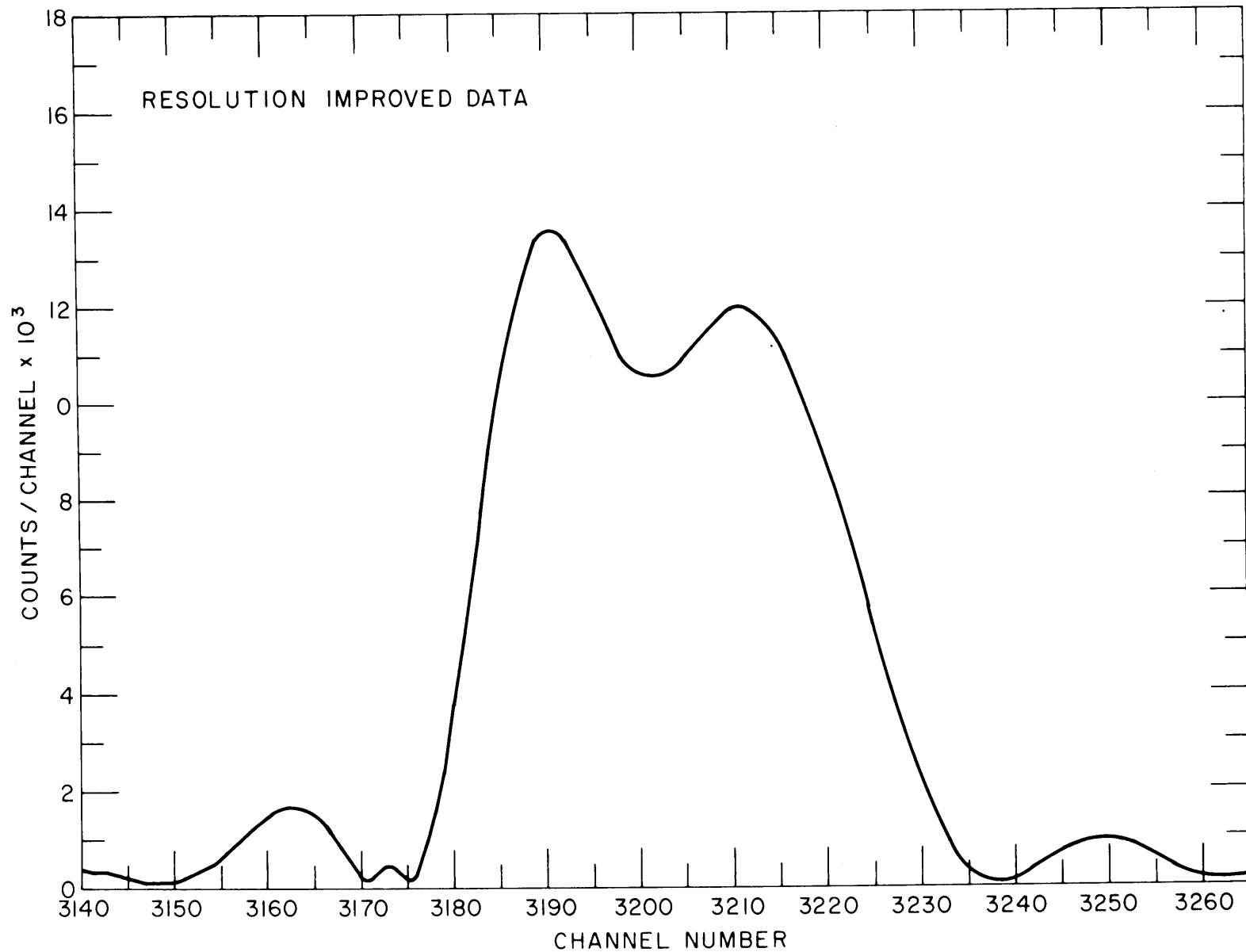PRODUCE FIG. 8.9. I/H(ω) IS THE INVERSE OF THE
TRANSFORM OF A SINGLE SPECTRAL PEAK.

FIG. 8.9 THE UNRESOLVED DOUBLET OF FIG. 8.6 SHOWING THE EFFECT OF THE FOURIER
TRANSFORMATION USING THE FILTER FUNCTION W (ω) SHOWN IN FIG. 8.8.
THE SMALL PEAKS ON EITHER SIDE ARE SPURIOUS PEAKS INTRODUCED
BY THE TRANSFORMATION PROCESS

A computer code, GAMANL, has been developed for carrying out the gamma spectra analysis discussed above. One of the problems encountered with the use of the Fourier transform equations in their usual form is that N^2 computation operations are required where N is the number of points in energy space, i.e., the number of channels in the spectrum. This means that for $N = 4096$, the computing time becomes quite long, being on the order of one-half hour. Two methods have been used to greatly reduce this computation time. The first method used was to section the data into n smaller segments and to take the transform of each segment separately. This results in $n\left(\frac{N}{n}\right)^2$ operations and reduces the computation time by a factor of $\frac{1}{n}$. For a section length of 16 channels flanked by 10 and 11 channels on each side to correct for end effects, the sectioning method for $N = 4096$ channels required $256\,(37)^2$ operations or time reduction of a factor of $\frac{256(37)^2}{(4096)^2} \simeq \frac{1}{210}$ as compared to the direct method.

The second method used the Fast Fourier Transform (FFT) as developed by Cooley and Tukey ($\underline{8}$). The time required by the FFT to transform N energy points is $N(\log_2 N)$, which reduces the computation time by a factor of $\log_2 N/N$ as compared with the usual transformation. Thus, for a 4096 channel spectra, the time used by the FFT is $\log_2 4096/4096 = 1/256$ of the direct transform. In addition, it gives a complete set of Fourier coefficients in ω space useful in the filter function determination. The sectioning does not give these coefficients in as convenient a form.

The program GAMANL is written in FORTRAN IV for use on the M.I.T. IBM 360, Model 65 computer. The complete analysis of a 4096 channel spectrum requires less than 100 seconds.

In addition to the present application, the above program has also been used under another government contract in the analysis of a wide variety of gamma-ray spectra, including some 150 very complex capture gamma-ray spectra ($\underline{9}$), with very satisfactory results. The most important feature of the program is the data smoothing technique which enables peak centers and the average background to be determined with reasonable accuracy by rather simple methods. To

get the maximum information from a spectrum, the smoothing technique should be combined with some of the more sophisticated peak analysis methods. However, for most applications the shorter, simpler methods described here seem adequate.

Work is continuing to optimize the program to suit the specific needs of the present work, for both prompt and decay gammas emitted by irradiated fuel rods.

8.5 References

(1) Bushuev, A. V. et al., "Use of a Germanium γ-Spectrometer for Studying Certain Reactor Characteristics," Soviet Atomic Energy, Vol. 22, No. 6, June 1967.

(2) Orphan, V. J. and N. C. Rasmussen, "A Ge(Li) Spectrometer for Studying Neutron Capture Gamma Rays," Nucl. Instr. and Methods, 48, No. 2 (1967).

(3) Sonstelie, R. R. and N. C. Rasmussen, Measurement of δ_{28} Based on Gamma Spectrometry, in "Heavy Water Lattice Project Final Report," MIT-2344-12, MITNE-86, September 30, 1967.

(4) Inouye, T. and N. C. Rasmussen, "A Computer Method for the Analysis of Complex Gamma-Ray Spectra," Trans. of the ANS, 10, 1, p. 38 (1967).

(5) Sheline, R. et al., "Levels in U^{239}," Phys. Rev., 151, 3, p. 1011 (1966).

(6) Groshev, L. V. et al., Atlas of Gamma-Ray Spectra from Radiative Capture of Thermal Neutrons, Pergamon Press, London, 1959.

(7) Inouye, T., "The Super Resolution of Gamma-Ray Spectrum," Nucl. Instr. and Methods, 30 (1964).

(8) Cooley, J. W. and J. W. Tukey, "An Algorithm for the Machine Calculation of Complex Fourier Series," Math. Comput., 19, 297 (1965).

(9) Rasmussen, N. C., Y. Hukai, T. Inouye and V. J. Orphan, "Thermal Neutron Capture γ-Ray Spectra of the Elements," MITNE-85 (prepublication).

APPENDIX A

BIBLIOGRAPHY OF PUBLICATIONS ON
HETEROGENEOUS REACTOR THEORY
AND SINGLE ROD METHODS

In this bibliography we list a selection of references which deal with various aspects of heterogeneous reactor theory and single fuel element neutronics. A brief comment is included on each.

1. Barden, S. E. et al., "Some Methods of Calculating Nuclear Parameters for Heterogeneous Systems," Proc. 1958 Geneva Conf., P/272. Application of heterogeneous method to finite arrays of rectangular shape.

2. Blaesser, G., "An Application of Heterogeneous Reactor Theory to Substitution Experiments," P/42/52, IAEA Symposium, Amsterdam, 1963. The method avoids many difficulties which are typical of homogenized treatment as, for example, determination of coupling constants.

3. Corno, S. E., "Interpretazione Teorica delle Esperienze di Moltiplicazione Neutronica su un Solo Elemento di Combustible," Energia Nucleare, 10, 11 (1963). A highly theoretical application of small source theory to the problem of a single rod in an exponential pile. (Series of three articles.)

4. Corno, S. E., "Theory of Pulsed Neutron Experiments in Highly Heterogeneous Multiplying Media," in Pulsed Neutron Research, Vol. II, IAEA, Vienna, 1965. A theory of pulsed neutron experiments applicable to a single fuel element.

5. Donovan, R., "Measurement of Heterogeneous Parameters," MIT-2344-12 (1967). Calculations based on measurements on a single element using foil techniques.

6. Durrani, S., E. Etherington and J. Ford, "Determinations of Reactor Lattice Parameters from Measurements on a Single Fuel Element Channel," APC/TN 1054. Another application of the method in (30) below.

7. Estabrook, F. B., "Single Rod Exponential Experiments," NAA-SR-925, p. 13. Reports other data on same experiments as in (12).

8. Feinberg, S. M., "Heterogeneous Methods for Calculating Reactors," Proc. 1955 Geneva Conf., P/669. One of the original and basic theoretical papers on heterogeneous methods.

9. Galanin, A. C., "The Thermal Coefficient in a Heterogeneous Reactor," Proc. 1955 Geneva Conf., P/666. One of the original and basic theoretical papers on heterogeneous methods.

10. Graves, W. E. et al., "A Comparison of Heterogeneous Nuclear-Reactor Lattice Theory with Experiment," Nucl. Sci. Eng., 31, p. 57-66 (1968). Comparison is made for thermal neutron densities and critical geometric bucklings.

11. Hassit, A., "Methods of Calculation for Heterogeneous Reactors," Progress in Nuclear Energy, Series I, Vol. II, p. 271-313 (1958). Describes the "mesh method" of solving the two group diffusion theory equations within the moderator region of the heterogeneous system using finite difference equations.

12. Heinzman, O. W. and S. W. Kash, "Intracell Flux Distributions for an Extensive Series of Heavy Water, Uranium Rod Lattices," NAA-SR-1548 (August 1956). Reports radial flux traverses about 1-inch-diameter single rods.

13. Higgins, M. J., "Fuel Rod Interaction Kernels," MIT-2344-12 (1967). Describes experimental determination of the rod interaction kernels and methods that can use these kernels to predict integral parameters for entire lattices.

14. Horning, W. A., "Small Source Model of a Thermal Pile," HW-24282 (1957). An early attempt at an analysis that could be used to relate theory and experiment.

15. Jonsson, A., "Heterogeneous Calculation of Fast Fission," AE-42 (Feb. 1961). An exact calculation of the collision probabilities is included.

16. Jonsson, A. and G. Naslund, "Heterogeneous Two Group Diffusion Theory for a Finite Cylindrical Reactor," AE-57 (June 1961), and other internal reports. Describes the basis for the computer code HETRO.

17. Jonsson, A. and G. Naslund, "Theory of Application of Heterogeneous Methods for D_2O Reactor Calculations," Proc. 1964 Geneva Conf., P/683. Extension of heterogeneous methods to finite cylindrical systems.

18. Klahr, C. N. et al., "Heterogeneous Calculation Methods," NYO-2680 (June 1961). A final report on small source reactor physics calculations using the HERESY code.

19. Lanning, D. D., "Heterogeneous Reactor Critical Conditions Using Small Source Theory," TID-7532, Part I (1957). The application of heterogeneous analysis using age theory, to reactors containing control rods.

20. Leslie, D. C. and A. Jonsson, "Improvements to the Theory of Resonance Escape in Heterogeneous Fuel," Papers I and II, Nucl. Sci. Eng., 22, p. 78-86 (1965) and Nucl. Sci. Eng., 23, p. 82-89 (1965). New and simple method of calculating Dancoff factors in regular arrays of cylindrical rods and cluster.

21. Leslie, D. C. and A. Jonsson, "The Calculation of Collision Probabilities in Cluster-Type Fuel Elements," Nucl. Sci. Eng., 23, p. 272-290 (1965). The method is analytic and comparable in speed to other codes for annular geometry.

22. Meetz, K., "Exact Treatment of Heterogeneous Core Structures," Proc. 1958 Geneva Conf., P/968. A theoretical paper which develops a mathematical formalism for such problems.

23. Papay, L. T., "Fast Neutron Fission Effect for Single Slightly Enriched Uranium Rods in Air and Heavy Water," MIT-2344-4 (1965). Describes the determination of δ_{28} for small diameter single rods.

24. Pershagen, B., G. Anderson and I. Carlvik, "Calculation of Lattice Parameters for Uranium Rod Clusters in Heavy Water and Correlation with Experiments," Proc. 1958 Geneva Conf., P/151. An example of the application of the Poisson summation in heterogeneous lattices.

25. Pilat, E. E. et al., "The Use of Experiments on Single Fuel Elements to Determine the Nuclear Parameters of Reactor Lattices," MIT-2344-10, MITNE-81 (Feb. 1967). Combines experiments on a single element with a theory which describes a lattice of such elements.

26. Rodeback, G. W., C. H. Skeen and J. W. Zink, "Single Element Measurements," Trans. Amer. Nucl. Soc., 2, 1 (June 1959). A preliminary report on (30).

27. Saji, G. and A. Axford, "Space-Time Kinetics for Heterogeneous Reactor Models," Nucl. Sci. Eng., 35, p. 319-331 (1969). A new theoretical formalism of the space-time kinetics is developed for heterogeneous reactor models.

28. Seth, S. S., "Measurement of Integral Parameters," MIT-2344-9 (1966) and MIT-2344-12 (1967). Report includes techniques to obtain single element integral parameters.

29. Stewart, J. D. et al., "MICRETE: A G-20 Program for Calculating Finite Lattices by the Microscopic Discrete Theory," AECL 2547 (Feb. 1966). Description of the program MICRETE for solving 2D reactor lattice problem using heterogeneous theory.

30. Zink, J. and G. Rodeback, "The Determination of Lattice Parameters by Means of Measurements on a Single Fuel Element," NAA-SR-5392 (1960. Actual experiments on a single fuel rod are used to infer parameters of graphite uranium lattices, with best results in the thermal energy region. Also reported in <u>Nucl. Sci. Eng.</u>, <u>9</u>, p. 16-25 (1961).